APC/C processivity and cell cycle regulation in meiosis I mouse oocytes.

Christopher Thomas

Institute for Cell and Molecular Biosciences,
Newcastle University

A thesis submitted for the degree of Doctor of Philosophy

September 2017

Abstract

Accurate cell division is a strictly ordered, highly regulated event. In mitosis, a robust spindle checkpoint ensures that chromosome division errors occur at a relatively low frequency, maintaining high levels of cyclin B1 and securin until chromosomes are accurately aligned. In contrast, in mouse oocytes, cyclin B1 and securin are targeted for destruction in late prometaphase I, at a time when the spindle is yet to fully migrate to the cortex and checkpoint proteins are still at kinetochores. This has been suggested to be symptomatic of an inefficient spindle checkpoint in meiosis I oocytes and a potential contributor to the high rates of aneuploidy observed in human oocytes. Curiously however, these observations have been made in mouse oocytes which ordinarily experience much lower rates of error. The seemingly early loss of cyclin B1 and securin rarely has a negative impact. This study demonstrates that cyclin B1 and securin destruction in late prometaphase I is not simply due to an inefficient spindle checkpoint, but instead due to controlled novel mechanisms of destruction within the oocyte. Meiotic cyclin B1 and securin destruction can in fact be split into two distinct periods; a later period that resembles mitotic destruction where the D-box is sufficient for APC/C targeting, and a much earlier period of destruction requiring previously unidentified motifs able to bypass the spindle checkpoint. Due to the location of these motifs, it is likely that they are hidden when in complex; cyclin B1 with Cdk1 and securin with separase. A model is proposed by which free pools of cyclin B1 and securin act as buffer zones, protecting Cdk1 activity and separase inhibition when the spindle checkpoint may become insufficient over the extended prometaphase period in the huge cell volume of an oocyte. Furthermore, meiotic cyclin A2 regulation is investigated. When put alongside cyclin B1 and securin data this begins to shed light on overall APC/C processivity in meiosis I.

Acknowledgements

I would firstly like to thank my supervisors Dr. Suzanne Madgwick and Dr. Mark Levasseur for continued support and guidance throughout the PhD. Without Mark's encouragement following my third year undergraduate project, I might still be working as a removals man. Though I imagine I would have been made to pass my driving test by now, in which case those blissful sleeps back and forth from London would be only history.

I feel extremely lucky to have been part of such a compact group, where constant co-operation, teamwork and discussion were not a privilege but a norm. I would also like to thank Dr. Jon Higgins and Dr. Owen Davies for critical discussion and expertise that have helped shape the project and drive it to where it is today.

My time in Newcastle wouldn't have been the same without the wonderful people I share an office with. Roy, congratulations! Come January you'll be #1 at the Times crossword in our office. Diana, thanks for everything. I hope there is pea pie for many years to come. Nik, best of luck in the van. Basquey, en el fondo todo lo que quiero es verte amenecer.

Finally, none of this would have been possible without the love and support of my family to whom I am eternally grateful.

Table of contents

List of figures

Publications

My PhD studies have resulted in two first author manuscripts, one currently in revision and a second in preparation.

Mark D. Levasseur, **Christopher Thomas**, Owen R. Davies, Jonathan M.G. Higgins and Suzanne Madgwick* – *Degron-masking controls cyclin B1-Cdk1 activity to prevent division errors in oocytes* (Unpublished – in revision) – **Joint first authorship**

Christopher Thomas*, Mark D. Levasseur, Owen R. Davies, Jonathan M.G. Higgins and Suzanne Madgwick* – *A novel motif promotes preferential degradation of free securin to protect against premature separase activation in meiosis I mouse oocytes.* (Unpublished – in preparation) – **First and corresponding authorship**

Chapter 1: General introduction.

In this chapter, I will introduce general themes underlying the study. These include progression through the female meiotic cell cycle, oogenesis and aneuploidy. I will also discuss how the method of spindle assembly and the checkpoint which protects this assembly vary between mitosis and meiosis. Each results chapter will include a separate, in-depth introduction focusing on the literature relevant to the data presented in that chapter.

1.1 Meiosis, oogenesis and aneuploidy

Meiosis is the specialised cell division in which a diploid progenitor cell undergoes two sequential rounds of division without an intermediate DNA synthesis phase, to produce a haploid gamete. The first meiotic division (MI) involves the division of the homologous pairs of chromosomes, in the case of humans from 46 to 23 pairs and in mice from 40 to 20 pairs. MI is therefore described as a reductional division. The second meiotic division (MII) is more like mitosis, in that sister chromatids are segregated in a division described as equational. Following MI and MII, the subsequent fusion of two haploid gametes, the egg from the maternal side and the spermatozoa from the paternal side, takes place during fertilisation to re-establish a diploid zygote with half the genetic material from each parent. A schematic diagram highlighting the important features of female meiosis I and II is shown in fig. 1.1.

Anomalies are extremely common in human gametes with ~9% of spermatozoa and ~21% of oocytes being abnormal. The types of abnormalities are very different and have a different impact on human wellbeing. Spermatozoa are produced in their millions and the majority of abnormalities are structural. On the other hand, most ovulatory cycles involve the release of a single oocyte and most abnormal oocytes are aneuploid (Martin 2008). This study was conducted in MI mouse oocytes and therefore the focus hereafter will be female rather than male meiosis.

Prior to meiosis I, connections or crossovers between homologous chromosomes are established during a process known as homologous recombination. This takes place during early oocyte development within the foetus and functions to allow exchange of genetic material between maternal and paternal chromosomes. Homologous pairs of maternal and paternal chromosomes are first paired together by the synaptonemal complex, a molecular ‘zipper’ that provides the scaffolding for crossover to take place (see Hunter 2015 for review).

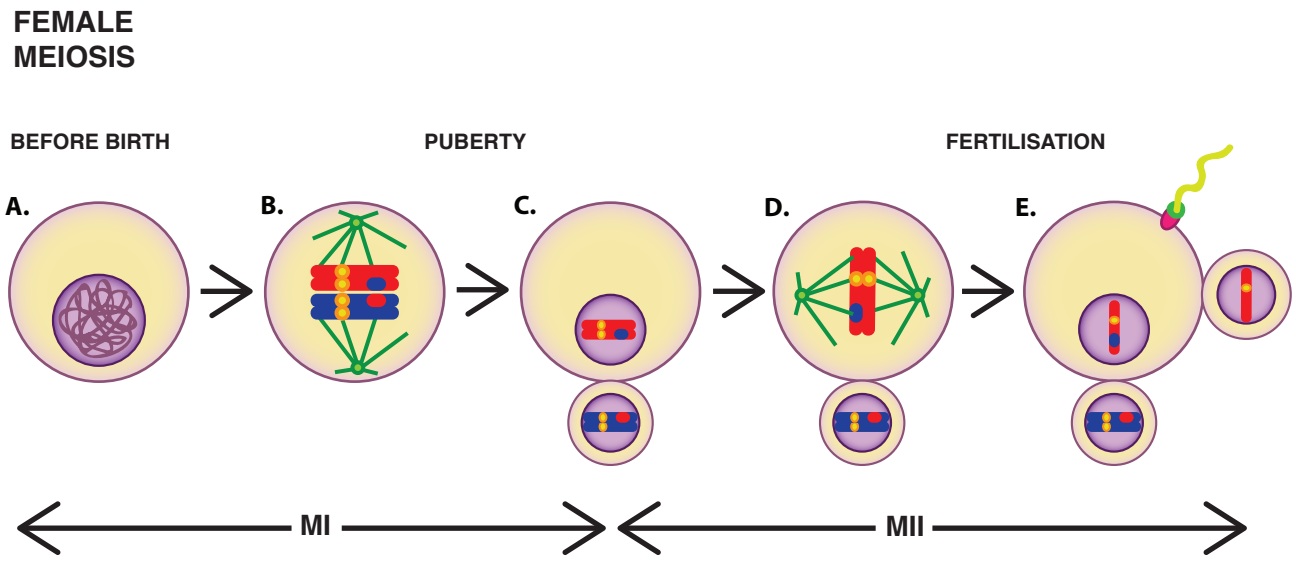

Figure 1.1. An overview of mammalian female meiosis. (A) Crossovers are established during early oocyte development in the foetus, allowing exchange of genetic material between maternal and paternal chromosomes. Any future offspring will therefore be genetically diverse from either parent cell. Following crossover, oocytes arrest in the germinal vesicle (GV) stage and are stored in the ovary. The oocyte remains in this prolonged growth phase until it is released from the ovary, following puberty. **(B)** When the egg is released from the ovary, during the monthly menstrual cycle, the GV breaks down (GVBD) and MI resumes. Bivalent pairs of chromosomes are aligned on the spindle over many hours, requiring multiple rounds of error correction to reposition homologous pairs. **(C)** Following alignment, there is an asymmetric division in which one half of homologous chromosomes remain within the large oocyte while the other half is lost in the extrusion of the first polar body (PB1) which eventually degenerates. **(D)** As the oocyte progresses into MII it is arrested in metaphase II and relocates to the oviduct. **(E)** If fertilised, the now mature egg progresses into anaphase II, in which sister chromatids are segregated. This is followed by extrusion of the second polar body, leaving a human egg with 23 maternal sister chromatids and the 23 paternal sister chromatids from the male nuclei. The membranes of these 2 pro nuclei dissolve to allow fusion of the genetic material and entry into the first mitosis and embryonic cell divisions.

Crossover between the sister chromatids of homologous pairs results in chromatids with a combination of maternal and paternal DNA. Any future offspring will therefore be genetically diverse from either parent cell.

Following crossover, there is a switch in the function of the cohesin ring structures that previously held sister chromatids together. While cohesin complexes located closer the centromere remain holding sisters together, those located distally to crossover sites switch towards holding homologous chromosomes together as crossover sites are resolved. This newly formed pair of chromosomes is termed a bivalent (Watanabe & Nurse 1999; Webster & Schuh 2017).

After formation of bivalents, oocytes arrest in the germinal vesicle (GV) or dictyate stage and are stored in the ovary, surrounded by a thin layer of follicular cells in a state known as the primordial follicle (Webster & Schuh 2017). Over multiple decades in humans, or many weeks in mice, the primordial follicle undergoes an extended growth phase, nursed by follicular cells (Herlands & Schultz 1984). The oocyte remains in this prolonged growth phase until a time when, following puberty, a cyclical increase in luteinising hormone (LH) released by the pituitary gland results in its release from the ovary (ovulation). The germinal vesicle of this prophase-arrested oocyte breaks down (GVBD) and MI resumes (Webster & Schuh 2017).

Bivalent pairs of chromosomes are then arranged and aligned on the meiotic spindle apparatus over many hours, requiring multiple rounds of error correction to reposition homologous pairs (Kitajima et al. 2011). The mechanisms of spindle assembly in human and mouse oocytes are not only vastly different from that in mitotic cells, but also distinct from each other. Mechanisms of meiotic spindle assembly will be discussed in more detail in section 1.3.

While chromosomes are aligning on the spindle, levels of cyclin B1-Cdk1 activity must be kept high to drive the progression of both mitotic and meiotic cell division (Ledan et al. 2001; Gavet & Pines 2010). At the same time, inhibition of separase by securin must be maintained to prevent premature cleavage of cohesin before chromosomes are bi-oriented and under tension (Ciosk et al. 1998). In mitosis, destruction of cyclin B1 and securin is restrained by the spindle checkpoint (discussed further in section 1.4) until all chromosomes become correctly aligned (Lara-Gonzalez et al. 2012). In brief, spindle checkpoint proteins serve to sequester Cdc20, a co-activator of the giant E3 ubiquitin ligase, the Anaphase Promoting Complex or Cyclosome (APC/C; Di Fiore et al. 2016). On correct alignment, the spindle checkpoint ceases and Cdc20 becomes free to bind to the APC/C and form a bipartite receptor

with the APC10 subunit that recognises short D-box degrons within APC/C substrates (Chao et al. 2012; He et al. 2013). Cyclin B1 and securin are then targeted for degradation via their D-box motifs driving mitotic exit and sister chromatid segregation. See Figure 1.2 for a schematic diagram showing regulation of mitotic progression.

In contrast to mitosis in which a single unattached kinetochore is sufficient to generate enough of a checkpoint signal to prevent degradation of metaphase APC/C substrates (Lara-Gonzalez et al. 2012), in meiosis I mouse oocytes cyclin B1 and securin degradation is initiated in late prometaphase (Homer et al. 2005). This takes place before all chromosomes are congressed and kinetochore attachments are stabilised (Kitajima et al. 2011) and is perhaps suggestive of a spindle checkpoint that is inefficient over the large volume of an oocyte. However this seems contradictory as mouse oocytes are rarely aneuploid, with errors present in only 1-2% of fertilised mouse eggs (Bond & Chandley 1983). In contrast, aneuploidy rates in human female oocytes are much higher and will be discussed in section 1.2.

In oocytes, prior to anaphase I, separase activation allows for cleavage of the Rec8 kleisin subunit, specific to meiotic cohesin (Buonomo et al. 2000). In MI this only occurs on chromosomes arms since while distal cohesin is readily targeted, proximal cohesin is protected from cleavage by Shugoshin-2 (Sgol2) which recruits PP2A, removing the phosphorylations essential for cohesin cleavage (Lee et al. 2008). This allows for segregation of homologous chromosomes while sister chromatids remain strongly attached over their centromeric regions. Following anaphase I, there is an asymmetric division in which one half of homologous chromosomes remain within the large oocyte while the other half is lost in the extrusion of the first polar body (PB1) which eventually degenerates. Important to note is the extended time over which MI is executed in mammalian oocytes, lasting 7-11 hours in mice and 24-36 hours in humans, this is in stark contrast to mitosis which often lasts less than an hour (Homer 2013).

As the oocyte progresses to MII it is arrested in metaphase II and relocates to the oviduct (Webster & Schuh 2017). If fertilised, the now mature egg completes MII (Clift & Schuh 2013). Shugoshin proteins that previously protected centromeric cohesin during the first meiotic division have been reported to dissociate away from the centromere in MII in a tension-dependent manner (Gómez et al. 2007; Nerusheva et al. 2014). However, a more recent study questions whether or not the tension model is the full story since in yeast, sister chromatid biorientation is not sufficient to permit Rec8 de-protection during meiosis II (Jonak et al. 2017). Instead they suggest that APC/C-Cdc20 targeting of Sgo1 and Mps1, and

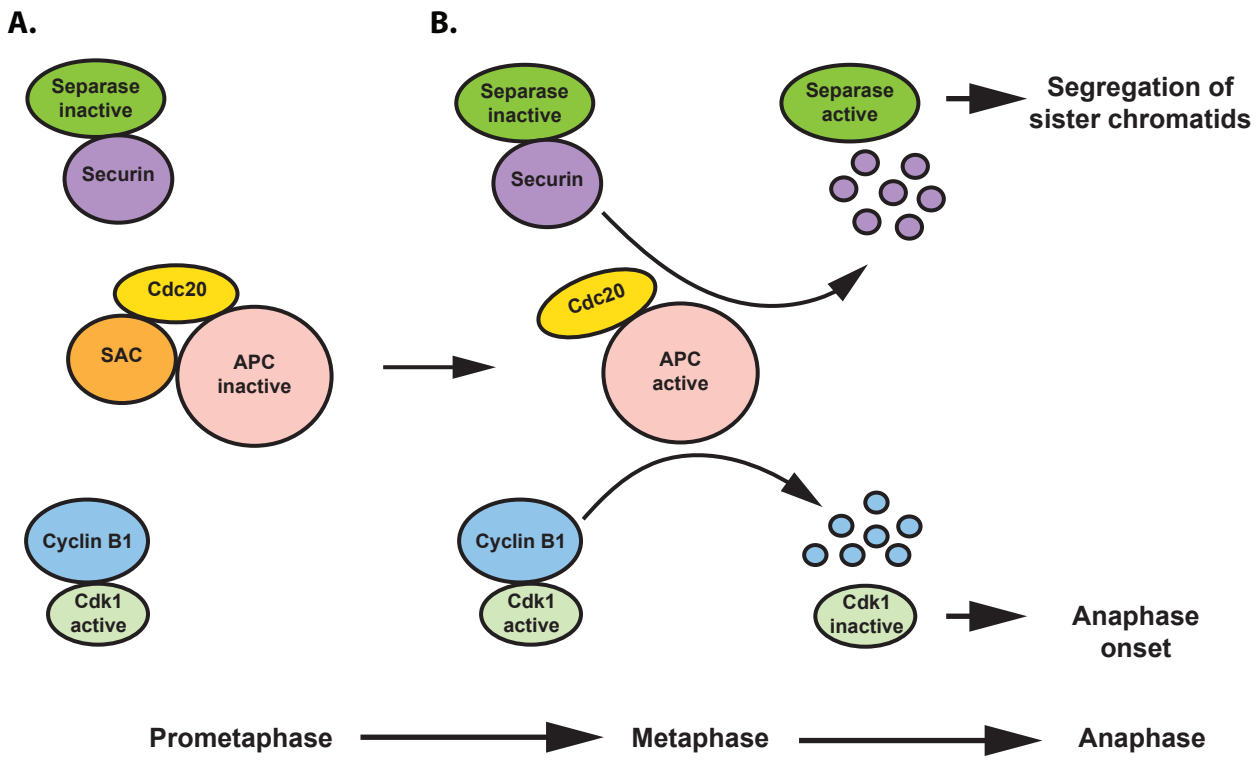

Figure 1.2. General model for the regulation of mitotic progression through APC/C-mediated cyclin B1 and securin destruction. (A) While chromosomes are aligning on the spindle, a robust spindle assembly checkpoint (SAC) inhibits APC/C activity through sequestration of APC/C co-activator Cdc20. This maintains high levels of cyclin B1-Cdk1 activity to drive the early stages of mitosis and high levels of securin which acts to inhibit separase, preventing premature cleavage of cohesin.**(B)** Once chromosomes are correctly aligned, the SAC ceases and APC/C-Cdc20 targets cyclin B1 and securin for proteasomal degradation via their D-box motifs.Cyclin B1 degradation inactivates Cdk1 which drives anaphase onset, while securin degradation activates separase allowing for cleavage of cohesin and segregation of sister chromatids.

subsequent removal of PP2A from centromeres is necessary. They propose that in yeast, Rec8 is protected until anaphase II onset, at which point it is phosphorylated in time with separase activation (Jonak et al. 2017). Co-localisation of I2PP2A with PP2A at the centromeres in metaphase II has also been shown to play a role in centromeric Rec8 de-protection through direct inhibition PP2A function (Chambon et al. 2013).

Together these mechanisms allow for segregation of sister chromatids in anaphase II. This is followed by extrusion of the second polar body, leaving a human zygote with 23 maternal sister chromatids and the 23 paternal sister chromatids from the male nuclei. The membranes of these 2 pro nuclei dissolve to allow fusion of the genetic material (syngamy) and entry into the first mitosis and subsequent embryonic cell divisions (Webster & Schuh 2017).

In oocytes, sister chromatid cohesion is lost in an age-dependent manner, partially mediated by down regulation of Sgo2 and cohesin (Lister et al. 2010; Wassmann 2013). This is thought to be a major contributor to the ageing effect. While this clearly has a great effect on segregation errors, instead this study focuses on understanding the roles of fundamental cell cycle proteins in younger, healthy oocytes.

In contrast to meiosis in mouse oocytes, human female meiosis is extremely error prone, with an estimated 10-30% of fertilised eggs carrying an incorrect number of chromosomes (Hassold & Hunt 2001). 80-90% of these errors are thought to originate in meiosis I (Homer 2011). This loss or gain of chromosomes is known as aneuploidy and is the leading genetic cause of miscarriage and developmental defects in babies that survive to term (Hassold & Hunt 2001). On top of this, there is an exponential increase in the frequency of meiotic missegregation observed in women over the age of 35 (Hassold & Hunt 2001). Indeed woman who conceive over the age of 40 are 30% more likely to become pregnant with a trisomic child (Nagaoka et al. 2012). A problem confounded by the growing trend in the western world towards having children later in life, a societal shift that has led to a 70% increase in trisomic pregnancies over a 30 year period (Touati & Wassmann 2016). While the reasons why human oocytes have such a high frequency of segregation errors when compared to mouse oocytes remains largely elusive, the question can at least begin to be answered by looking at the different mechanisms they employ to assemble their MI spindle. However to begin with, I will introduce the mechanisms of mitotic spindle assembly.

1.2 Mechanisms of spindle assembly

In mitotic cells, two centrosomes positioned at opposite spindle poles form the basis for bipolar spindle establishment. Initially positioned together at the start of mitosis, having duplicated in G1/S phase, the centrosomes must separate and position themselves at opposite poles across the nucleus prior to nuclear envelope breakdown (NEBD) (Tanenbaum & Medema 2010). Following NEBD, microtubules emanating from each of these poles firstly capture and then accurately align chromosomes on the spindle. Microtubules then retract, mediating chromosome segregation in anaphase. The presence of more than two centrosomes within a cell, a situation often observed in cancer, is associated with multipolar spindle formation and an increase in segregation defects (Silkworth et al. 2009; Webster & Schuh 2017).

In contrast, spindle assembly in mouse oocytes is mediated by self-arranging microtubule organising centres (MTOCs) lacking any canonical centrosomes (Schuh & Ellenberg 2007). Early spindle assembly in mouse meiosis involves microtubule nucleation from around 80 newly-fragmented MTOCs, which form a large sphere throughout the ooplasm (Schuh & Ellenberg 2007; Clift et al. 2009). MTOCs then merge over time and the oocyte goes through multiple rounds of error correction, eventually forming the characteristic barrel-shaped bipolar spindle in the center of the oocyte (Schuh & Ellenberg 2007; Kitajima et al. 2011).

Even between closely related mammalian species, the mechanism of meiotic spindle assembly seems to be divergent. In human female meiosis, the mechanism of spindle assembly is different once again, taking place independently of both centrosomes and MTOCs (Holubcova et al. 2015). Instead, microtubule nucleation is mediated directly by the chromosomes themselves and the small GTPase, Ran (Holubcova et al. 2015). A T24N mutation that blocks the GTPase function on Ran causes a delayed and disorganised spindle assembly, yet does not prevent assembly altogether (Holubcova et al. 2015). Microtubules nucleating directly from chromosomes form an aster, which over a prolonged period of around 16 hours eventually develops into a stable bipolar spindle (Holubcova et al. 2015). This method of chromosome-mediated spindle assembly is intrinsically error-prone and may begin to explain why human oocytes have such a higher frequency of segregation defects when compared to mice.

1.3 The Spindle Checkpoint in mitosis and meiosis

1.3.1 The spindle checkpoint in mitosis

The spindle checkpoint detects microtubule occupancy of kinetochores; the multi-protein microtubule attachment site located near the centromere of each chromosome. A graded checkpoint response is stimulated at these sites of attachment, the strength of which is directly related to kinetochore occupancy by microtubules (Collin et al. 2013; Touati & Wassmann 2016). While chromosomes are aligning on the spindle, there are often errors made in attachments as the cell attempts to perfect bi-orientation. The response at sites of erroneous attachment is to stimulate the assembly of the mitotic checkpoint complex (MCC), a multi-protein complex that directly sequesters the APC/C co-activator, Cdc20 (Chao et al. 2012).

Central to MCC assembly is Aurora B, a key component of the Chromosomal Passenger Complex (CPC), enriched at incorrectly attached kinetochores (Musacchio 2015) and involved in a positive feedback loop with Mps1 where both proteins are recruited to unattached kinetochores (Santaguida et al. 2010). The process of MCC assembly begins when Mps1 phosphorylates MELT motifs within the kinetochore scaffold protein Knl1, allowing for recruitment of spindle checkpoint proteins Bub1, Bub3, BubR1, Mad1, Mad2 and Cdc20 (Musacchio 2015). The MCC, which comprises Bub3, BubR1, Mad2 and Cdc20 is then subsequently enriched in the cytoplasm and functions to inhibit APC/C through direct sequestration of both APC/C-bound and free Cdc20 (Di Fiore et al. 2016). Mechanisms of Cdc20 sequestration by the MCC are discussed in more detail in chapter 5.

1.3.2 The spindle checkpoint in meiosis

In meiosis, checkpoint proteins are present and are similarly recruited to unattached kinetochores (Sun & Kim 2012; Touati & Wassmann 2016). However, unlike in mitosis where a single unattached kinetochore is sufficient to prevent destruction of cyclin B1 (Lara-Gonzalez et al. 2012), MI is characterised by a lengthy period of cyclin B1 destruction which initiates several hours ahead of metaphase, before chromosome alignment is achieved. Furthermore, this destruction initiates prior to stabilisation of kinetochore attachments and while checkpoint proteins remain on kinetochores (Kitajima et al. 2011; Gui & Homer 2012; Lane et al. 2012; Lane & Jones 2014). These data together suggest that while all the same checkpoint proteins appear to be present in oocytes as mitotic cells, somehow the response elicited is less efficient. This has been previously suggested to be due to the large volume of

an oocyte in which a diffusible checkpoint signal may become much weaker. In the following chapters, I will dispute that the situation is this simple and present an alternative model for cyclin B1 and securin destruction.

While a number of studies have demonstrated that mouse oocytes with multiple attachment errors fail to block anaphase onset (LeMaire-Adkins et al. 1997; Yuan 2002; Hodges et al. 2005; Nagaoka et al. 2011), all were carried out in genetically abnormal strains. Ordinarily mouse oocytes repair these attachment errors and the rate of aneuploidy (1-2%) is much lower than in human oocytes (20-25%) (Hook 1985; Hassold & Hunt 2001), this could be at least partially explained by the fact a human oocyte is 50% larger in diameter than a mouse oocyte (Griffin et al. 2006). However, pig oocytes that are only marginally smaller than human oocytes experience aneuploidy rates of around 10%, much higher than mouse oocytes yet still clearly much lower than the human error rates (Hornak et al. 2011). Pig oocytes have a spindle assembly mechanism that bears resemblance to that of both mice and humans; mediated by self-organising MTOCs yet also chromosome-dependent (Miyano et al. 2007). Perhaps a combination of a chromosome-dependent spindle assembly mechanism in humans that favours segregation errors (Holubcova et al. 2015), combined with an inefficient checkpoint over the large volume of an oocyte can begin to address the high error rates in human oocytes.

Spindle assembly mechanisms, oocyte size and the ageing effect are all features of oocyte biology linked to the frequency of segregation defects in female meiosis, features vastly different to those presented by a normal mitosis. Since the same cell cycle proteins underpin and drive both meiotic and mitotic division, it seems reasonable to predict that the regulation of key cell cycle proteins will vary between mitosis and meiosis, adapted to a very different type of cell division. However, when compared to the depth and breadth of mitotic cell cycle studies, there are few independent, comparative cell cycle studies in mammalian female meiosis. In mouse oocytes, both cyclin B1 and securin are destroyed from late prometaphase while chromosomes are not aligned, yet this is not associated with an increase in divisional errors. From our understanding of how these proteins behave in mitosis, these observations are at complete odds with each other. In this thesis, I aim to expand upon our understanding of these key cell cycle mediators in mouse oocyte meiosis.

Chapter 2: Methods

2.1 Mouse oocyte collection and culture

Outbred four to eight week old female CD1 mice were purchased from Charles River and housed in the Comparative Biology Centre at Newcastle University. Germinal vesicle (GV) stage oocytes were collected from excised ovaries by shredding with a sterile 25-gauge needle. Cumulus cells were then mechanically stripped using hand pulled mouth pipettes, made by heating glass Pasteur pipettes over a Bunsen flame until soft. Pulling results in a fine, whisker-like shaft with an internal diameter just wider than that of an oocyte. All animals were handled in accordance with the ethics approved by the UK Home Office Animals (Scientific Procedures) Act 1986. For bench handling, microinjection and imaging experiments, oocytes were cultured on a heated stage at 37°C in M2 medium (Sigma) and where necessary, held in GV arrest until imaging by the addition of 30nM 3-isobutyl-1-methyl xanthine (IBMX; Sigma). M2 medium also contained penicillin G (0.06g/l) and streptomycin sulphate (0.05g/l). Prior to imaging, oocytes were kept in petri dishes in small drops of M2 medium covered with embryo-tested mineral oil (Sigma) to prevent evaporation. When not being handled, petri dishes were covered with tin foil lids to prevent unnecessary light exposure. Only oocytes that underwent GVBD with normal timings and had a diameter within 95-105% of the population average were used. Where necessary and at the times indicated, nocodazole (Sigma) was added to the media at a concentration of 150 nM, and the Mps1 inhibitor reversine (Sigma) at 100 nM (Kolano et al. 2012). SiR Hoechst was added to media at 250 nM, 30 minutes prior to imaging (Lukinavičius et al. 2015).

2.2 Plasmid constructs

Wild-type human cyclin B1 (NM_031966), securin (NM_001282382) and cyclin A2 (NM_001237) sequences were amplified from pre-existing gene targets within the lab. Wild-type Cks1 (EF026652) was amplified from pWZL Neo Myr Flag CKS1B, a gift from William Hahn & Jean Zhao (Boehm et al. 2007) (Addgene plasmid # 20461). Amplified products were then subcloned using the SLIC technique (detailed in section 2.3) into MDL9; a modified pRN3 vector that contains a 5 amino acid C-terminal linker (AGAQF) to Venus Fluorescent Protein (VFP). All mutations were made as detailed in section 2.4. The Cdk1 FRET sensor (Addgene plasmid #26064; a gift from Jonathan Pines; Gavet & Pines 2010) and the separase

biosensor (a gift from Jan van Deursen; Nam & van Deursen 2014) were both amplified and cloned into pRN3 vectors.

2.3 One-Step Sequence- and Ligation-Independent Cloning (SLIC)

The MDL9 or pRN3 vector was linearized by incubation with BglII (Promega) for 3 hours at 37 °C. The full digestion reaction was then run on a 1% agarose TAE w/EtBr gel. The 4kb digested vector was excised and extracted from the gel (GeneJET Gel Extraction Kit (Thermo Scientific)) and eluted in 10 mM Tris-HCl; pH 8.5. Inserts were amplified using primers designed to include a specific recognition site for BglII flanked on either side by a ≥15 bp extension homologous to the BglII-cut vector ends and a 10 bp insert-specific extension. This specifically creates 15 bp sequence length homologues to the vector. PCR reactions for SLIC were done using KOD polymerase (Merck), to give blunt-ended products. PCR products were then purified using a GeneJET PCR Purification Kit (Thermo Scientific), with elution in 10 mM Tris-HCl, pH 8.5. Concentrations of both vector and insert were measured on a NanoDrop 2000 UV-Vis Spectrophotometer to calculate a 1:3 vector to insert molar ratio. Vector and insert were then combined along with H_2O, BSA, NEB's buffer 2 and T4 DNA Polymerase (0.4 µl) and incubated for 2.5 minutes in a 22 °C water bath. This reaction takes advantage of the 3' to 5' endonuclease activity of T4 DNA polymerase, creating the complementary overhangs with which the vector and insert will anneal during a 10 minute incubation period on ice. Following this, the plasmids were transformed into competent E. Coli cells (NovaBlue Singles competent cells (Novagen)) and plated on Agar containing ampicillin. SLIC was carried out according to the protocol in (Jeong et al. 2012).

2.4 Mutagenesis by crossover PCR

Mutations and linked constructs were generated using multi-round arm extension crossover PCR. The first round for any given mutation construct involved two separate, 30-cycle DreamTaq (Thermo Fisher) PCR reactions, reactions A and B. Reaction A used the normal 5' SLIC primer designed as above with a 3' primer designed with homology to 15 bp either side of the desired site of mutagenesis. The point changes mutations were included in the sequence of the primer arm. Reaction B was the reverse, a 5' primer designed with homology to 15 bp either side of the site of mutagenesis, with the desired mutation in the primer sequence and a standard 3' SLIC primer. From reactions A and B, we get two PCR products, one running from the start of the sequence to 15 bp after the site of mutagenesis and one from 15 bp before

the site of mutagenesis to the end of the sequence, each containing the desired mutation. A third reaction is then carried out as a standard SLIC reaction, described in section 2.3, using only the 5' and 3' SLIC primers. However, rather than a wild-type gene template, instead the target is 0.5 µl of finished reaction A and 0.5 µl of finished reaction B. This allows for the homologous 30 bp mutation spanning regions of product A and B to anneal during the PCR reaction and assemble a full-length protein with the desired mutation.

2.5 Sequencing

Colonies selected from transformation plates were grown in LB broth in an oscillating (180 rpm) 37 °C incubator overnight. Plasmid DNA was then isolated using a GeneJET Plasmid Miniprep Kit (Thermo Scientific) and quantified by a NanoDrop Spectrophotometer. 5 µl samples (100 ng/µl) were sent to Eurofins UK for sequence analysis. Returned sequences were checked via nucleotide BLAST search (http://www.ncbi.nlm.nih.gov) for accuracy before cRNA preparation.

2.6 Preparation of cRNA and morpholino oligomers for microinjection

cRNA for microinjection was prepared using a T3 mMESSAGE mMACHINE kit (Ambion Inc.). Following SLIC and sequence confirmation, approximately 1 µg of plasmid DNA was digested with SfiI for 5 hours at 50 °C. Once the reaction was complete, proteinase K was added for a final hour at 50 °C to remove any protein contamination. The reaction mix was then phenol/chloroform extracted, and followed by the addition of Pellet Paint (Merck) and $1/10^{th}$ volume of Na Acetate, pH 5.5, precipitated in 100% EtOH for >1 hour at -80 °C. The DNA pellet was then washed and resuspended in nuclease-free H_20, all of which was used in a transcription reaction containing RNA polymerase enzyme mix, ribonucleotides and reaction buffer according to the manufacturer's protocol. This reaction mix was incubated for 2 hours at 37 °C, with addition of DNase for the final 15 minutes. Overnight lithium chloride precipitation at -20 °C followed by centrifugation extracted the cRNA from solution. The final cRNA pellet was then washed and resuspended in nuclease-free H_20 and aliquots were stored at -20 °C for later use. Maximal stability was conferred on all cRNA constructs by the presence of a 5' globin UTR upstream and both 3' UTR and poly (A)-encoding tracts downstream of the gene.

Morpholino antisense oligomers (MO; Gene Tools) were used to knockdown gene expression. MOs were designed to recognize the 5' UTR of APC3 and Cdc20. As per the manufacturer's instructions, all MOs were stored at room temperature then heated for 5 minutes at 65 °C prior to use to resolubilise the oligos. MOs were then used at a micropipette concentration of 1 mM.

2.7 Microinjection and imaging

Oocyte microinjection of MOs and cRNA constructs were carried out on the 37 °C heated stage (Intracel) of an inverted epifluorescence microscope (Olympus; 1X71) in a chamber containing 1 ml of M2 media covered with mineral oil to prevent evaporation. A pre-fabricated holding pipette with a 30° bend (Hunter Scientific) was connected to a syringe (IM-5B, Narishige, Japan) filled with mineral oil, allowing for a fine hydraulically driven inward and outward flow of oil to position and hold oocytes during injection. The holding pipette was positioned centrally by eye to the base of the chamber using a three-way coarse manipulator (MMN-1, Narishige, Japan).

Microinjection micropipettes were made from filamented borosilicate glass capillaries, outer diameter of 1.5 mm and inner diameter of 0.86 mm (Harvard Apparatus Ltd.). Microinjection needles were made using a micropipette puller (Model P-97, Sutter Instruments, California, USA). Freshly pulled needles were then broken by gently brushing through cotton wool and checked for size and suitability using a bench top stereomicroscope (Nikon Optiphot Pol) at 10x magnification.

Microinjection pipettes were then loaded with cRNA or MO using a glass Microliter syringe (Hamilton) and microloader tip (Eppendorf). Loaded microinjection pipettes were fitted into a microelectrode holder prefilled with 120 mM KCl in 10 mM HEPES, pH 7.4 and connected to an electrometer (Electro 705, World Precision Instruments). The microelectrode holder was attached to a Pneumatic PicoPump (PV830, World Precision Instruments) via plastic tubing. This apparatus was manipulated using both a three-way coarse manipulator (MMN-1, Narishige, Japan) and a three-axis oil hydraulic micromanipulator (MMO-203, Narishige, Japan). Micropipettes were positioned just above the egg and then pushed through the zona pellucida. A brief pulse of negative capacitance overcompensation provided by the 'Tickler' function on the Electro 705 electrometer provides a momentary oscillation assisting passage into the oolemma. The cRNA or MO was then injected by a brief pulse of compressed air to the back of the micropipette provided by the Pneumatic PicoPump. This procedure ensures a

high rate of survival, typically >90%. The final volume of injection was estimated by the diameter of displaced ooplasm and was typically between 0.1-0.3% of total volume.

Images were captured on an Olympus IX71 inverted epifluorescence microscope using a CCD camera (Micromax, Sony Interline chip, Princeton Instruments) and analysed using MetaFluor software (Molecular Devices). All experiments were performed at 37 °C. To generate the resulting fluorescent protein profiles, bright-field and fluorescence images were recorded at 10 minute intervals.

2.8 Confocal microscopy of separase biosensor

Separase biosensor-injected oocytes were imaged on a Nikon A1R confocal laser microscope. Imaging began at 5 hours post GVBD to minimise oocyte laser exposure. Oocytes were imaged at 10 minute intervals over a 6 hour period in a temperature-controlled, humidified chamber set at 37 °C. Bright-field and fluorescent images were recorded in NIS-Elements (Nikon) and processed in Fiji (Schindelin et al. 2012). All oocytes extruded polar bodies.

2.9 Western blots

Mitotic U2OS cells and MEFs were prepared by lysis in Laemmli buffer following mechanical shake off of metaphase cells after an 8 hour incubation in 100 nM nocodazole. Oocytes were collected 5.5 hours after GVBD ± 15 min and lysed in Laemmli buffer. The cyclin B1:Cdk1 purified complex was purchased from Thermo Fisher Scientific; PV3292. Protein samples were boiled for 5 minutes at 95 °C, loaded into the wells of a Bis-Tris NuPAGE gel (Thermo Fisher), then fractioned at 180 V for 1 hour in an XCell SureLock Mini-Cell Electrophoresis tank (Invitrogen) attached to a PowerPac HC High Current power supply (BioRad). Gels were run in MOPS running buffer (Thermo Fisher). A multicolour protein ladder (Spectra, Thermo Fisher) was loaded into the first lane as a size marker. Following electrophoresis, gels were removed from casing and transferred onto a polyvinylidene fluoride (PVDF) membrane at 30 V overnight in a Mini Trans-Blot tank (Bio-Rad) attached to a PowerPac HC High Current power supply (BioRad). Transfer buffer contained 25mM Tris buffer, 192mM glycine, 20% methanol. PVDF membrane required pre-wetting in methanol for 30 seconds followed by incubation for 10 minutes in transfer buffer. Following transfer, membranes were blocked in 5% non-fat dry milk (Bio-Rad) in phosphate buffered saline 0.05% Tween 20 (PBST) for 1 hour at room temperature before addition of

primary antibodies. For cyclin B1, immunoblots were incubated at RT for 2 hours with anti-cyclin B1 (Abcam ab72) at 1:250. For Cdk1, immunoblots were incubated at RT for 2 hours with anti-Cdk1/Cdk2 (Santa Cruz sc-53219) at 1:200. After the overnight incubation, membranes were washed in PBST (3 x 10 minutes changing wash solution in between) then incubated with anti–mouse IgG (7076P2; Cell Signalling) horseradish peroxidase (HRP)-linked secondary antibody for 1 hour at RT in 2.5% non-fat dry milk in PBST. Membranes were given a final wash step in PBST (2 x 10 minutes) followed by a 10 minute wash in phosphate buffered saline (PBS) before a 5 minute incubation in ECL Select (RPN2132; GE Healthcare) to detect protein-bound HRP-labelled secondary antibodies. Membranes were then exposed to Hyperfilm x-ray film (Amersham Biosciences) and developed using a SRX101 film processor (Konica). The exposure time depended on the strength of the signal.

2.10 Data analysis

Real-time destruction profiles were recorded in MetaFluor (Molecular Devices) and data was automatically logged in Excel. By taking an average VFP intensity reading from a defined region of interest around the oocyte, these were plotted over time and aligned at PB1 extrusion unless otherwise stated. Average cleavage profiles for separase biosensor experiments were produced in Fiji (Schindelin et al. 2012) by first creating a clipping mask to the DNA using the far red signal from Sir Hoechst treatment. The GFP and mCherry intensity readings from the clipping mask were then plotted over time and aligned at PB1 extrusion and the GFP/RFP ratio was calculated. Statistics were exported from MetaFluor and Fiji into Excel (version 14.4.8, Microsoft) where all destruction traces were produced. Typically when only two constructs were being compared, both the average traces and individual traces were shown, whereas when 3 or more constructs were being compared, for clarity, only the average traces are shown but with error bars = +/- SEM.

2.11 Other techniques

Molecular structure images were generated using the PyMOL Molecular Graphics System, version 1.3 Schrödinger, LLC. Sequence conservation alignments were made by importing protein sequences from Uniprot and aligning in Jalview, version 15.0, (Waterhouse et al. 2009). All figures were prepared in Adobe Illustrator CC, version 17.1.0.

Chapter 3: A second destruction motif in the N-terminal helix of cyclin B1 mediates late prometaphase destruction in mouse oocytes.

3.1 Introduction

Cdk1 is the only cyclin-dependent kinase that is essential to the eukaryotic cell cycle (Santamaría et al. 2007). Throughout early mitosis, Cdk1 is activated by its binding partner cyclin B1. Cyclin B1 must be maintained at a level sufficient to generate enough cyclin B1:Cdk1 activity ("Cdk1 activity") to drive the early stages of cell division (Gavet & Pines 2010). By monitoring the status of kinetochore microtubule attachments, spindle checkpoint proteins safeguard cyclin B1 levels, preventing its destruction, thereby inhibiting anaphase until all chromosomes have congressed and their kinetochores have established stable attachments (Lara-Gonzalez et al. 2012). Thereafter, a sharp drop in Cdk1 activity via cyclin B1 destruction is equally important to drive the events of anaphase and cytokinesis (Sullivan & Morgan 2007).

The goal of the spindle checkpoint is to attenuate the activity of the anaphase promoting complex or cyclosome (APC/C), an E3 ubiquitin ligase which directs the degradation of a number of cell cycle proteins. To ensure accurate passage through all stages of chromosome alignment and segregation, the APC/C must process its substrates in strict order, an order largely achieved via distinct substrate degradation motifs. The most common of these motifs is the classic destruction motif, the D-Box, that directs cyclin B1 destruction in metaphase (Glotzer et al. 1991).

In the absence of checkpoint activity, the APC/C and its co-activator Cdc20 form a bipartite co-receptor for D-Box docking (He et al. 2013). This allows cyclin B1 to be ubiquitinated on several lysine residues and to be delivered to the 26S proteasome-mediated degradation (Yamano et al. 1998). Prior to chromosome alignment, each unattached kinetochore generates a checkpoint signal which is sufficient to prevent Cdc20 from binding to the D-box of metaphase substrates (Lara-Gonzalez et al. 2012). Chromosome misalignment in mitosis therefore strongly inhibits cyclin B1 destruction to prevent premature chromosome segregation and the possibility of aneuploid daughter cells. Metaphase then coincides with the initiation of cyclin B1 destruction.

Female mammalian meiosis is also driven by Cdk1 activity (Ledan et al. 2001) and governed by the same checkpoint as mitosis (Gorbsky 2015). Yet, unlike mitosis, meiosis I (MI) is characterised by a lengthy period of cyclin B1 destruction which initiates several hours ahead of metaphase, before chromosome alignment is achieved, prior to the stabilisation of kinetochore attachments, and while checkpoint proteins remain on kinetochores (Brunet et al. 1999; Davydenko et al. 2013; Gui & Homer 2012; Kitajima et al. 2011; Lane et al. 2012; Lane & Jones 2014; Nagaoka et al. 2011; Sebestova et al. 2012). Indeed, at the initiation of cyclin B1 destruction, nearly half of all mouse oocytes have chromosomes not located near the spindle equator (Lane et al. 2012).

Surprisingly however, during this prolonged period of cyclin B1 destruction, the vast majority of mouse oocytes continue to perfect chromosome alignment and undergo a division which produces a euploid egg. Indeed the rate of aneuploidy observed in fertilised mouse eggs is only 1-2% (Bond & Chandley 1983), a figure far lower than the estimated error rate of 20-25% in human eggs (Hassold & Hunt 2001). A key puzzle, therefore, is how cyclin B1 evades the spindle checkpoint in mouse oocytes, and why the early loss of cyclin B1 does not negatively impact oocyte competency.

3.2 Results

3.2.1 Cyclin B1 levels are in excess and do not report Cdk1 activity in MI mouse oocytes.

In contrast to mitotic cells where Cdk1 protein levels are in excess of cyclin B1, we find that this balance is reversed in prometaphase I mouse oocytes, a finding also reported in prophase I mouse oocytes (Kanatsu-Shinohara et al. 2000). Mass amounts of cyclin B1 and Cdk1 protein were initially determined in a range of known numbers of mitotically enriched U2OS cells by immunoblotting alongside known masses of a purified cyclin B1:Cdk1 complex (Fig. 3.1A-C). The average mass of cyclin B1 and Cdk1 per 1000 U2OS cells was calculated to be 0.68ng and 0.4ng respectively. Using molecular weights based on the amino acid sequences, molar masses were calculated demonstrating the molar ratio of cyclin B1:Cdk1 in mitotically enriched U20S to be approximately 1:1.

Mass amounts of cyclin B1 and Cdk1 protein were then determined in late prometaphase I oocytes (5.5 hours post GVBD) by immunoblotting alongside a range of known numbers of U2OS cells (Fig. 3.1D-E). The average mass of cyclin B1 per single oocyte was calculated to be equal to that of 16.3 U2OS cells or 11.09 pg. The average mass of Cdk1 per single oocyte was calculated to be equal to 2.7 U2OS cells or 1.09 pg. Molar amounts were then determined, generating a ratio of approximately 6:1 cyclin B1:Cdk1 in late prometaphase I mouse oocytes. Interestingly in mouse embryonic fibroblasts (MEFs), Cdk1 is once again in excess (Fig. 3.1D). This suggests the cyclin B1 excess observed in meiosis is quickly lost by early mitotic divisions. Consequently, though exogenous fluorescently-tagged cyclin B1 reports changes in Cdk1 activity during mitosis (as confirmed by a Cdk1 activity FRET biosensor (Gavet & Pines 2010)), we reasoned that early cyclin B1 destruction in mouse oocytes might instead reflect the proteolysis of free cyclin B1 rather than Cdk1-bound cyclin B1.

Mouse oocytes were microinjected with cRNA encoding the Cdk1 FRET biosensor then imaged at 10 minute intervals from prophase to anaphase I. Average fluorescence intensity readings were taken from a defined region of interest around each oocyte, plotted over time and aligned using the first polar body (PB1) extrusion as a reference point.

Indeed, after validating the Cdk1 FRET biosensor for its use in oocytes, we find that Cdk1 activity is stable during the first ~1.5 hours of cyclin B1 destruction, only declining in the final hour before polar body (PB1) extrusion (Fig. 3.2C). Fluorescent cyclin B1 levels

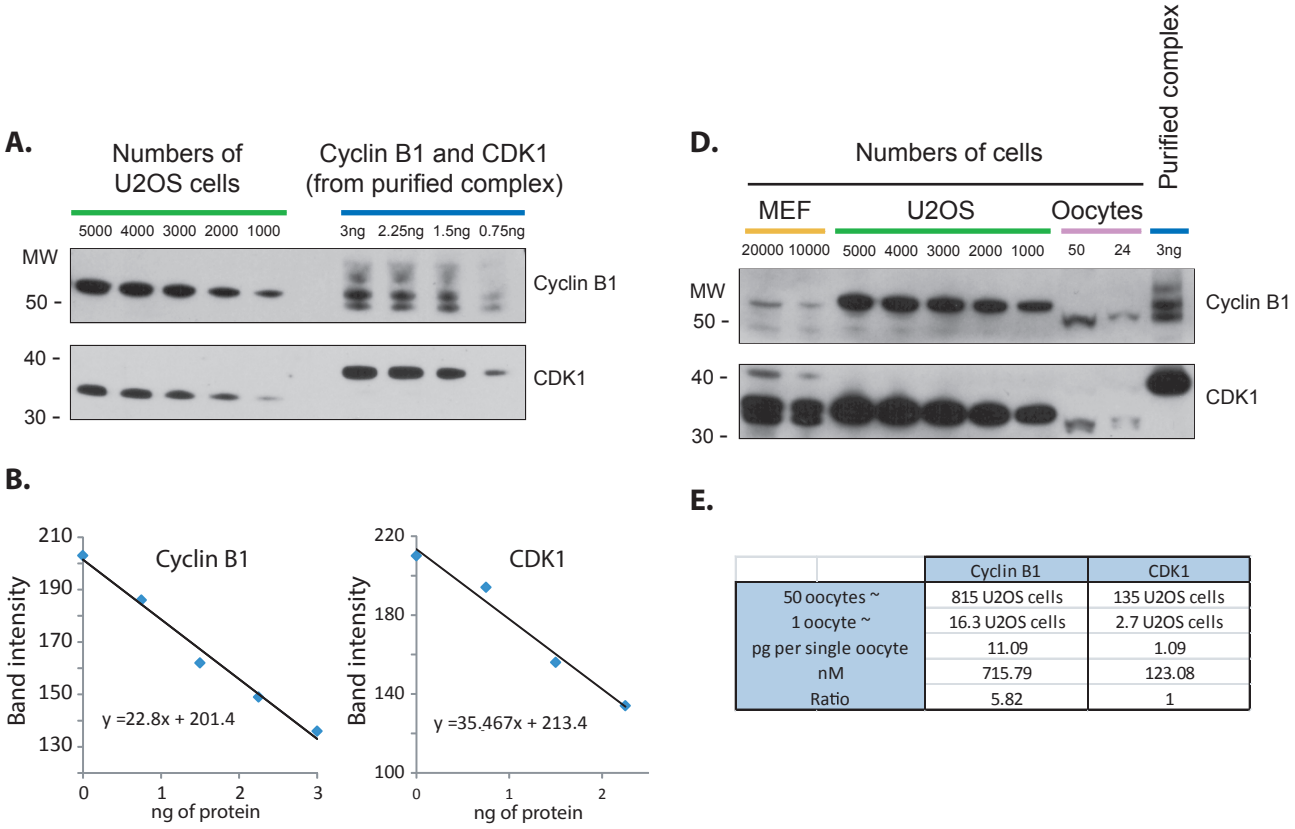

U2OS cells	CDK1 band intensity	CDK1 in 1000 cells	Cyclin B1 band intensity	Cyclin B1 in 1000 cells
1000	203	*	185	0.72
2000	183	0.42	171	0.67
3000	171	0.40	156	0.66
4000	158	0.39	147	0.66
Average per 1000 cells		= 0.40 ng		= 0.68 ng

	Cyclin B1	CDK1
50 oocytes ~	815 U2OS cells	135 U2OS cells
1 oocyte ~	16.3 U2OS cells	2.7 U2OS cells
pg per single oocyte	11.09	1.09
nM	715.79	123.08
Ratio	5.82	1

Figure 3.1. Quantification of cyclin B1 and CDK1 in mouse oocytes 5.5 h post GVBD using a 1:1 cyclin B1:CDK1 protein complex. (A) Western blot of known amounts of cyclin B1 and CDK1 recombinant protein (purified complex) alongside known numbers of mitotic U2OS cells to quantify cyclin B1 and CDK1 protein bands in U2OS cells (cell numbers indicated above). **(B)** Band densities of 'purified complex' lanes in part 'A' plotted relative to protein amount in ng. **(C)** Calculated amounts of cyclin B1 and CDK1 in 1000 U2OS cells using U2OS lane band densities in part 'A' and the equation of the line generated in part 'B'. **(D)** Western blot of mitotic mouse embryonic fibroblasts (MEFs), U2OS cells, oocytes collected 5.5 hours post GVBD and 1.5 ng of cyclin B1 + 1.5 ng of CDK1 recombinant protein (cell numbers indicated above). Note the difference in the balance of cyclin B1 and CDK1 in the mitotic cycles of MEFs, here CDK1 is in excess. **(E)** Using the same strategy as in 'B' and 'C', cyclin B1 and CDK1 band densities from part 'D' were used to relate cyclin B1 and CDK1 protein levels in oocytes to an equivalent number of U2OS cells. From this cyclin B1 and CDK1 protein amounts were calculated per oocyte. We calculate the ratio of cyclin B1:CDK1 to be approximately 6:1.

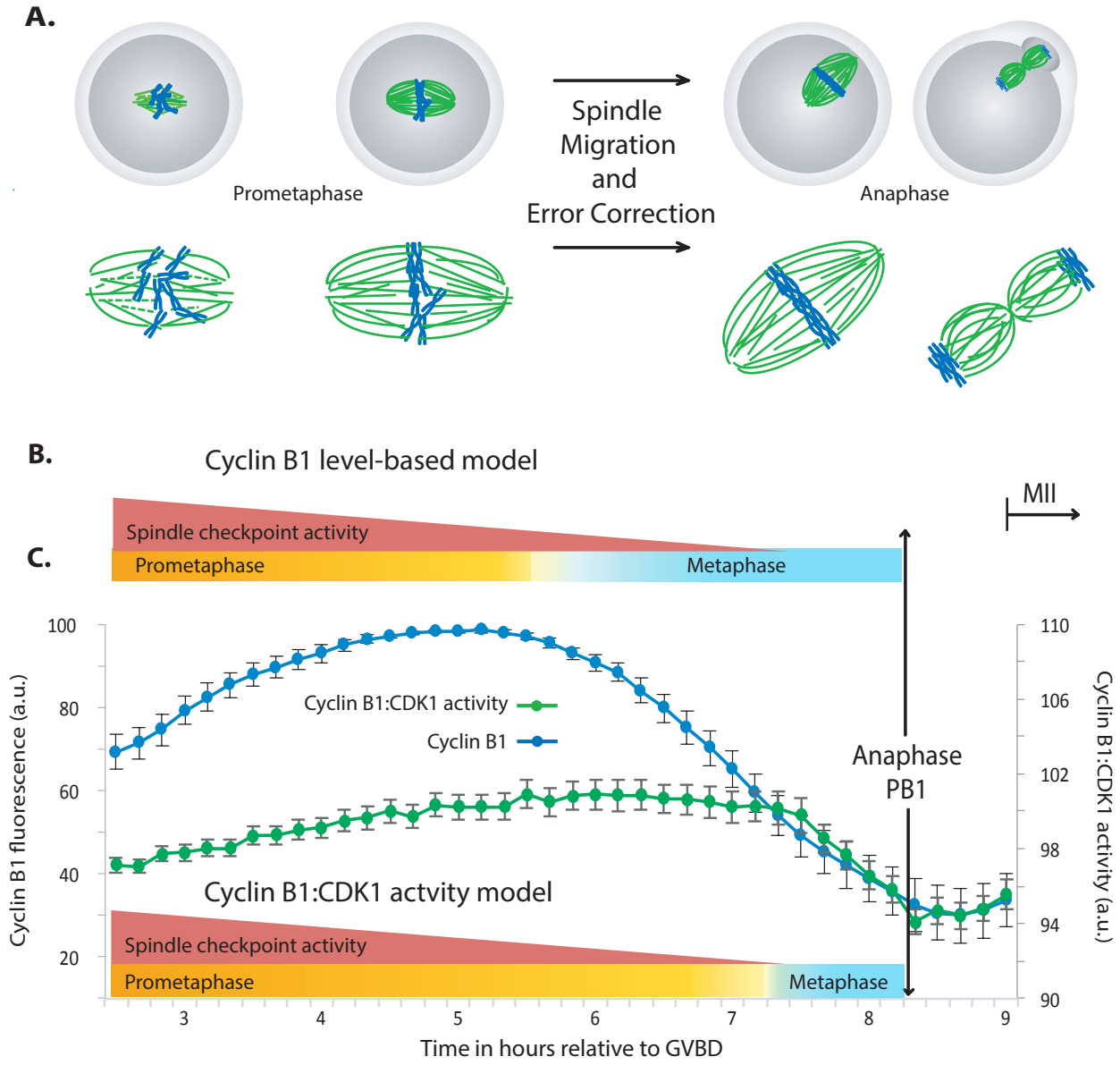

Figure 3.2. Cyclin B1 levels do not reflect CDK1 activity in MI mouse oocytes. (A) MI spindle assembly, chromosome alignment and PB1 extrusion. Homologous chromosome pairs (blue) align on the spindle apparatus (green). **(B)** Stages of MI based on the timing of cyclin B1 destruction. Spindle checkpoint activity (red bar), prometaphase (yellow bar) and metaphase (blue bar) are shown. **(C)** Levels of cyclin B1-Venus (blue trace, n=16 oocytes, means ± SEM) alongside CDK1 activity determined using a FRET biosensor (green trace, n=72). Retimed stages of MI based on the time of CDK1 activity loss are also shown (colours as in B).

therefore misinform our view of MI progression. If prometaphase and metaphase are timed in relation to the loss of Cdk1 activity (Fig. 4.2C), rather than the initiation of cyclin B1 degradation (Fig. 3.2B), a clear picture of MI emerges. Metaphase, during which Cdk1 activity declines, now coincides with the time at which stable end-on kinetochore-microtubule attachments are formed and checkpoint proteins are maximally depleted from kinetochores (Kitajima et al. 2011; Lane et al. 2012). However, this does not explain why cyclin B1 levels decline in prometaphase.

3.2.2 D-box only recognition is not sufficient for a normal cyclin B1 destruction profile in mouse oocyte meiosis.

Given that, in oocytes, two pools of cyclin B1 exist (Cdk1-bound and non-Cdk1-bound), and that the majority of cyclin B1 is lost before a decline in Cdk1 activity, we wanted to determine whether free cyclin B1 is destroyed in preference to Cdk1-bound cyclin B1. Initially we tested two fluorescent cyclin B1 reporters, a Y170A mutant of full-length cyclin B1 unable to bind to Cdk1 (Y170A; Bentley et al 2007) and the N-terminal 90 amino acids of cyclin B1 (N90; Fig. 3.3A) . Y170A was used as a marker to represent free cyclin B1 while N90 was used to represent the tail of cyclin B1 that remains accessible when the protein is in complex with Cdk1 (Brown et al. 2015). Both constructs contain the D-box sequence and neighbouring lysine residues known to be necessary and sufficient for recognition by APC/C-Cdc20 and subsequent proteolysis in mitosis (Pines 2011; Yamano et al. 1998), however N90 critically lacks other well conserved regions of the protein, namely the N-terminal helix and cyclin box/fold regions of the protein.

When cRNA encoding these proteins is microinjected into oocytes we find that while the destruction profile of Y170A is similar to that of wild-type (WT) cyclin B1, N90 is not destroyed until much later (~80 minutes) and concurrently with the loss of Cdk1 activity (Fig. 3.3B). The difference seen in protein destruction kinetics is not an artefact of contrasting levels of exogenous protein or as a result of differences in translation efficiency. Overexpression levels are matched for each protein and no higher than 15% endogenous. Furthermore, the use of cycloheximide (CHX) to block translation does not change the order of destruction (data not shown). This raises the possibility that an additional binding motif or degron exists in cyclin B1 between residues 90-433, which promotes its earlier degradation.

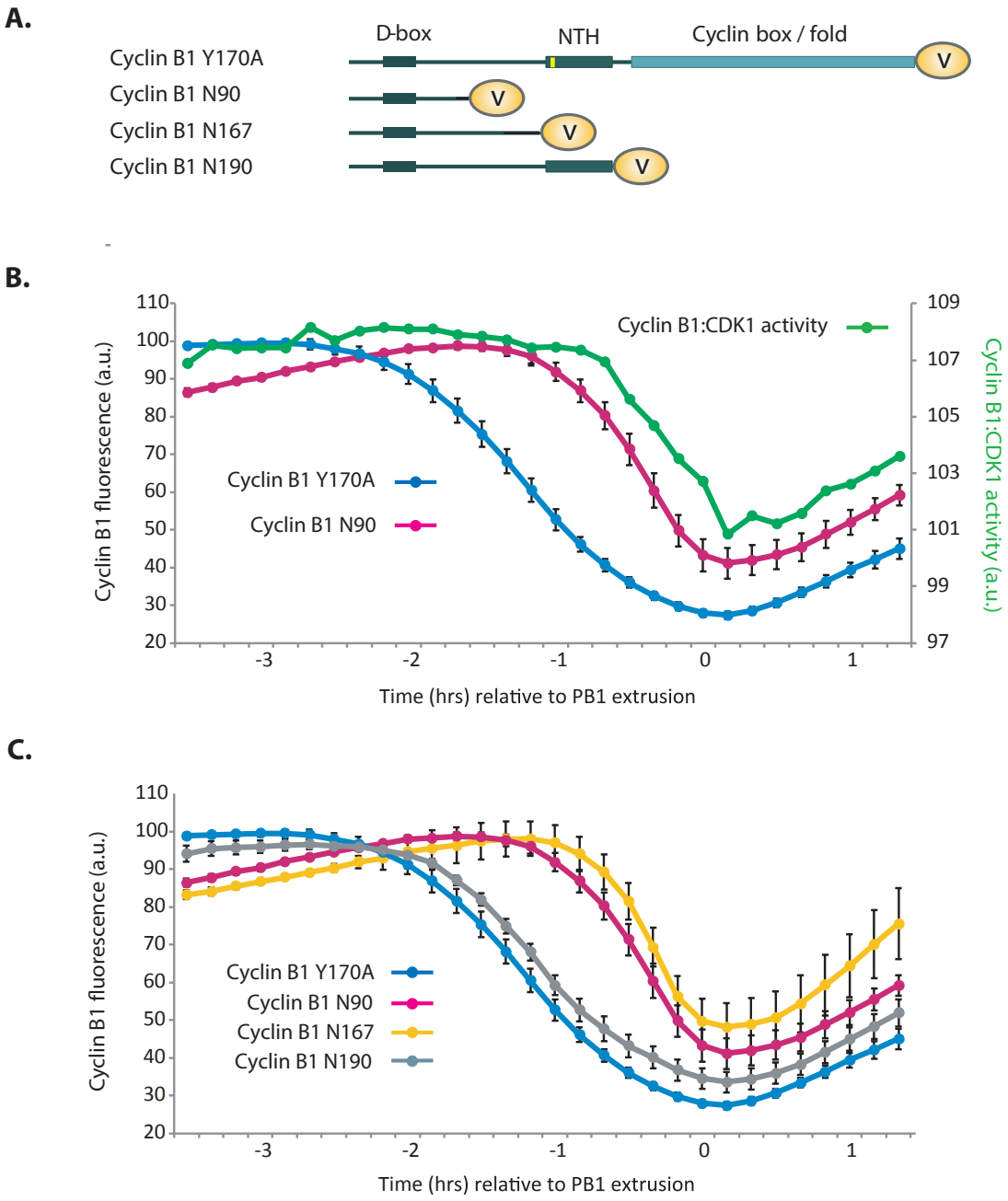

Figure 3.3. D-box only recognition is not sufficient for a normal cyclin B1 destruction profile. **(A)** Schematic of Venus-tagged cyclin B1 Y170A, a non-CDK1-binding mutant and cyclin B1 N90 constructs. **(B)** Levels of Venus-tagged cyclin B1 Y170A (n=32) and cyclin B1 N90 (n=34) alongside CDK1 activity (n=72, secondary axis) during MI. **(C)** Levels of Venus-tagged cyclin B1 Y170 (n=32); N90 (n=34); N167 (n=38) and N190 (n=38) during MI. Traces are aligned to the first polar body extrusion (PB1). Error bars = SEM throughout.

3.2.3 A second destruction motif exists within the N-terminal helix (NTH) of cyclin B1.

To test if a second destruction motif exists within cyclin B1, one that facilitates its prometaphase destruction, we made the following stepwise extensions to the C-terminus of N90; N146, N167 and N190. We found that a destruction profile resembling that of full-length Y170A was recovered between residues 167 and 190 (Fig. 3.3C). Between residues 167 and 190 lies the N-terminal helix (NTH) of cyclin B1 (residues 170-196, Fig. 3.4D), an integral part of the Cdk1 binding interface (Brown et al. 2015). Coupling the NTH to N90 (N90+NTH) is sufficient to convert N90 from a late substrate to a much earlier WT-like destruction target (Fig. 3.4B), thus confirming that the region required for early degradation lies completely within the NTH.

Alanine mutagenesis of Y170A revealed residues within the NTH that are essential for early cyclin B1 destruction (only the final mutant is shown; figs 3.4A and 3.4C). We suggest that 7 residues, DIY (173-175) and LRQL (178-181), constitute a novel motif (hereafter named the PM-motif) able to direct APC/C-mediated proteolysis of free cyclin B1 in late prometaphase. Indeed, a PM motif mutant lacking these 7 residues (Y170A lacking the PM motif), B1 PM mutant is destroyed over the same late time period as N90 (Figs 3.4C and 3.4E). Again this order of destruction is maintained where Y170A and PM mutant expressing oocytes are matured in the presence of CHX.

3.2.4 Masking of the NTH region of cyclin B1 on Cdk1 binding.

The crystal structure of the human cyclin B1:Cdk1 in complex with Cks2 (Brown et al. 2015) supports our hypothesis that the PM motif would be masked when cyclin B1 is bound to Cdk1. The NTH forms a crucial part of the interaction, sitting deep in the interface between cyclin B1 and Cdk1 (Fig. 3.5A), making it likely that Cdk1 binding would obscure the PM-motif, leaving only the D-box of cyclin B1 accessible. We propose the following model; unbound excess cyclin B1 is targeted preferentially in late prometaphase via its PM motif; Cdk1-bound cyclin B1 is then destroyed later, in metaphase, via its D-box, thus protecting Cdk1 activity.

Figure 3.4

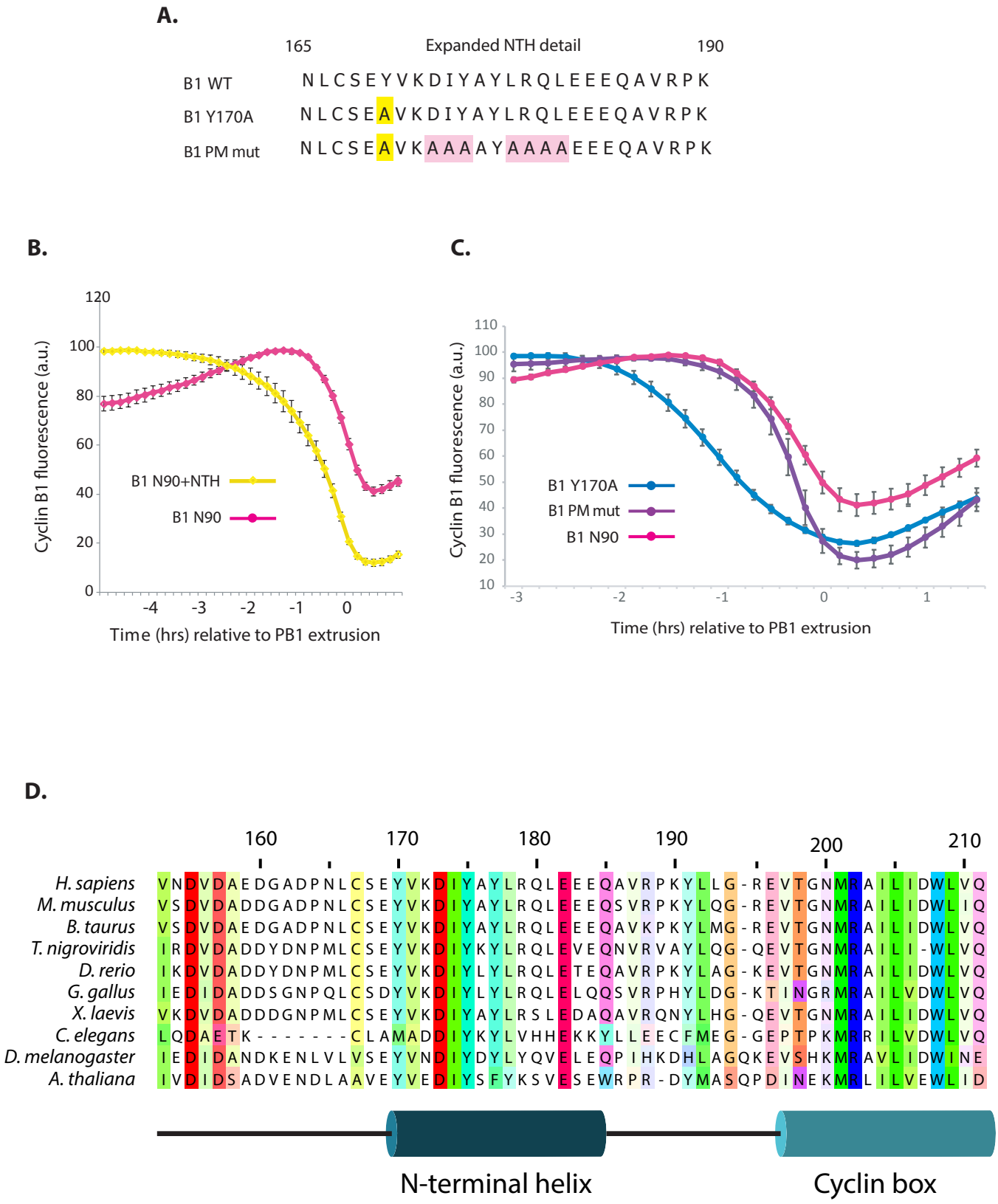
A.
165
Expanded NTH detail
190
B1 WT
N L C S E Y V K D I Y A Y L R Q L E E E Q A V R P K
B1 Y170A
N L C S E A V K D I Y A Y L R Q L E E E Q A V R P K
B1 PM mut
N L C S E A V K A A A A Y A A A A E E E Q A V R P K
B.
Cyclin B1 fluorescence (a.u.)
B1 N90+NTH
B1 N90
Time (hrs) relative to PB1 extrusion
C.
Cyclin B1 fluorescence (a.u.)
B1 Y170A
B1 PM mut
B1 N90
Time (hrs) relative to PB1 extrusion
D.
160
170
180
190
200
210
H. sapiens V N D V D A E D G A D P N L C S E Y V K D I Y A Y L R Q L E E E Q A V R P K Y L L G - R E V T G N M R A I L I D W L V Q
M. musculus V S D V D A D D G A D P N L C S E Y V K D I Y A Y L R Q L E E E Q S V R P K Y L Q G - R E V T G N M R A I L I D W L I Q
B. taurus V S D V D A E D G A D P N L C S E Y V K D I Y A Y L R Q L E E E Q A V K P K Y L M G - R E V T G N M R A I L I D W L V Q
T. nigroviridis I R D V D A D D Y D N P M L C S E Y V K D I Y K Y L R Q L E V E Q N V R V A Y L Q G - Q E V T G N M R A I L I - W L V Q
D. rerio I K D V D A D D Y D N P M L C S E Y V K D I Y L Y L R Q L E T E Q A V R P K Y L A G - K E V T G N M R A I L I D W L V Q
G. gallus I E D I D A D D S G N P Q L C S D Y V K D I Y L Y L R Q L E L Q Q S V R P H Y L D G - K T I N G R M R A I L V D W L V Q
X. laevis V K D V D A D D D G N P M L C S E Y V K D I Y A Y L R S L E D A Q A V R Q N Y L H G - Q E V T G N M R A I L I D W L V Q
C. elegans L Q D A E T K - - - - - - - C L A M A D D I Y K Y L V H H E K K Y L L E E C F M E G - G E P T P K M R R I L V D W L V Q
D. melanogaster I E D I D A N D K E N L V L V S E Y V N D I Y D Y L Y Q V E L E Q P I H K D H L A G Q K E V S H K M R A V L I D W I N E
A. thaliana I V D I D S A D V E N D L A A V E Y V E D I Y S F Y K S V E S E W R P R - D Y M A S Q P D I N E K M R L I L V E W L I D
N-terminal helix
Cyclin box

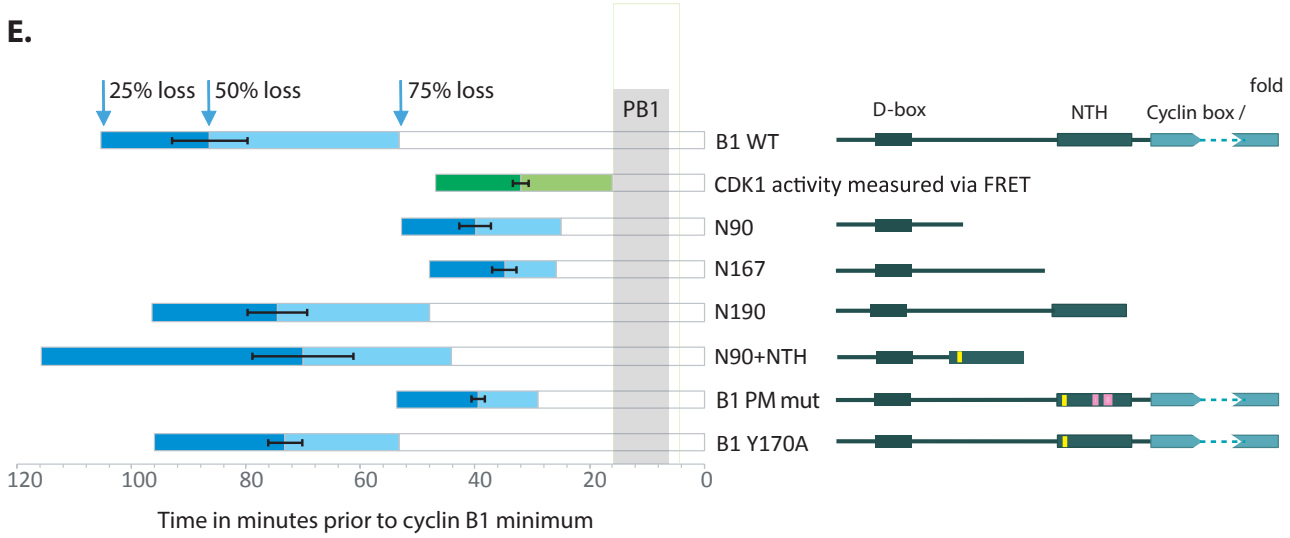

Figure 3.4. A second destruction motif exists within the NTH of cyclin B1. (A) NTH sequence detail. WT, Y170A and PM mutant (B1 PMmut) sequences are shown. **(B)** Destruction profiles of B1 N90+NTH (yellow, n=22) and B1 N90 (pink, n=34). **(C)** B1 N90, Y170A and PM mut destruction profiles. **(D)** Sequence alignment of NTH-containing region in cyclin B1 orthologs. **(E)** Destruction of Venus tagged cyclin B1 truncations and mutants. Other than wild type cyclin B1 (B1 WT), all lack the ability to bind CDK1 and therefore act as reporters of destruction timing without perturbing endogenous CDK1 activity. Schematic representations of cyclin B1 constructs are shown down the right hand side (cyclin box / fold not to scale) while the bars to the left indicate destruction timings. The length of each bar indicates the number of minutes ahead of the minimum fluorescence/maximum destruction point (time 0). The open, white bars indicate the point at which 75% of the destruction has taken place. The light blue extension to this bar indicates the point at which 50% of the destruction has taken place (error bars = SEM), followed by a dark blue extension indicating the point at which 25% of the destruction has taken place. Similarly, CDK1 activity loss, as measured via FRET, is shown in green. The period over which PB1 extrusions occur is shaded in grey.

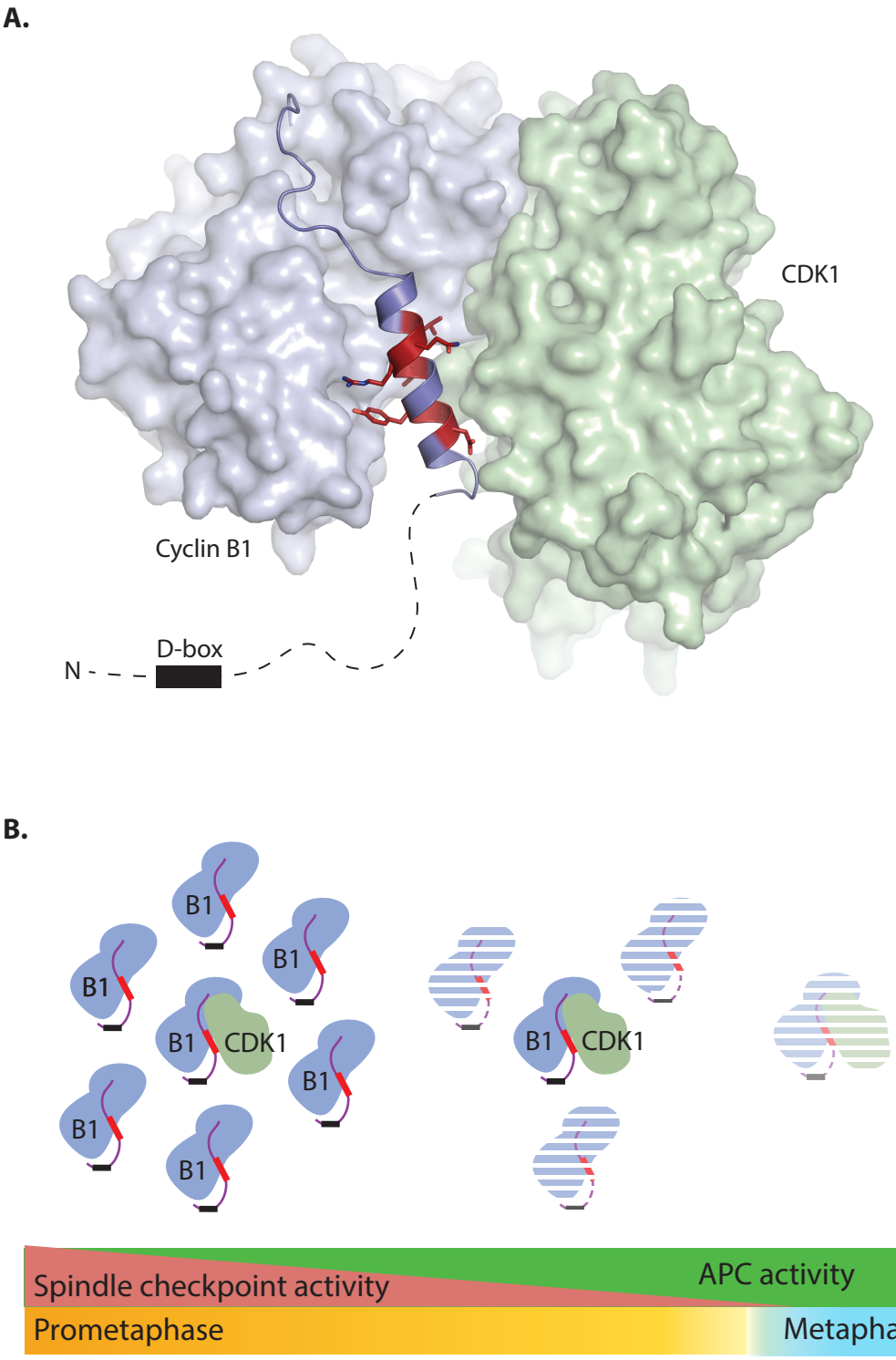

Figure 3.5. Masking of the NTH region of cyclin B1 on CDK1 binding. (A) Surface representation of cyclin B1:CDK1 from the crystal structure of its complex with CKS2 (Brown et al., 2015) (pdb accession 4Y72). The NTH and preceding loop are excluded from the surface and their backbones are instead shown, with residues 173-DIY-175 and 178-LRQL-181 highlighted in red. The flexible N-terminal extension harbouring the D-box is illustrated. (B) Model of cyclin B1 degradation in mouse oocytes as spindle checkpoint activity declines and APC/C-Cdc20 activity increases.

3.3 Discussion

An estimated 20-25% of human oocytes missegregate their chromosomes, making aneuploidy the number one genetic cause of miscarriages and birth defects (Hassold & Hunt 2001). 80-90% of these segregation errors are thought to occur in MI (Homer 2011). The seemingly precocious destruction of cyclin B1 observed in mouse oocyte MI has previously been suggested to contribute to aneuploidy and evidence of an oocyte-specific defect in the spindle checkpoint which allows the cell cycle to proceed despite chromosome alignment errors. However, mouse oocytes are rarely aneuploid. Misaligned chromosome pairs are a common feature of mouse oocytes during the initial period of cyclin B1 destruction, yet almost all achieve biorientation before anaphase onset (Lane et al. 2012). Mouse oocytes continue to perfect chromosome alignment and undergo a division yielding a euploid egg. It therefore became of primary interest how cyclin B1is able to bypass the spindle checkpoint in mouse oocytes, and why its early degradation does not negatively affect oocyte competency.

In stark contrast to the situation in mitosis in which Cdk1 is present in excess over cyclin B1 (Arooz et al. 2000), we show that in oocytes it is instead cyclin B1 that is present in large excess. By quantifying the ratio of cyclin B1:Cdk1 in prometaphase I mouse oocytes we find cyclin B1 to be approximately 6-fold in excess of Cdk1. This excess of cyclin B1 is lost by early mitotic divisions, evident in the dramatic switch back to a large Cdk1 excess observed in early embryonic mitosis (MEFs). This therefore suggests a meiosis specific translation program that generates a large excess of cyclin B1. How cyclin B1:Cdk1 ratio evolves through MII and the first embryonic divisions remains a point of future interest.

What is clear is that early cyclin B1 degradation is not associated with a decrease in Cdk1 activity; Cdk1 activity is instead preserved until the final hour before PB1 extrusion. This late drop in Cdk1 activity coincides with timings for maximal removal of checkpoint proteins from the kinetochore and the formation of stable end-on kinetochore microtubule attachments (Kitajima et al. 2011; Lane et al. 2012). We therefore suggest that early destruction represents that of an excess pool of free cyclin B1 whose degradation will not directly compromise Cdk1 activity.

To address how free cyclin B1 could evade an active checkpoint in late prometaphase while Cdk1-bound cyclin B1 was protected, we used reporters for free and Cdk1-bound cyclin B1. We show that an N-terminal truncation (N90) of cyclin B1, representing the tail region of cyclin B1 that remains accessible on Cdk1 binding, was targeted for degradation much later than a full length non-Cdk1-binding cyclin B1, in time with a drop in Cdk1 activity. Critically

the truncated construct contains the D-box and neighbouring lysine residues previously shown to be necessary and sufficient for degradation in mitosis (Glotzer et al. 1991). This raised the possibility that, similar to other APC/C substrates such as cyclin A2, an additional sequence exists between residues 90-433 which functions to promote degradation in the presence of an active checkpoint (Di Fiore et al. 2015).

After multiple rounds of serial truncation and point mutation we arrived at a discrete motif in the N-terminal helix (centred around residues ^{173}DIY^{175} and ^{178}LRQL^{181}). We have named this motif the PM motif due to its ability to direct **P**ro **M**etaphase destruction. Mutating this motif delays cyclin B1 degradation until the metaphase drop in Cdk1 activity. Pinpointing the PM-motif to within the NTH suggests how the cellular destruction machinery is able to discriminate between Cdk1-bound and free cyclin B1. Excess free cyclin B1 is targeted via its D-box and PM-motif, both of which are essential for timely degradation when the checkpoint is still active in prometaphase. In contrast, Cdk1 binding obscures the PM-motif, leaving only the D-box of cyclin B1 accessible. This protects a proportion of cyclin B1 and maintains Cdk1 activity until the checkpoint is satisfied in metaphase (see Fig. 3.5B for model); the availability of the PM motif grants APC/C preferential targeting of non-Cdk1-bound cyclin B1 in situations where chromosomes have not yet achieved full alignment. We suggest that in mouse oocytes, PM-motif-mediated destruction of free cyclin B1 may couple the timing of a prolonged late prometaphase to the progressive positioning of chromosomes.

Chapter 4: A hidden motif in securin mediates late prometaphase destruction in mouse oocytes

4.1 Introduction

Mitosis

Successful cell division relies on chromosomes first organising and correctly aligning on the spindle followed by the separation of sister chromatids into two genetically identical sets of chromatids, an event tightly coordinated with metaphase exit. Two key events within the cell are critical to this process. Firstly, the removal of Cdk1 activity via cyclin B1 degradation (discussed in Chapter 3) which initiates a cascade of Cdk1 substrate dephosphorylations (Sullivan & Morgan 2007), and secondly degradation of securin allowing for separase activation (Ciosk et al. 1998; Uhlmann et al. 1999). If these events become disconnected, as demonstrated by artificial stabilisation of Cdk1 activity during normal separase activity, anaphase becomes extremely problematic with cells unable to form stable kinetochore microtubule attachments (Kamenz & Hauf 2014; Rattani et al. 2014).

In order to prevent precocious separation of sister chromatids, separase must be kept inactive state until a time when all chromosomes are correctly orientated on the spindle. Prior to anaphase, separase is kept inactive via a number of intricate mechanisms. Firstly, separase is inhibited by its binding partner securin which is present in excess of separase in mitotic cells (Hellmuth et al. 2014; Kamenz et al. 2015). Human securin is a relatively short and unstructured protein that binds across the surface of separase, acting as a pseudo substrate by occupying the Scc1 recognition site (Sánchez-Puig et al. 2005; Nagao & Yanagida 2006; Lin et al. 2016). Not only does securin function to inhibit separase, it also has an activating role. Separase is less active and less stable before it complexes with securin, than it is once released from securin, thereby preventing premature proteolytic activity prior to securin binding (Holland & Taylor 2008).

While in a typical eukaryotic cell most separase is inhibited by securin, cyclin B1-Cdk1 has also been shown to have the capacity to bind and inhibit separase (Stemmann et al. 2001; Gorr et al. 2005), likely able to completely take over this role given that securin is dispensable in mice (Mei et al. 2001; Wang et al. 2001). Phosphorylation of serine residue S1126 of separase by Cdk1 provides a platform for Pin1, a mitotic peptidyl-prolyl isomerise, to bind.

Pin1 then isomerises the bond between the phosphorylated serine and its adjacent proline residue (Hellmuth et al. 2015). This both renders separase more prone to aggregation and allows cyclin B1-Cdk1 to bind and inhibit separase (Hellmuth et al. 2015). In vertebrate cells, this inhibition is mutual, with separase having an inhibitory effect on cyclin B1-Cdk1. Where securin is the chief separase inhibitor, once separase is liberated and isomerised by Pin1, residual cyclin B1-Cdk1 is seen to complex with active separase. Abolishing cyclin B1 binding to separase by mutating a key serine residue (S1121) in separase results in segregation errors that are rescued by Cdk1 inhibition (Shindo et al. 2012). Correct polar body extrusion in mouse oocytes has also been shown to be dependent on Cdk1 inhibition by separase (Gorr et al. 2006). Whether separase is inhibited primarily by securin or by cyclin B1-Cdk1 varies depending on cell type and developmental state. Primordial germ cells and early stage embryos rely primarily on cyclin B1-Cdk1-mediated inhibition, whereas in female mouse meiosis II, human cancer cells and healthy human mitotic cells, securin is largely responsible for separase inhibition (Nabti et al. 2008; Huang et al. 2009; Kamenz & Hauf 2017).

Upon accurate chromosome alignment and termination of the spindle checkpoint, the APC/C in conjunction with its co-activator Cdc20 targets securin and cyclin B1 via their D-box motifs for ubiquitination and subsequent proteasomal degradation (Yamano et al. 1998; Hagting et al. 2002). Unlike cyclin B1, securin also contains a KEN box (residues 9-11) in addition to its destruction box. Since the KEN box can be targeted by the APC/C and its anaphase co-activator Cdh1, KEN box recognition is thought to take place much later in mitosis when the APC/C switches from Cdc20 to Cdh1 co-activation (Pfleger & Kirschner 2000). Where in mitosis a D-box mutation in cyclin B1 renders it non-degradable (Glotzer et al. 1991), securin with a mutated D-box but an intact KEN box is still degradable, however its destruction is delayed until anaphase when the APC/C switches from Cdc20 to Cdh1 co-activation (Hagting et al. 2002). APC/C-mediated securin destruction releases the inhibitory hold on separase which in turn cleaves the kleisin subunit of the cohesin ring structure which holds sister chromatids together during metaphase (Uhlmann et al. 1999). Together separase activity and Cdk1 inactivation due to cyclin B1 destruction drive anaphase and mitotic exit.

Securin destruction in mitosis begins at metaphase, once the spindle checkpoint is satisfied and mirrors that of cyclin B1, with degradation of both proteins required before sister chromatids can properly separate (Hagting et al. 2002).

Meiosis

Like mitosis, securin is known to be targeted for destruction in time with cyclin B1 in mouse oocytes (Homer et al. 2005). Unlike mitosis, this is at a time when checkpoint proteins are still detectable at the kinetochore (Lane et al. 2012). Beyond this, very little is known about securin destruction and separase inhibition in meiosis I. How and why securin is degraded throughout late prometaphase I is unknown. The similarities in degradation timings and APC/C recognition of cyclin B1 and securin, their overlapping roles in mitosis and the critical need for the synchronous loss of both proteins made it a primary line of interest to further investigate securin in meiosis. Specifically, whether securin exhibits a similar biphasic pattern of destruction to that of cyclin B1 in mouse oocytes.

4.2 Results

4.2.1 The D-box of securin is not sufficient for a wild-type (WT) destruction profile in MI mouse oocytes.

Given that securin is targeted for degradation in time with cyclin B1 in oocytes (Homer et al. 2005), I wanted to determine whether securin also showed a biphasic destruction profile similar to that of cyclin B1 (Levasseur et al. 2017 unpublished). Furthermore, I wanted investigate whether late prometaphase I destruction of securin was similarly mediated by a second destruction box working alongside the D-box.

Employing a strategy similar to that of the cyclin B1 PM motif discovery, two fluorescent securin reporters were initially tested, full-length securin (securin FL) and the N-terminal 101 residues of securin (securin N101). Both constructs contain the KEN box, D-box and neighbouring lysine residues necessary for APC/C recognition and subsequent proteolysis (Zur & Brandeis 2001; Hagting et al. 2002), however N101 critically lacks highly conserved regions within the C-terminal half of the protein (Fig. 4.1A).

Mouse oocytes were microinjected with cRNA encoding the securin VFP construct of interest then imaged at 10 minute intervals from prophase I to anaphase I. Average fluorescence intensity readings were taken from a defined region of interest around each oocyte, plotted over time and aligned using first polar body (PB1) extrusion as a reference point.

Securin FL was consistently targeted for destruction much earlier (~80 minutes) than securin N101 (Fig. 4.1B). When these destruction profiles were combined with data from our cyclin B1 study, it was revealed that not only were securin FL and cyclin B1 FL targeted for degradation simultaneously, securin N101 was degraded in time with cyclin B1 N90 (which contains the D-box and neighbouring lysine residues but critically lacks the PM motif that mediates late prometaphase I destruction) and concurrently with the loss of Cdk1 activity (Fig. 4.1C). This raises the possibility that, similar to cyclin B1 and other APC/C substrates such as cyclin A2, an additional sequence in the C-terminus of securin may cooperate with the D-box to direct APC/C-mediated degradation during prometaphase I in oocytes.

4.2.2 A second destruction motif exists within the C-terminus of securin.

To test if a second destruction motif exists within securin, one that facilitates its prometaphase destruction, a number of stepwise extensions were made to the C-terminus of securin N101.

Figure 4.1

A.

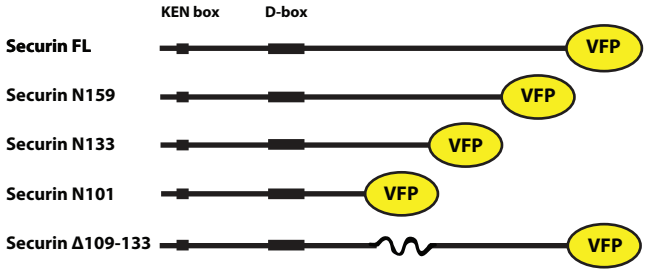

B.

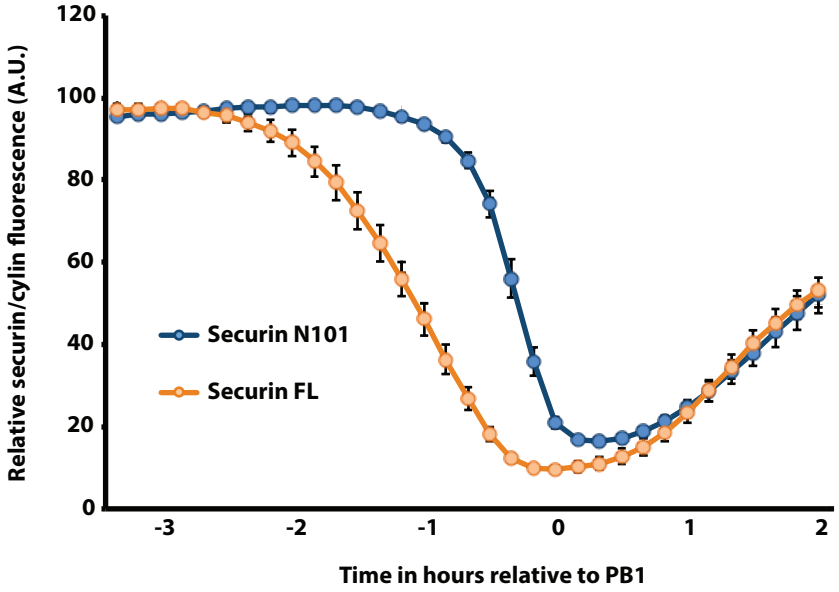

C.

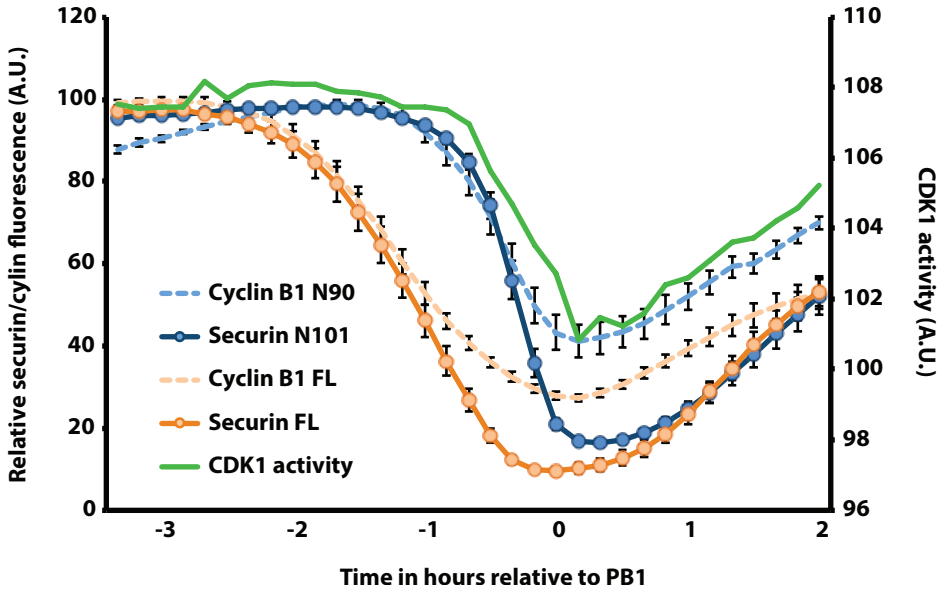

D.

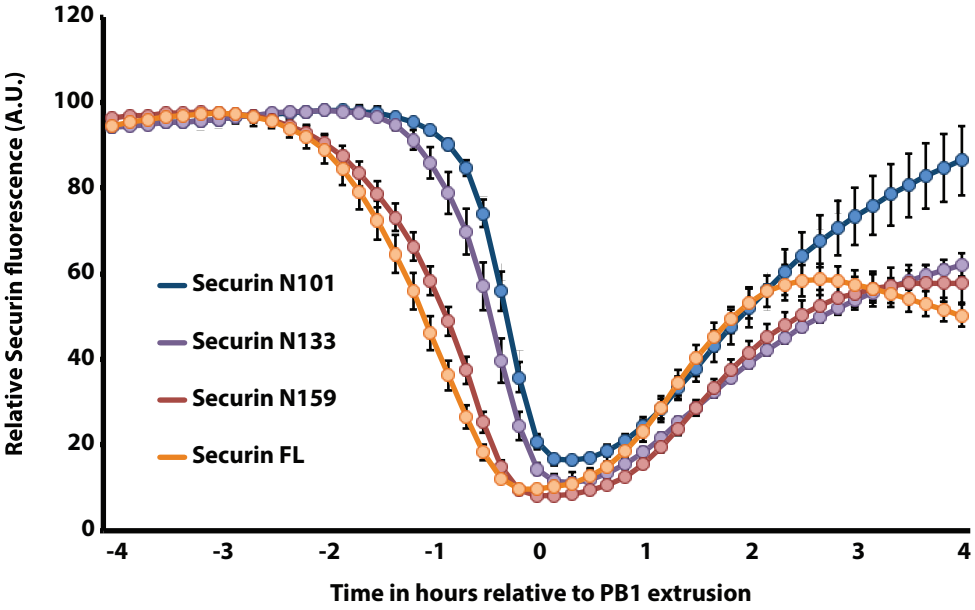

E.

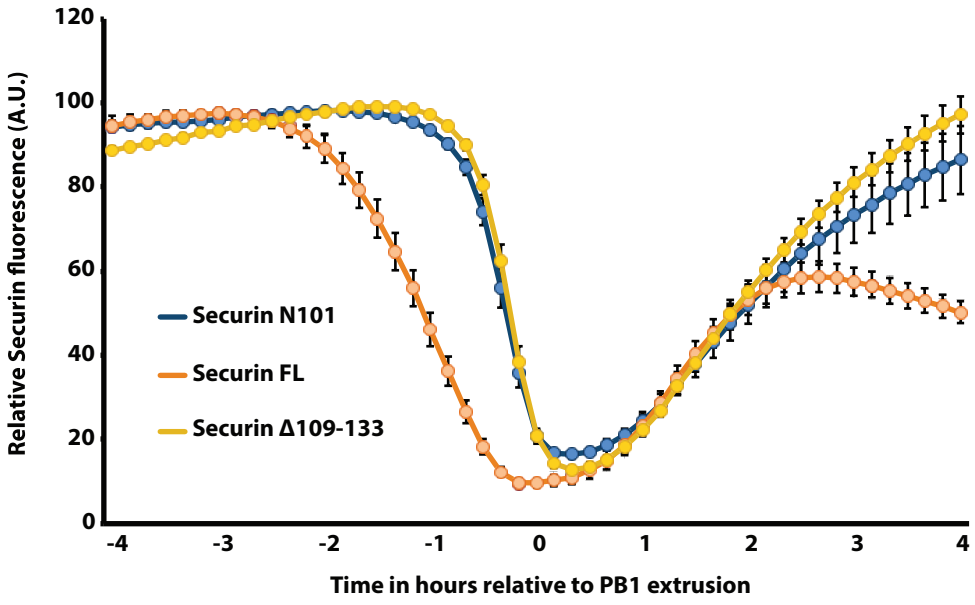

Figure 4.1. D-box only recognition is not sufficient for a normal securin destruction profile in MI mouse oocytes. (A) Schematic showing VFP-tagged securin truncations and mutations. **(B)** Average securin FL::VFP (orange, n=25) and securin N101::VFP (blue, n=23) destruction traces aligned at PB1 extrusion. **(C)** Average securin FL::VFP (orange, n=25), securin N101::VFP (blue, n=23), cyclin B1 FL::VFP (orange dotted, n=32) and cyclin B1 N90::VFP (blue dotted, n=34) destruction profiles alongside CDK1 activity (n=72, secondary axis) during MI aligned at PB1 extrusion. **(D)** Average securin FL::VFP (orange, n=25), securin N159::VFP (red, n=23), securin N133::VFP (purple, n=22) and securin N101::VFP (blue, n=23) destruction profiles aligned at PB1 extrusion. **(E)** Average securin FL::VFP (orange, n=25), securin N101::VFP (blue, n=23) and securin Δ109-133 (yellow, n=23) destruction profiles aligned at PB1 extrusion. Error bars = +/- SEM.

Initial extension constructs were securin N133 and N159, two extensions of securin N101 that separated regions of high conservation within the protein. Securin N159 was targeted for destruction in time with securin FL whereas securin N133 was targeted for destruction approximately 50 minutes after this (Fig. 4.1D). However, when residues 109-133 were replaced with a neutral linker in a full-length securin construct (securin Δ109-133), it was then targeted in time with securin N101 (Fig. 4.1E). To fully mimic wild-type destruction, it appears that a region within residues 109-133 is essential for prometaphase targeting of securin in meiosis, alongside additional information present between residues 133-159.

To narrow down the residues important in mediating prometaphase I securin destruction, residues 109-133 were divided into three blocks based on sequence conservation (Fig. 4.2A) and alanine mutagenesis was used to assess the importance of each group of residues in the timing of securin degradation (Fig. 4.2B). The first mutant, securin DAYPEIE-A, initially predicted to eliminate prometaphase targeting due to its similarity to the PM motif in cyclin B1 was instead targeted in time with securin FL, whereas securin FFPFNP-A and DFESFD-A where both degraded at a later time (Fig. 4.2C). Securin FFPFNP-A was targeted for destruction approximately 60 minutes after securin FL but still ~20 minutes ahead of securin N101 (Fig. 4.2D), whereas securin DFESFD-A was targeted in time with securin N101 (Fig. 4.2E). This suggests that essential residues for wild-type prometaphase securin degradation lie within both regions. The interaction which mediates this early degradation is likely strengthened by residues within FFPFNP. However, DFESFD-A gave the most striking phenotype and opened up the possibility of identifying discrete residues critical for prometaphase destruction.

Further point mutations within DFESFD highlighted a pair of conserved phenylalanine residues, F125 and F128, which when substituted for alanines (securin FxxF-A) delayed degradation by ~90 minutes in time with securin N101 (Fig. 4.2F). These two phenylalanine residues appear to constitute crucial residues of a novel interacting region (hereafter named the FxxF motif) able to direct APC/C-mediated proteolysis of securin in late prometaphase I in mouse oocytes. Destruction timings for all securin truncations and mutations are summarised in figure 4.3.

To confirm that the differences observed in degradation timing between securin FL and securin FxxF-A was not simply due to differences between protein expression of the two different mRNA constructs, oocytes were treated with cycloheximide (CHX) to block protein synthesis (Fig. 4.2G). On addition of CHX, securin FL was evident (~10% of the total protein was lost). The rate of degradation then increased ~3.5 hours after CHX addition. Securin

Figure 4.2

A.

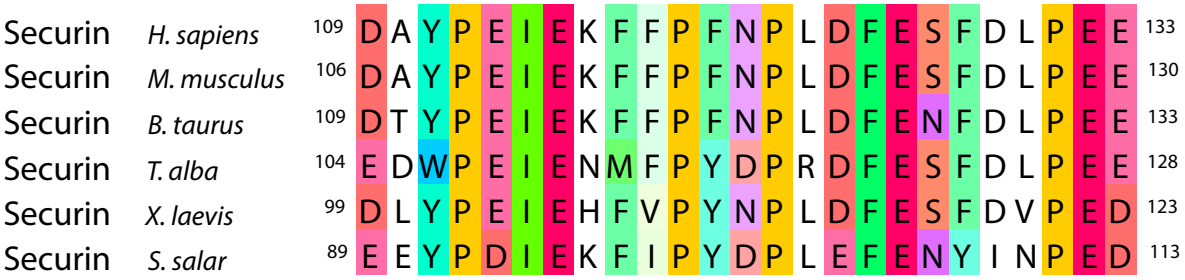

B.

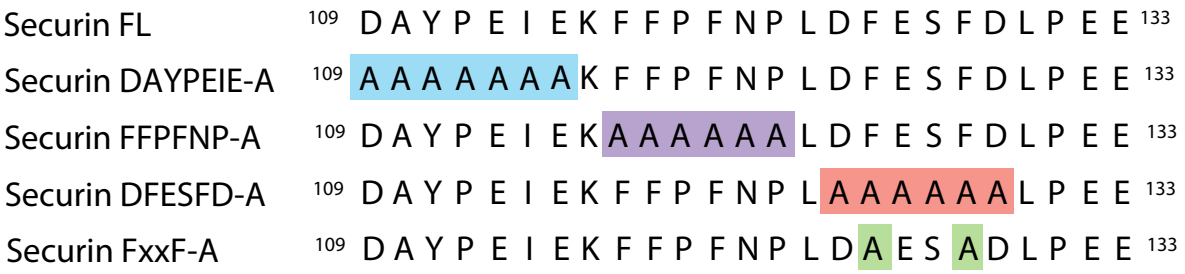

C.

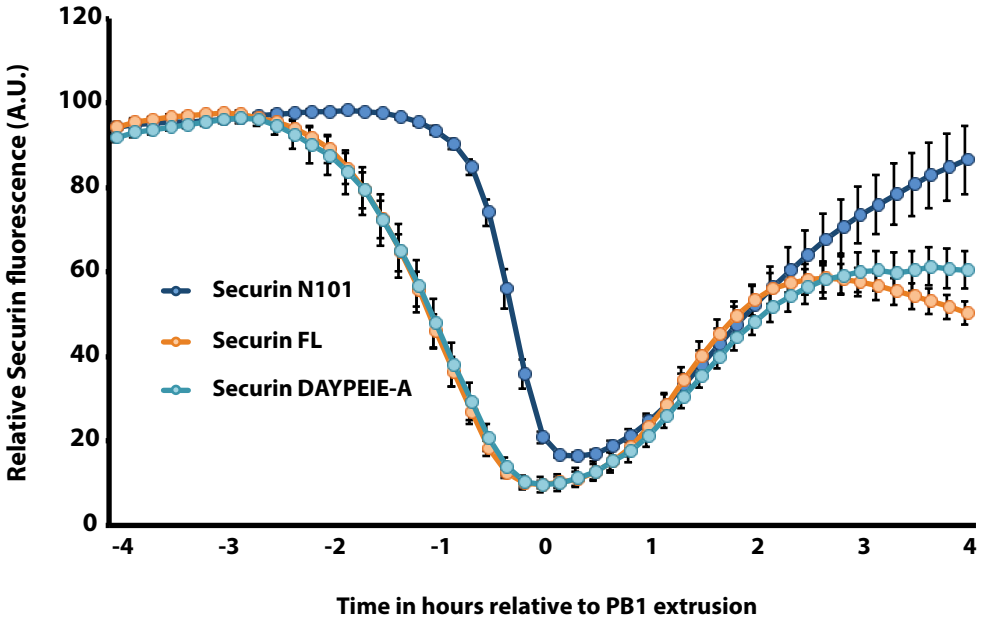

Figure 4.2

D.

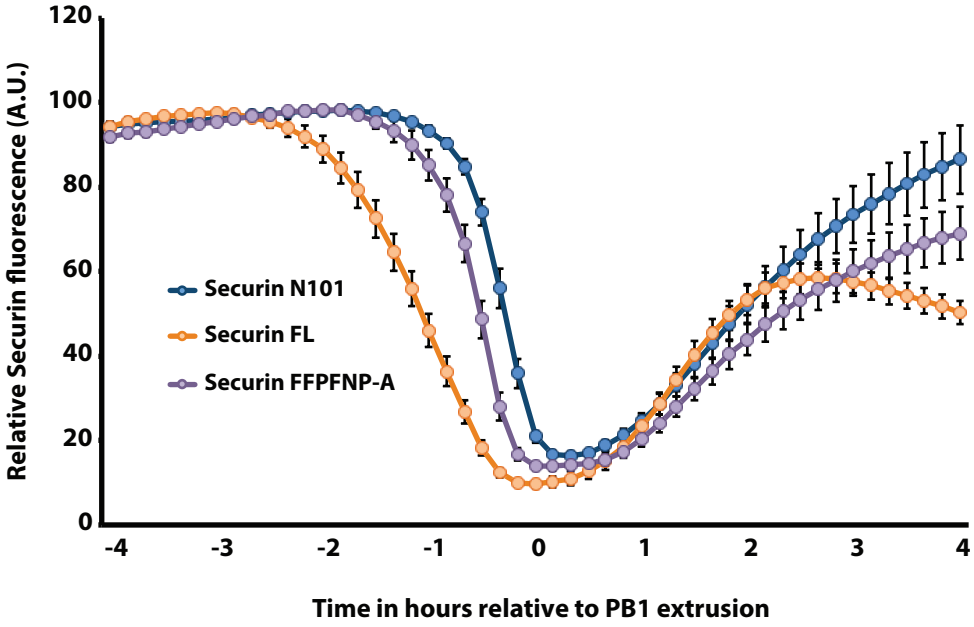
Relative Securin fluorescence (A.U.)
120
100
80
60
40
20
0
-4
-3
-2
-1
0
1
2
3
4
Securin N101
Securin FL
Securin FFPFNP-A
Time in hours relative to PB1 extrusion

E.

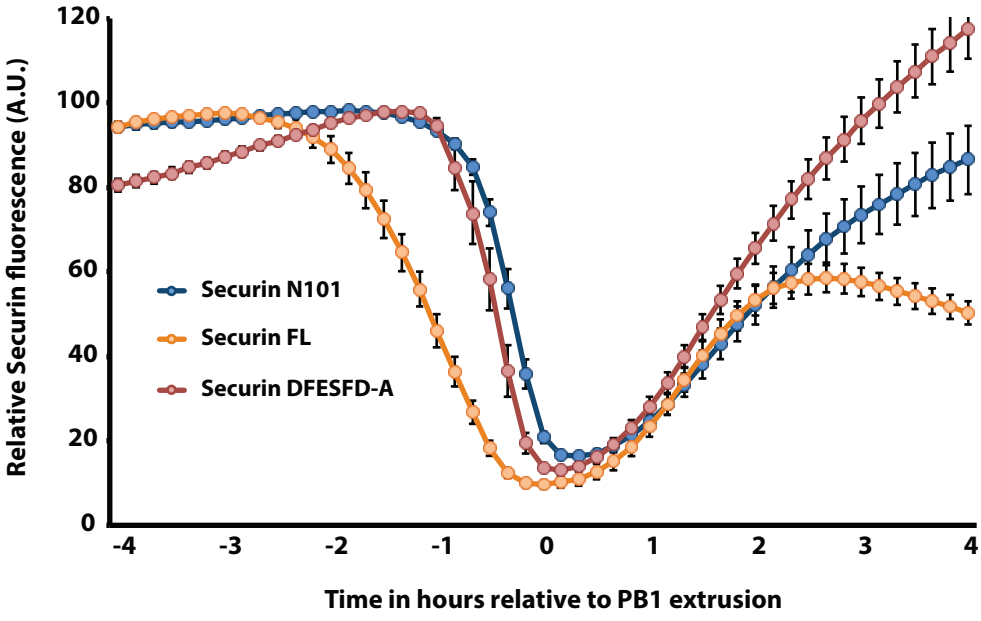
Relative Securin fluorescence (A.U.)
120
100
80
60
40
20
0
-4
-3
-2
-1
0
1
2
3
4
Securin N101
Securin FL
Securin DFESFD-A
Time in hours relative to PB1 extrusion

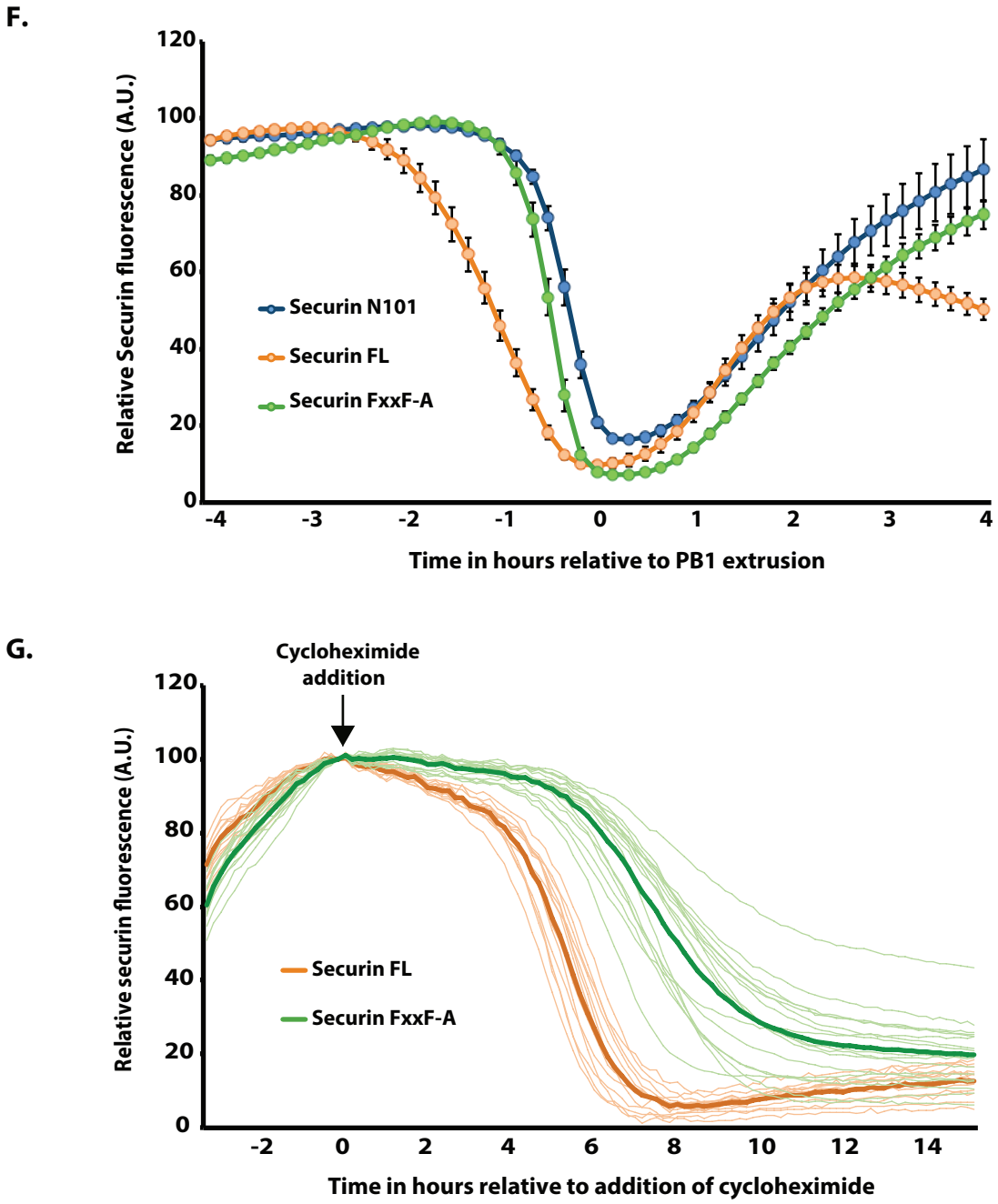

Figure 4.2. A second destruction motif exists within the C-terminus of securin. (A) Alignment of residues 109-133 in securin orthologs. **(B)** Securin residues 109-133 sequence detail showing the nomenclature of Venus-tagged securin mutations. **(C)** Average securin FL::VFP (orange, n=25), securin N101::VFP (blue, n=23) and securin DAYPEIE-A::VFP (light blue, n=19) destruction traces aligned at PB1 extrusion. **(D)** Average securin FL::VFP (orange, n=25), securin N101::VFP (blue, n=23) and securin FFPFNP-A (purple, n=23) destruction traces aligned at PB1 extrusion. **(E)** Average securin FL::VFP (orange, n=25), securin N101::VFP (blue, n=23) and securin DFESFD-A (red, n=20) destruction traces aligned at PB1 extrusion. **(F)** Average securin FL::VFP (orange, n=25), securin N101::VFP (blue, n=23) and securin FxxF-A (green, n=20) destruction traces aligned at PB1 extrusion. **(G)** Average securin FL::VFP (orange, n=24) and securin FxxF-A (green, n=27) on addition of cycloheximide to inhibit protein synthesis. Traces are aligned to the addition of cycloheximide at 3 hours post GVBD. Error bars = +/- SEM.

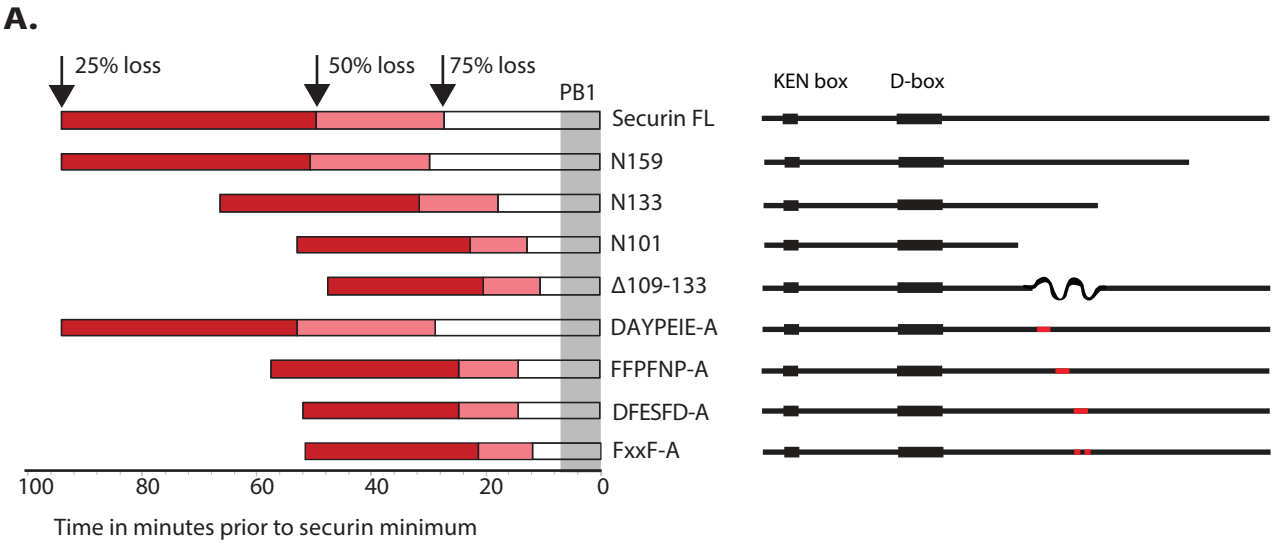

Figure 4.3. Securin constructs destruction timings. (A) Destruction of Venus-tagged securin truncations and mutants. Schematic representations of securin constructs are shown down the right hand side, while the bars to the left indicate destruction timings. The length of each bar indicates the number of minutes ahead of the minimum fluorescence/maximum destruction point (time 0). The open, white bars indicate the point at which 75% of the destruction has taken place. The light red extension to this bar indicates the point at which 50% of the destruction has taken place (error bars = SEM), followed by a dark red extension indicating the point at which 25% of the destruction has taken place. The period over which PB1 extrusions occur is shaded in grey.

FxxF-A protein appears to be turned over far less readily, instead remaining mostly stable until it was targeted for degradation ~5 hours after CHX addition. Critically, the securin FxxF-A becomes a target ~90 minutes after securin FL, consistent with results from non CHX-treated oocytes.

4.2.3 The FxxF motif is likely to be masked when securin is bound to separase.

The recently solved structure of the *S. cerevisiae* separase-securin complex (Luo & Tong 2017) has allowed us to see that residues Y276 and F279 which correspond to F125 and F128 in the human protein sit deep within a hydrophobic binding pocket on the surface of separase (Fig. 4.4A), making it likely that these two residues are obscured when securin is in complex with separase, yet visible when securin is free. This provides a mechanism by which an unbound pool of securin could be targeted preferentially in late prometaphase ahead of separase-bound securin, preventing premature separase activation.

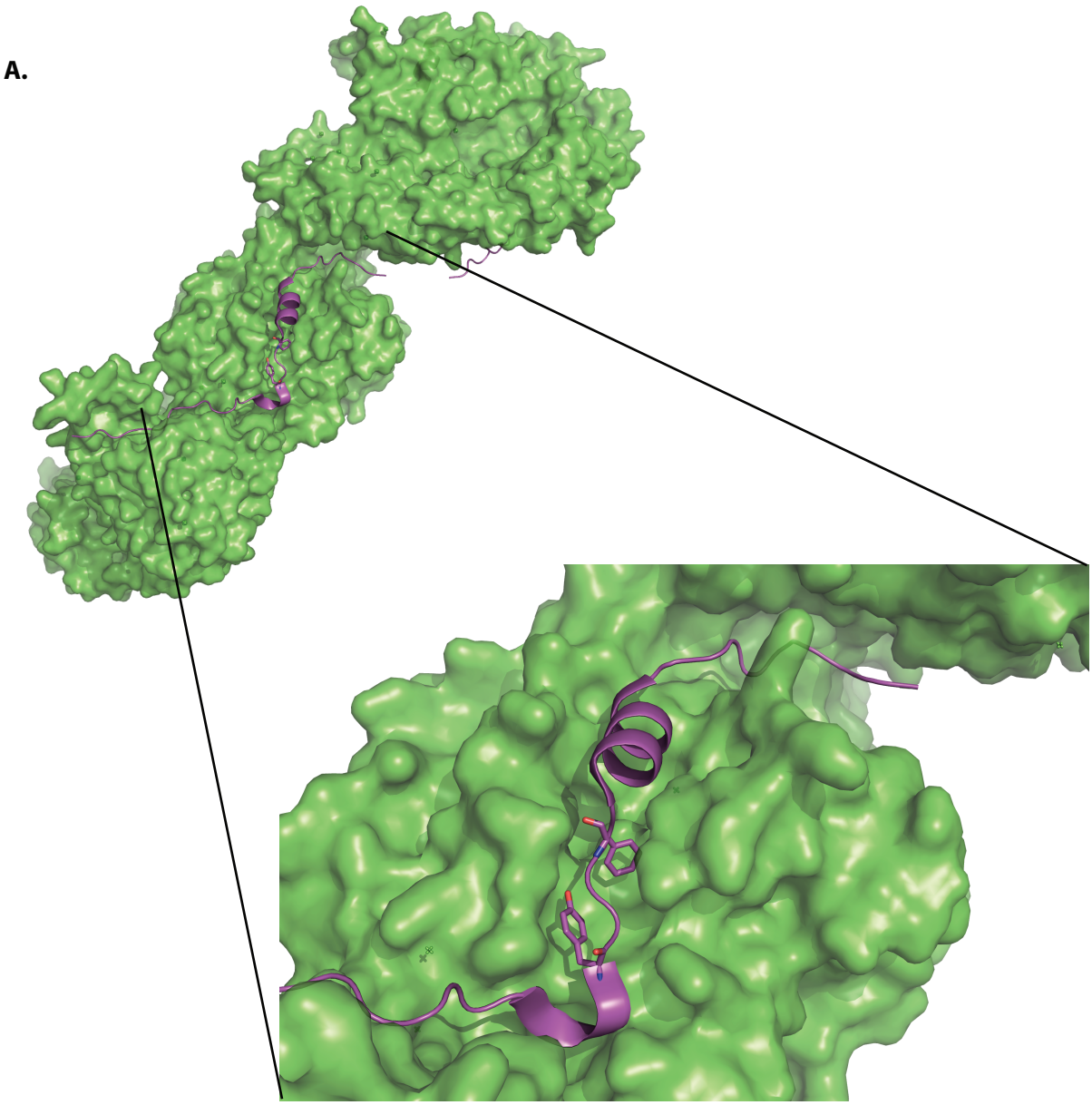

Figure 4.4. The FxxF motif is likely to be masked when securin is in complex with separase. (A) Molecular surface of the separase interaction segment of securin (purple) bound to separase (green) from the crystal structure of the Saccharomyces cerevisiae separase-securin complex (Luo & Tong, 2017.). The side chains of securin residues Y276 and F276, which correspond to F125 and F128 in the human protein, are shown as stick models**. (B)** Alignment of FxxF motif-containing region in securin orthologs.

4.3 Discussion

Securin destruction in mitosis begins at metaphase, once the spindle checkpoint is satisfied and mirrors that of cyclin B1. Degradation of both proteins is required before sister chromatids can properly separate (Hagting et al. 2002). In mouse oocytes, securin has also been shown to be targeted for destruction in time with cyclin B1 (Homer et al. 2005). Beyond this however, there is very little meiosis specific securin data with the majority of studies carried out in mitosis. Since we know that cyclin B1 is regulated in a different way in meiosis (chapter 3), given that securin and cyclin B1 are destroyed synchronously, it became important to explore the possibility of a similar biphasic destruction mechanism for securin in meiosis I mouse oocytes.

To address this question, mouse oocytes were microinjected with cRNA encoding full-length securin alongside an N-terminal truncation containing only the D-box and neighbouring lysine residues yet critically missing highly conserved regions within the C-terminus of the protein. It was found that the destruction of full-length securin mirrors that of full-length cyclin B1 in oocytes as previously observed by Homer et al. 2005, initiating at a time point when checkpoint proteins are still observed at the kinetochore (Kitajima et al. 2011; Lane et al. 2012) and the spindle is yet to migrate to the cortex (Verlhac et al. 2000). A D-box only N-terminal truncation is targeted approximately 80 minutes later than full-length securin and critically in time with a cyclin B1 mutant lacking its PM motif. Given that an additional motif was necessary to permit late prometaphase destruction of cyclin B1 (Chapter 3; Levasseur et al. 2017 unpublished), this made it likely an additional sequence may exist in the C-terminus of securin; a motif able to cooperate with the D-box and direct APC/C-mediated degradation in prometaphase I oocytes prior to full checkpoint satisfaction.

To investigate this and narrow down the region within the C-terminus of securin mediating prometaphase destruction, a number of extensions based on sequence conservation were made to the initial N-terminal truncation. This revealed that a region within residues 109-133 is essential for prometaphase degradation of securin in meiosis (Fig. 4D-E).

Based on sequence similarity to the PM motif of cyclin B1 (DIYxxLRQL), it was predicted that the region surrounding securin residues ^{109}DAY^{111} was a likely candidate, mediating late prometaphase degradation in oocytes. A theory strengthened by a report that in humans, primates and rodents, securin residues 108-113 (DDAYPE) form an unconventional βTrCP recognition motif that targets securin for SCF$^{\beta TrCP}$-mediated degradation, principally following UV-irradiation damage, but also involved in securin turnover in normal cells

(Limón-Mortés et al. 2008). Surprisingly however, an alanine mutation that eliminated residues 109-115 was still degraded during prometaphase and mirrored the destruction profile of full-length securin (4.2B-C).

Further mutations within residues 109-133 highlighted a pair of conserved phenylalanine residues, F125 and F128, which when substituted for alanines in an otherwise wild-type securin delayed degradation by ~80 minutes in time with the D-box only N-terminal truncation (Fig. 4.2F) and critically the cyclin B1 PM mutant. I suggest that these two phenylalanine residues constitute crucial residues of a novel interacting region (hereafter named the FxxF motif) able to direct APC/C-mediated proteolysis of securin in late prometaphase I in mouse oocytes. While the presence of F125 and F128 are clearly essential for wild-type destruction, I also acknowledge that neighbouring residues and regions also play an important role, namely residues within ^{117}FFPFNP^{122} and the region spanning residues 133-159. Interestingly, whilst degradation timings of the securin FxxF mutant and the cyclin B1 PM mutant appear to mirror each other, much like the wild-type proteins, the motifs themselves have very little in common.

The recently solved structure of the *S. cerevisiae* separase-securin complex (Luo & Tong 2017) has allowed us to visualise how the FxxF motif might be positioned when securin is in complex with separase as yeast separase shares the same elongated same as human separase. Residues Y276 and F279 which correspond to F125 and F128 in the human protein sit deep within a hydrophobic binding pocket on the surface of separase (Fig. 4.4A), making it likely that these two residues are obscured when securin is in complex with separase, yet visible when securin is free. This provides a mechanism by which an unbound pool of securin could be targeted preferentially in late prometaphase ahead of separase-bound securin, preventing premature separase activation. Important to note is that whilst the primary amino acid sequence of securin is generally poorly conserved through evolution, the D-box and region surrounding the FxxF motif are well conserved down to yeast (see Appendix for full alignment of securin orthologs).

Initial quantification blots suggest that securin is in large excess over separase in oocytes. Securin is known to be in excess in mitotic cells (Hellmuth et al. 2014). In MEFs, U2OS and HeLa, we are able to detect both separase and securin bands via immunoblot. However in mouse oocytes, while we are readily able to detect securin, we have not been able to detect separase (investigations are on going) despite neighbouring wells giving strong separase band for mitotic cells (MEFs, U2OS and HeLa). This suggests that in meiosis, securin is in huge excess of separase. An excess of free-securin may be targeted preferentially during late

prometaphase via its visible FxxF motif, potentially as a buffer zone, allowing the oocyte time to manage its highly complex spindle assembly without affecting separase inhibition prematurely. This theory will be discussed in further detail in chapter 7.

The idea of preferential targeting of free securin is not without president. In HeLa cells, separase-bound securin is dephosphorylated by PP2A-B56 phosphatase, whereas free securin exists in a phosphorylated state and is thus a preferential APC/C target, though this destruction takes place only after checkpoint satisfaction (Hellmuth et al. 2014).

It has been suggested that securin is present in excess of separase in mitosis, with free securin present at 4-5x the abundance of separase-bound securin in HeLa cells (Hellmuth et al. 2014). Why then is free securin destruction not seen in mitosis, prior to checkpoint satisfaction? It is important to note that HeLa cells are an immortalised cancer cell line and likely do not reflect the securin to separase ratio in healthy somatic cells. This may explain why the FxxF motif does not appear to target securin for prometaphase destruction in mitosis, however it may still have a role in housekeeping should securin become overexpressed. Another possibility is that some degree of prometaphase securin destruction does take place in mitosis yet is undetectable due to the relative speed of the metaphase anaphase transition in comparison to meiosis. Other studies have also noted securin to be in excess of separase though here without rigorous quantification (Ciosk et al. 1998; Shindo et al. 2012; Kamenz et al. 2015).

Possible mechanisms for the prometaphase destruction of securin in meiosis will be discussed in chapters 5 and 6. Clues to solving this can be taken from known prometaphase APC/C substrates such as cyclin A, Nek2A and HOXC10 which are degraded rapidly in prometaphase as soon as the nuclear envelope breaks down (NEBD) (Elzen & Pines 2001; Geley et al. 2001; Gabellini et al. 2003; Hayes et al. 2006). The mechanism by which the FxxF motif mediates prometaphase securin destruction in oocytes, as well as the role of this novel mechanism in protecting separase inhibition, will be addressed in chapter 5.

Chapter 5: The FxxF motif in securin functions alongside a D-box to promote preferential degradation of free securin ahead of separase activation in meiosis I mouse oocytes.

5.1 Introduction

In chapter 4, the existence and location of a novel and conserved FxxF motif within the C-terminus of securin was uncovered. The FxxF motif permits destruction in late prometaphase, two hours ahead of a securin mutant construct lacking this motif. This destruction takes place at a time when weak Mad2 staining is still detectable at kinetochores (Lane & Jones 2014) and the meiotic spindle is yet to fully migrate to the cortex (Verlhac et al. 2000; Kitajima et al. 2011). In this chapter I will begin to discuss how this motif promotes destruction during a period of active checkpoint signalling and further aim to explore the roles of other known destruction motifs, namely the KEN box and D-box, in meiotic securin destruction. In addition to understanding the mechanism by which securin seems able to bypass an active checkpoint, the aim was to investigate the relationship between this prometaphase destruction and meiotic separase activity. Precocious separase activity would likely have disastrous consequences, therefore the early loss of securin seems at odds with the requirement of the oocyte.

In mitosis, the majority of securin destruction is mediated by the large multi-subunit E3 ubiquitin ligase the anaphase promoting complex or cyclosome (APC/C) (Hagting et al. 2002). However further studies have also highlighted a number of additional E3 ligases at least partially responsible for securin destruction in a number of different situations and cell types. The $SCF^{\beta TrCP}$ has been shown to mediate destruction when securin becomes abnormally hyper-phosphorylated through inhibition of the phosphatase PP2A, a situation that may arise in certain cancers (Gil-Bernabé et al. 2006). The same group also showed that UV irradiation had a similar effect, SCF-mediated securin degradation was triggered following a standard exposure to UV (100 J/m^2). Here a discrete motif within the C-terminus of securin (DDAYPE) was identified as being responsible for mediating the interaction with the SCF. In the same study, the SCF was also shown to have a role in securin turnover in healthy cells (Limón-Mortés et al. 2008). More recently, Parkin, an E3 ubiquitin ligase involved in Parkinson's disease has been observed to interact with Cdc20 and Cdh1, targeting securin and a number of other substrates including cyclin B1 and Nek2A for mitotic degradation

alongside the APC/C (Lee et al. 2015). In mouse embryonic fibroblasts (MEFs), Smurf1 directly interacts with securin and targets it for proteasomal degradation. When Smurf1 is knocked down, sister chromatid segregation is strongly inhibited and marked delay in anaphase onset is observed (Wei et al. 2017), likely due to an extended period of separase inhibition.

While there is far less known about securin degradation in meiosis, one study has suggested securin degradation in mouse oocytes to be entirely APC/C-dependent, due to securin stabilisation when the D-box is mutated (Herbert et al. 2003). However, since a new motif has been identified within securin, it becomes critical revisit this theory and investigate how the D-box, KEN box and FxxF motif are working together to mediate meiotic degradation.

The APC/C is able to recognise its substrates through two co-activators, Cdc20 and Cdh1, each of which contain WD40 domains serving as major sites for substrate recognition (Kraft et al. 2005; Chao et al. 2012). Through domains within the APC/C subunits and its co-activators, the APC/C is able to recognise a range of short motifs, known as degrons (Davey & Morgan 2016). Aside from the two well-characterised APC/C degrons (the D-box and KEN box), there exists also the newly discovered ABBA motif, originally identified in cyclin A and consisting of the consensus motif Fx[ILV][FHYx[DE]. The ABBA motif has been shown to outcompete a similar motif within BubR1 for an ABBA-binding domain in Cdc20 thus permitting APC/C activation during an active checkpoint (Di Fiore et al. 2015).

As well as the newly discovered FxxF motif (chapter 4), and in addition to the D-box, human securin contains a further classic APC/C degron, namely a KEN box. In mitosis, securin degradation begins in metaphase once the spindle checkpoint is satisfied and is mediated primarily by APC/C-Cdc20. This degradation requires only the D-box and not the KEN box (Hagting et al. 2002). However when key D-box residues are replaced via alanine mutagenesis, the KEN box takes over and degradation is pushed back to a later time point, following anaphase (Hagting et al. 2002). This KEN box only mediated degradation likely indicates a time in mitosis when APC/C-Cdh1 activity replaces that of APC/C-Cdc20. If both the KEN box and D-box are mutated in tandem, securin is largely stabilised in mitotic cells (Hagting et al. 2002). While not strictly degrons, human securin also contains two TEK boxes, mutation of which impairs initiation of ubiquitin chain formation by E2 ubiquitin conjugating enzyme, Ube2C (Jin et al. 2008).

Securin destruction in mouse oocytes begins 3 hours ahead of polar body extrusion (Chapter 4) at a time when weak Mad2 staining is still detectable at kinetochores, suggesting that a

reduced yet active checkpoint is still signalling (Lane et al. 2012). In mitosis, while chromosomes are still correctly aligning on the spindle, APC/C activation is strongly inhibited by the spindle checkpoint, a diffusible "wait anaphase" signal propagated from unattached kinetochores (Musacchio & Salmon 2007). The spindle checkpoint signal is generated primarily through the action of Mad2 and BubR1 (Sczaniecka et al. 2008), which act to sequester Cdc20 in a number of ways. As part of the mitotic checkpoint complex (MCC), Mad2 prevents association of free Cdc20 with the APC/C by outcompeting APC8 for binding of the KILR motif in Cdc20 (Izawa & Pines 2014). The MCC can then bind a second APC/C-bound Cdc20 through a conserved ABBA-KEN-ABBA binding cassette, preventing Cdc20 from interacting with APC3 (whilst still bound to APC8) and hence removing the bipartite D-box receptor formed with APC10 (Izawa & Pines 2014; Di Fiore et al. 2016). Cdc20 therefore shows a shift in the way it interacts with the APC/C depending on whether the checkpoint is on or off. When the checkpoint is on Cdc20 interacts with APC8 only, whilst when the checkpoint is satisfied and MCC production ceases, Cdc20 is free to also interact with APC3 and form a D-box receptor with the neighbouring APC10, thus initiating cyclin B1 and securin degradation (Izawa & Pines 2011). While chromosomes are still aligning during prometaphase both APC/C co-activators are suppressed. The spindle checkpoint acts to inhibit Cdc20, and Cdh1 is inhibited through Cyclin B1-Cdk1 phosphorylation (Zachariae 1998).

In contrast to mitotic cells where MCC complexes formed in the cytoplasm are sufficient for correct prometaphase timing (Maciejowski et al. 2010), mouse oocytes also require kinetochore localisation of MPS1 (whose role is discussed in Chapter 1) for correct timing of prometaphase I (Hached et al. 2011). This supports a long held theory that diffusible MCC complexes are insufficient over a large volume (Minshull et al. 1994), as is the case in a mouse oocyte. This is further evident in a recent study in C. *elegans* embryonic cells, where the strength of checkpoint was directly related to the ratio of kinetochores to cytoplasmic volume ratio (Galli & Morgan 2016).

Unlike in mitosis, where a single unattached kinetochore is sufficient to induce cell cycle arrest (Rieder et al. 1994), it has previously been suggested that APC/C activation in mouse oocytes can take place in the presence of multiple incorrect attachments since cyclin B1 and securin are destroyed so early (Gui & Homer 2012; Lane et al. 2012). Late prometaphase destruction of cyclin B1 and securin has therefore previously been considered as evidence of this inefficient or diluted checkpoint, resulting in a precocious degradation of APC/C metaphase substrates. However, previous chapters have shown that D-box only mediated

degradation is still insufficient for wild-type prometaphase destruction and that additional discrete motifs within the two proteins are also required.

In mitosis, there is a delay observed between the initiation of securin degradation and the activation of separase. In some systems, this delay is at least in part due to the phosphorylation state of securin. In human cells, phosphorylated free securin is targeted preferentially over separase-bound securin due to dephosphorylation by PP2A in complex with separase, thus delaying separase activation (Hellmuth et al. 2014). In budding yeast, the situation is reversed and Cdk1-dependent phosphorylation of securin has in fact been shown to delay degradation (Lu et al. 2014).

Securin destruction is observed for 3 hours ahead of polar body extrusion in meiosis I mouse oocytes. In chapter 4 it was hypothesised that preferential degradation of free securin via its FxxF motif may function to protect against premature separase activation, since a later second wave of securin destruction relying only on its D-box does not begin until 90 minutes prior to PB1 extrusion. However, initiation of separase activation even 90 minutes ahead of PB1 extrusion would still likely be catastrophic due to cohesin cleavage so far ahead of anaphase. It is therefore, alongside the role of the KEN box and D-box, a primary point of interest to investigate the exact timing and regulation of separase activity in oocytes.

5.2 Results

5.2.1 Meiotic securin destruction is D-box-dependent but not KEN box-dependent.

Following identification of a discrete FxxF motif within the C-terminus of securin (chapter 4) I wanted to investigate how this functioned alongside the D-box and KEN box to mediate meiotic destruction. Alignment of metazoan securin orthologs showed that while the consensus D-box motif is well conserved throughout; the canonical KEN box is lost even in mouse, where it is replaced by KDN. The mouse KDN sequence in securin would be unlikely to be recognised as a functional KEN motif since if the Cdc20 KEN box is mutated to KDN in mouse cell lines, Cdc20 is stabilised (Zur & Brandeis 2002) (Fig. 5.1A). This suggests that while the KEN box has been shown to be functional in humans when the D-box is mutated (Hagting et al. 2002), its functional significance seems of far less evolutionary importance than the D-box.

To assess the functionality of securin degrons in meiosis, three mutant securin constructs were tested, a KEN box mutant in which all three core residues were replaced with alanines (KEN>AAA, securin KEN mutant), a D-box mutant in which the three key residues forming the consensus motif, the arginine in position 1, the leucine in position 4 and the asparagine in position 8 were replaced with alanines (RKALGTVN>AKAAGTVA, securin D-box mutant) and finally a double mutant that combined both degron mutations (securin KEN/D-box mutant). Securin KEN mutant was targeted with an identical destruction profile to that of a wild-type securin construct (securin FL; Fig. 5.1B), while mutation of the D-box inhibited FL securin destruction (Fig. 5.1C-D). Though largely stabilised, in contrast to a previous study that found D-box mutation to completely stabilise securin in mouse oocytes, evidence of destruction was still observed in the fluorescence profiles of individual oocytes injected with securin D-box mutant, however this effect is lost in the average trace. Degradation here never exceeds 25% and is completely lost in the securin KEN/D-box mutant, which is completely stable (Fig. 5.1D). This suggests that while meiotic securin degradation is largely D-box dependent, when the D-box is mutated a small amount of destruction can be maintained via the KEN box. However, unlike in mitotic studies there does not appear to be a significant change in the timing of KEN-box mediated degradation, indeed some destruction profiles for securin D-box mutant constructs show targeting even ahead of securin FL (Fig. 5.1C).

Figure 5.1

A.

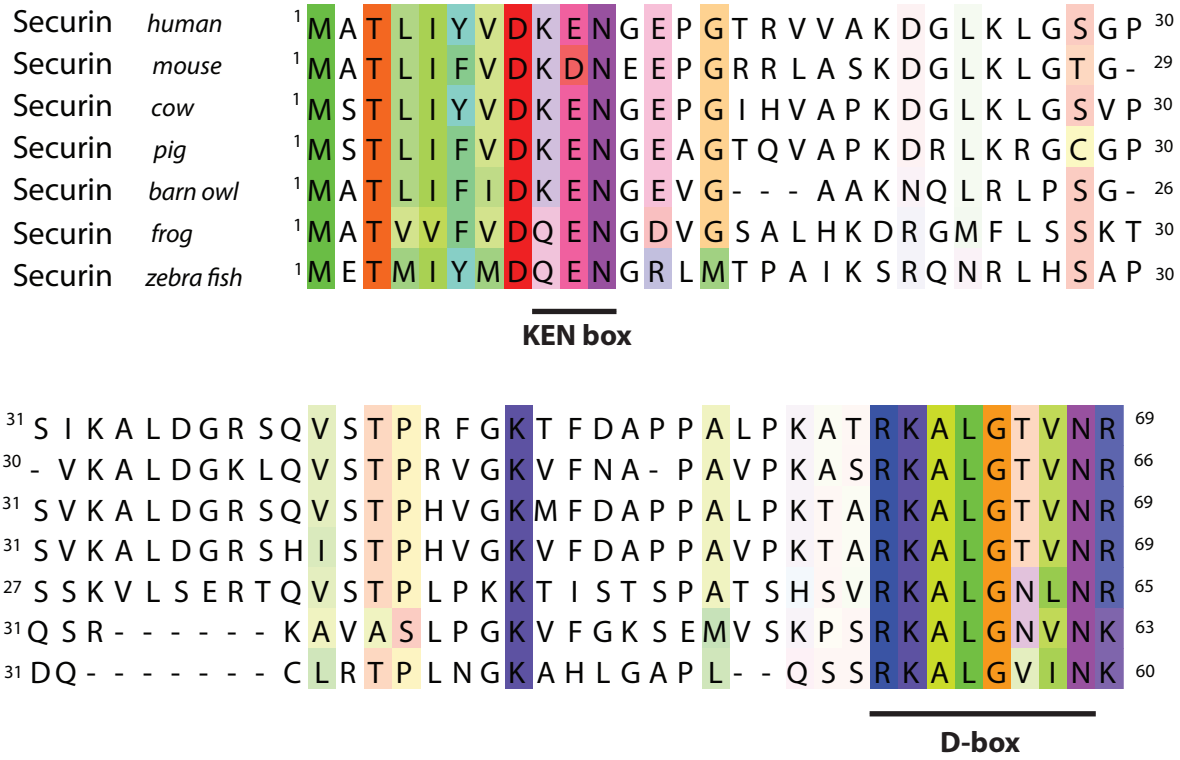
Securin human 1 MATLIYVDKENGEPGTRVVAKDGLKLGSGP 30
Securin mouse 1 MATLIFVDKDNEEPGRRLASKDGLKLGTG- 29
Securin cow 1 MSTLIYVDKENGEPGIHVAPKDGLKLGSVP 30
Securin pig 1 MSTLIFVDKENGEAGTQVAPKDRLKRGCGP 30
Securin barn owl 1 MATLIFIDKENGEVG---AAKNQLRLPSG- 26
Securin frog 1 MATVVFVDQENGDVGSALHKDRGMFLSSKT 30
Securin zebra fish 1 METMIYMDQENGRLMTPAIKSRQNRLHSAP 30
KEN box
31 SIKALDGRSQVSTPRFGKTFDAPPALPKATRKALGTVNR 69
30 -VKALDGKLQVSTPRVGKVFNA-PAVPKASRKALGTVNR 66
31 SVKALDGRSQVSTPHVGKMFDAPPALPKTARKALGTVNR 69
31 SVKALDGRSHISTPHVGKVFDAPPAVPKTARKALGTVNR 69
27 SSKVLSERTQVSTPLPKKTISTSPATSHSVRKALGNLNR 65
31 QSR------KAVASLPGKVFGKSEMVSKPSRKALGNVNK 63
31 DQ-------CLRTPLNGKAHLGAPL--QSSRKALGVINK 60
D-box

B.

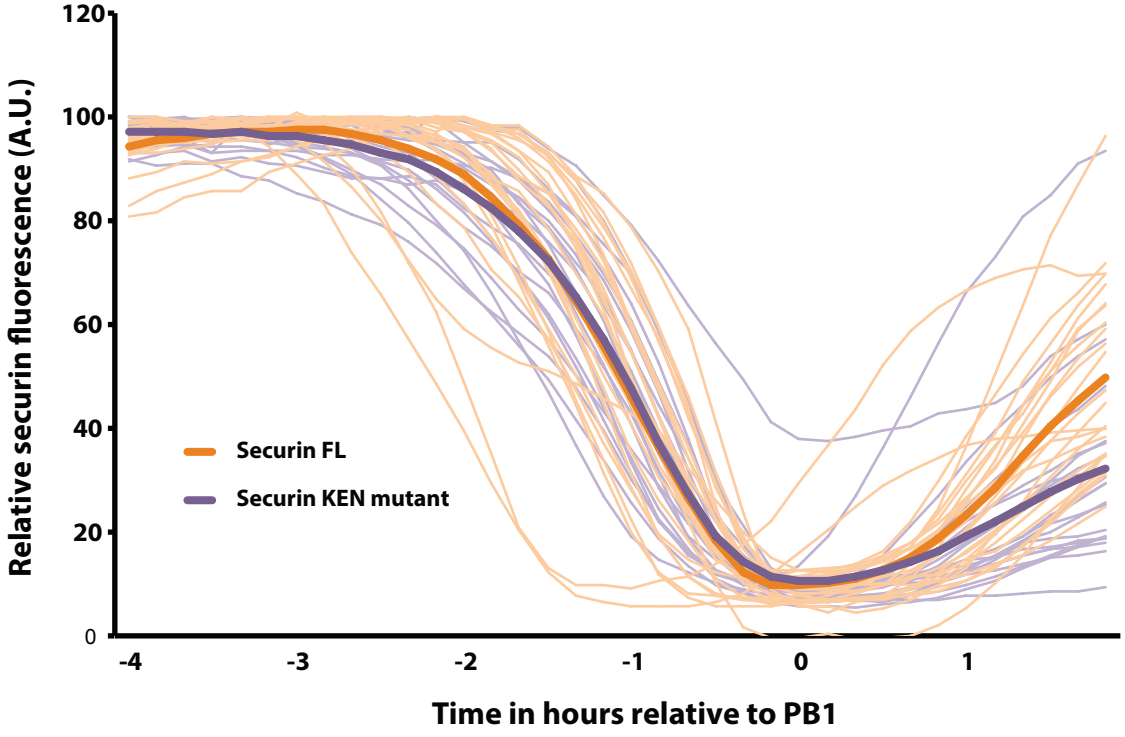
Relative securin fluorescence (A.U.)
120
100
80
60
40
20
0
-4
-3
-2
-1
0
1
Time in hours relative to PB1
Securin FL
Securin KEN mutant

Figure 5.1

C.

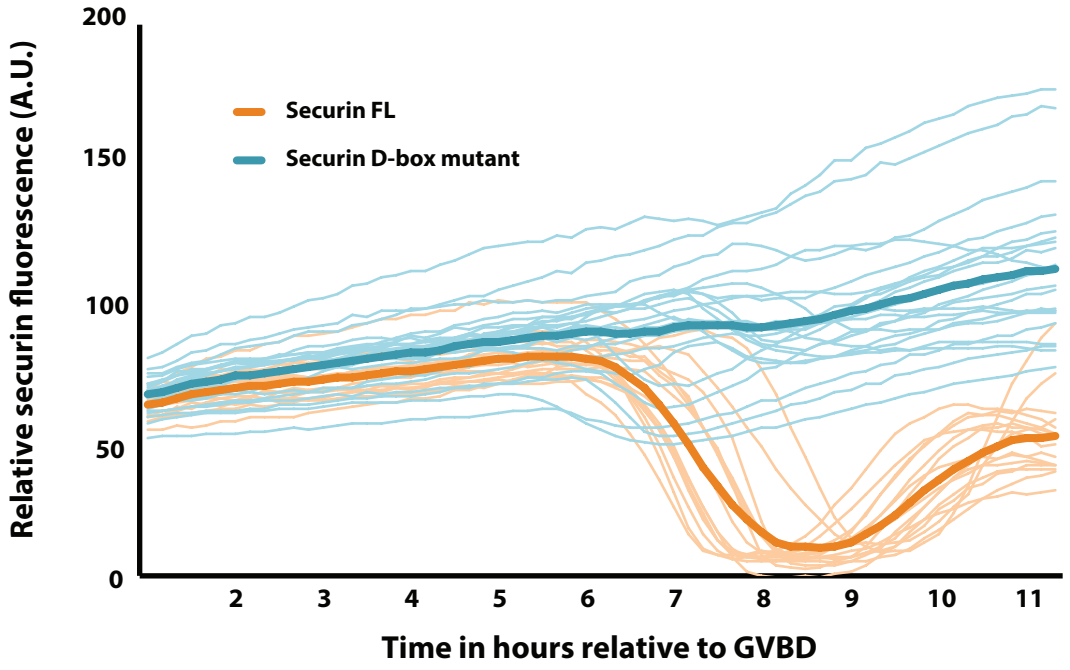
Relative securin fluorescence (A.U.)
200
150
100
50
0
Securin FL
Securin D-box mutant
2
3
4
5
6
7
8
9
10
11
Time in hours relative to GVBD

D.

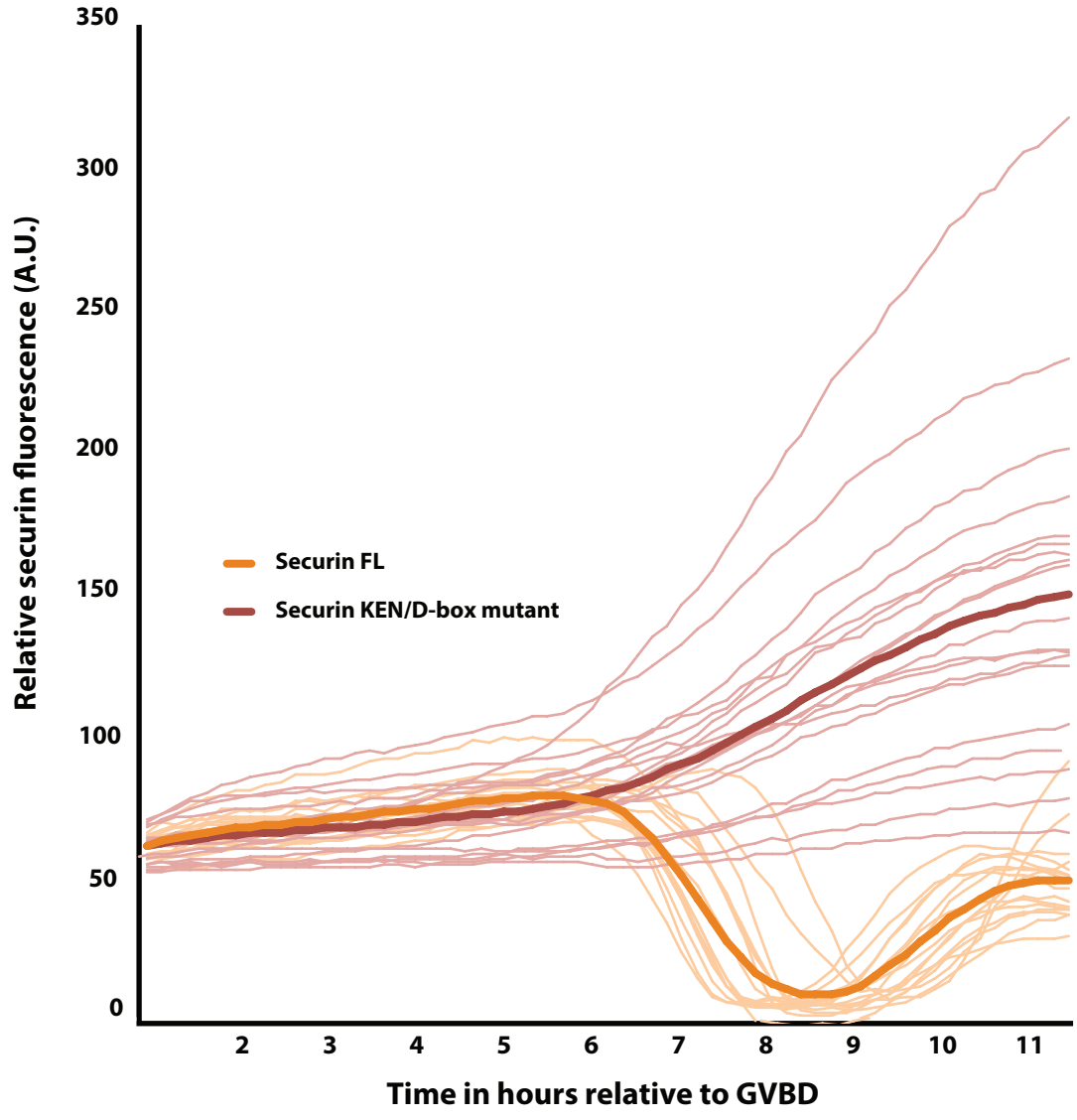
Relative securin fluorescence (A.U.)
350
300
250
200
150
100
50
0
Securin FL
Securin KEN/D-box mutant
2
3
4
5
6
7
8
9
10
11
Time in hours relative to GVBD

Figure 5.1. Meiotic securin destruction is D-box dependent but not KEN box dependent. **(A)** Alignment of residues 1-69 in securin orthologs containing both KEN box and D-box motifs. (**B)** Average securin FL::VFP (orange, n=25) and securin KEN mutant::VFP (purple, n=20) destruction profiles aligned at PB1 extrusion. **(C)** Average securin FL::VFP (orange, n=16) and securin D-box mutant::VFP (light blue, n=23) destruction profiles aligned at GVBD. **(D)** Average securin FL::VFP (orange, n=16) and securin KEN/D-box mutant::VFP (red, n=19) destruction profiles aligned at GVBD. Both securin D-box mutant and securin KEN/D-box mutant were largely stabilized and blocked anaphase progression, therefore destruction profiles are aligned at GVBD rather than PB1 extrusion. Fine traces represent destruction profiles from individual oocytes, heavy traces represent the average destruction profile resulting from all injected oocytes of a given contruct.

5.2.2 The FxxF motif in securin functions to bypass an active checkpoint in late prometaphase I oocytes and is involved in preferential targeting of free securin once the spindle checkpoint is satisfied.

Securin destruction in mouse oocytes begins in late prometaphase at a time when Mad2 staining is still detectable at kinetochores (Lane et al. 2012), however it is not known exactly how much control the spindle checkpoint has over FxxF-driven degradation. To investigate this, oocytes were treated with 150 nM nocodazole to depolymerise microtubules. This activates the checkpoint such that PB1 extrusion is blocked in >95% of oocytes. It was observed that while the rate of full-length securin degradation was dramatically reduced, it was still almost fully degraded by 20 hours, whereas securin FxxF-A was almost completely stabilised (Fig. 5.2A). This suggests that the destruction of securin in late prometaphase I is not simply due to a checkpoint signal that is insufficient over the large volume of an oocyte, but that the FxxF motif is actively involved in bypassing a checkpoint signal that can still sufficiently block D-box only APC/C substrates.

To further investigate the role of the FxxF motif in securin degradation, oocytes were treated with 100nM reversine to inhibit MPS1 and block the assembly of new MCC complexes. As expected, reversine treatment rapidly accelerated the meiotic cell cycle, with securin degradation beginning ~30 minutes after drug addition (Fig 5.2B). In reversine-treated oocytes, securin FL was still consistently targeted for destruction ~60 minutes ahead of securin FxxF-A (Fig 5.2B). This demonstrates that whilst the FxxF motif is necessary to bypass an active checkpoint, even once the spindle checkpoint is inactivated, FL securin (in which the FxxF motif is visible) is still the preferential APC/C substrate ahead of separase-bound securin in which only the D-box is visible.

5.2.3 APC3 and Cdc20 levels are rate limiting for prometaphase securin destruction.

Wild-type meiotic securin destruction begins in late prometaphase and is mediated via the FxxF motif which functions to bypass an active spindle checkpoint (Fig 5.2A). However, the FxxF motif must function alongside the D-box, given D-box mutation largely stabilises securin destruction (Fig 5.1C). The requirement for a D-box would suggest APC/C-Cdc20 activity is responsible for early securin degradation, as the D-box is recognised by a bipartite receptor formed between the WD40 domain of Cdc20 and APC/C subunit APC10 (Chao et al.

Figure 5.2

A.

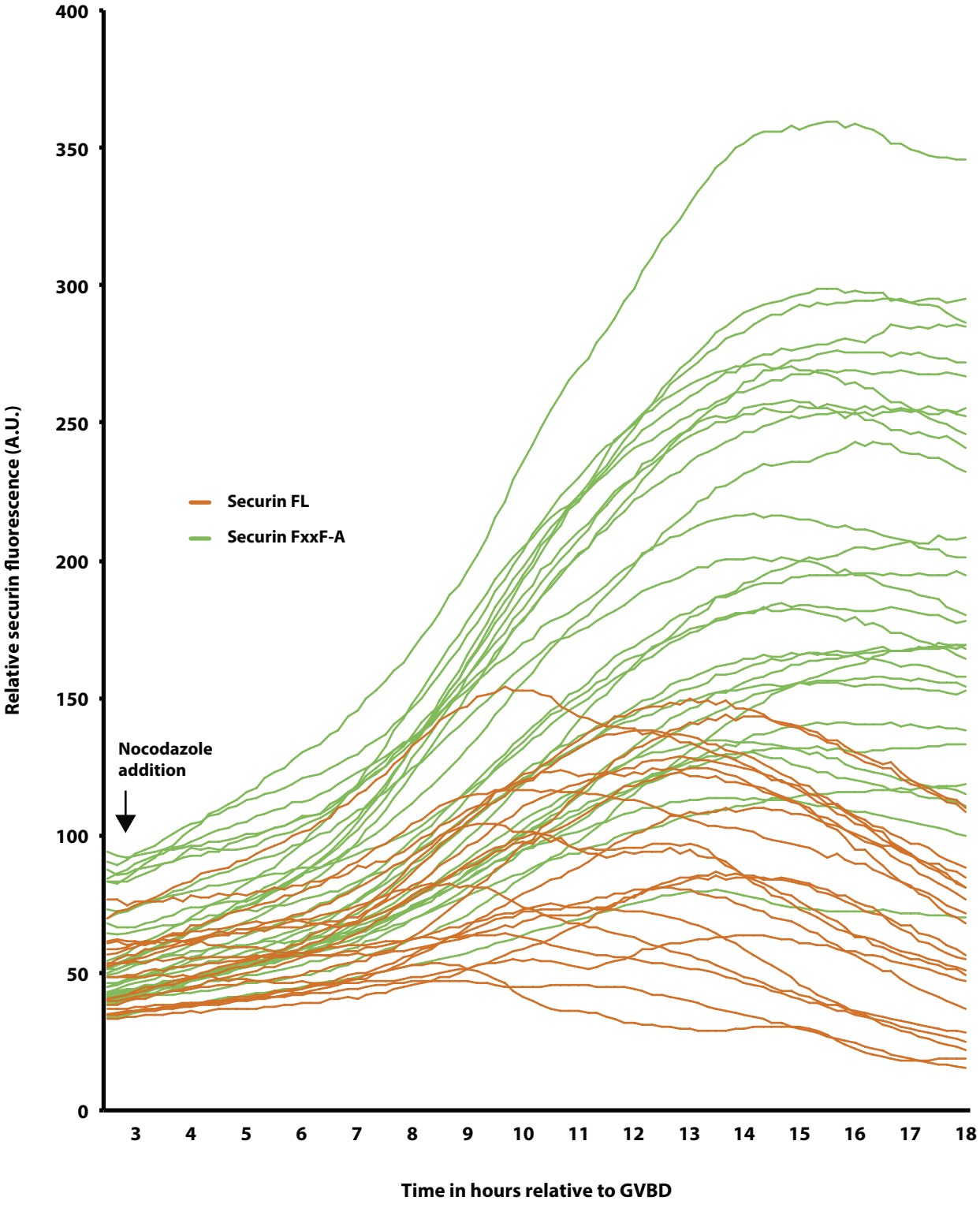
Relative securin fluorescence (A.U.)
400
350
300
250
200
150
100
50
0
Securin FL
Securin FxxF-A
Nocodazole addition
3
4
5
6
7
8
9
10
11
12
13
14
15
16
17
18
Time in hours relative to GVBD

B.

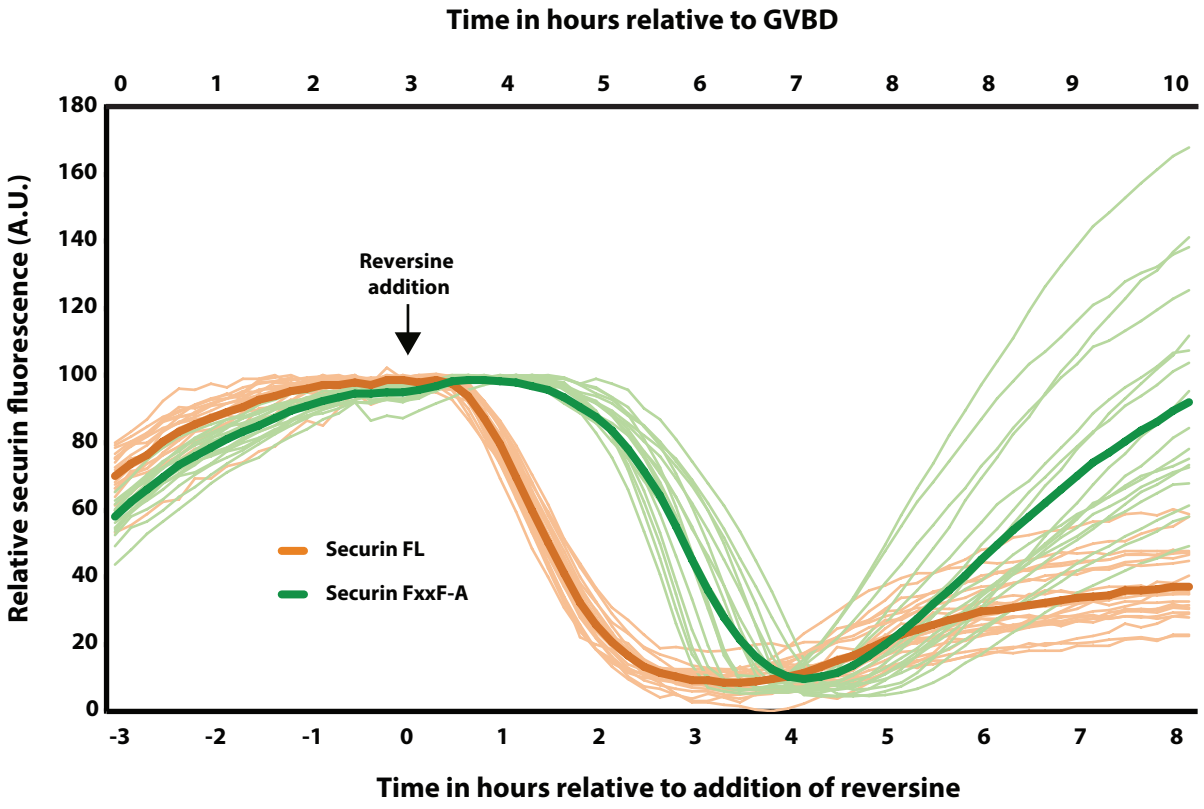

Figure 5.2. The FxxF motif in securin functions to bypass an active checkpoint and is involved in preferential targeting of free securin once the SAC is satisfied. (A) Average securin FL::VFP (orange, n=20) and securin FxxF-A (green, n=30) destruction profiles on addition of nocodazole to arrest oocytes in prometaphase. Traces are aligned to GVBD as oocytes did not extrude polar bodies. **(B)** Average securin FL::VFP (orange, n=21) and securin FxxF-A (green, n=18) on addition of reversine to inhibit MCC formation. Traces are aligned to reversine addition, however a second x-axis above the graph shows timing relative to average GVBD. Fine traces represent destruction profiles from individual oocytes, heavy traces represent the average destruction profile resulting from all injected oocytes for a given construct.

2012). To test this, a pool of oocytes was injected with an APC3 morpholino oligomer (MO), to knock down APC3 gene expression and thus inhibit APC/C activity (Nilsson et al. 2009), followed by a separate injection of securin FL. In these oocytes, securin degradation was drastically reduced in comparison with control securin FL oocytes (Fig. 5.3A). In a similar experiment Cdc20 levels were knocked down and gave a surprising result. Securin FxxF-A was completely stabilised, yet while the rate of securin FL destruction was reduced, destroyed over a 5 hour time period rather than 3 hours, it was still fully degraded (Fig. 5.3B). This suggests that early securin targeting is permitted at much lower concentrations of Cdc20, perhaps due to the high affinity of combining an FxxF motif with a D-box. In comparison, late D-box only degradation requires much higher levels of Cdc20 for APC/C targeting. Interestingly, when Cdc20 is knocked down by MO injection, securin FL is targeted for degradation ~2 hours ahead of securin FL in control oocytes (Fig 5.3B), yet polar body extrusion is blocked. This could be due to upregulation of Cdh1 in Cdc20 MO-injected oocytes, a situation in which the spindle checkpoint may be less able to prevent premature APC/C activation. However, this requires further investigation.

5.2.4 Meiotic securin destruction begins 2.5 hours ahead of separase activation in meiosis I mouse oocytes.

I hypothesise that early meiotic securin degradation represents destruction of a free pool of securin, targeted preferentially via a FxxF motif that is obscured when securin is bound to separase, thus preventing premature activation of separase while chromosomes are correctly aligning. Following this initial phase of destruction a second wave of securin destruction initiates 90 minutes ahead of PB1 extrusion. Here the D-box alone is sufficient to target securin for degradation, however the gradual activation of separase this far ahead of anaphase would be potentially catastrophic for faithful chromosome segregation. Separase activation from this early time point would lead to cohesin cleavage and homolog dissociation before the cell was ready to proceed into anaphase. We therefore reasoned that separase activity must still be delayed even after the 2nd wave of securin destruction is initiated.

To address this, the H2B-mCherry-Scc1$^{147-467}$-eGFP separase activity biosensor was used (Nam & van Deursen 2014) (Fig. 5.4C). The sensor is targeted to chromosomes via its histone H2B tag and shows a colour shift from yellow to red as separase becomes active and cleaves two cut sites within the Scc1 peptide, causing eGFP dissociation into the cytoplasm leaving only mCherry signal on the DNA. Separase activation was typically observed 20-30 minutes

A.

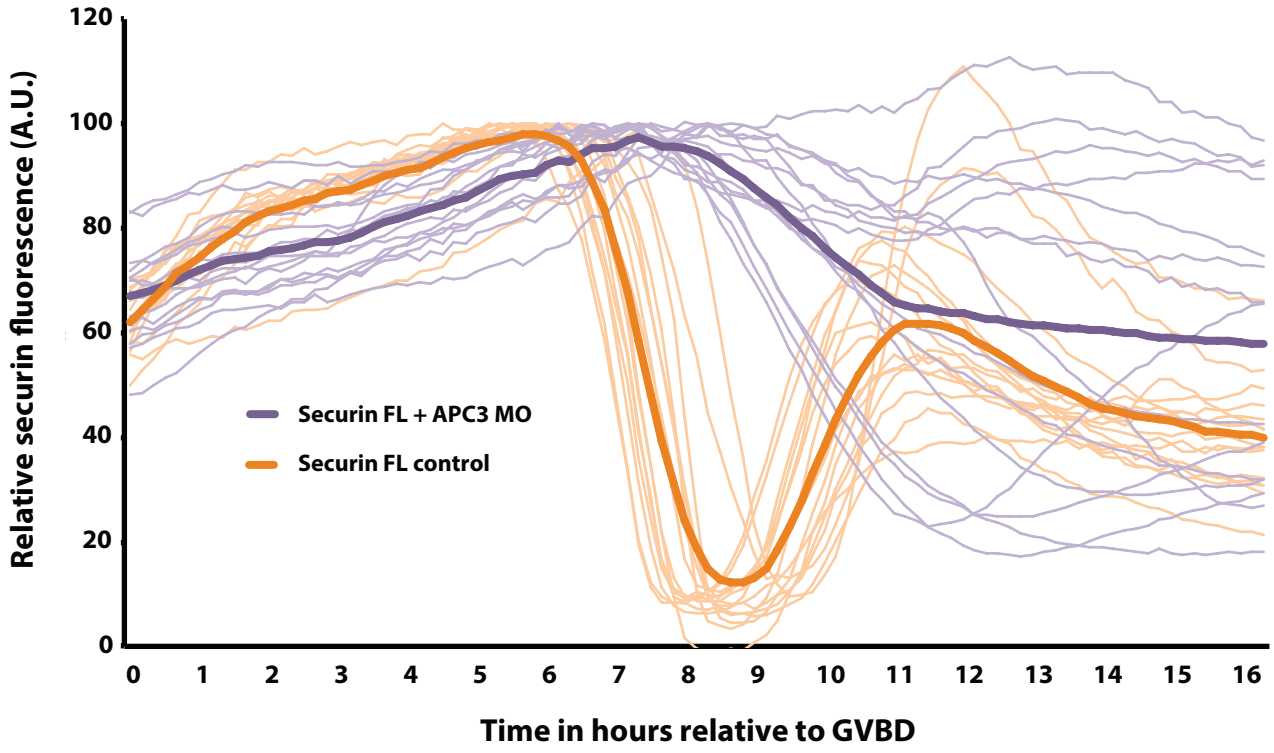

Figure 5.3. APC3 and Cdc20 levels are rate limiting for meiotic securin destruction. (A) Average securin FL::VFP (orange, n=16) and securin FL + APC3 morpholino oligomer (MO) (purple, n=15) destruction profiles aligned at GVBD. **(B)** Average securin FL + Cdc20 MO::VFP (orange, n=19), securin FxxF-A + Cdc20 MO (green, n=19) and control securin FL::VFP (orange dashed, n=16) destruction profiles aligned at GVBD. Traces were aligned at GVBD as both APC3 and Cdc20 MOs prevented polar body extrusion. Fine traces represent destruction profiles from individual oocytes, heavy traces represent the average destruction profile resulting from all injected oocytes for a given construct.

Figure 5.3

B.

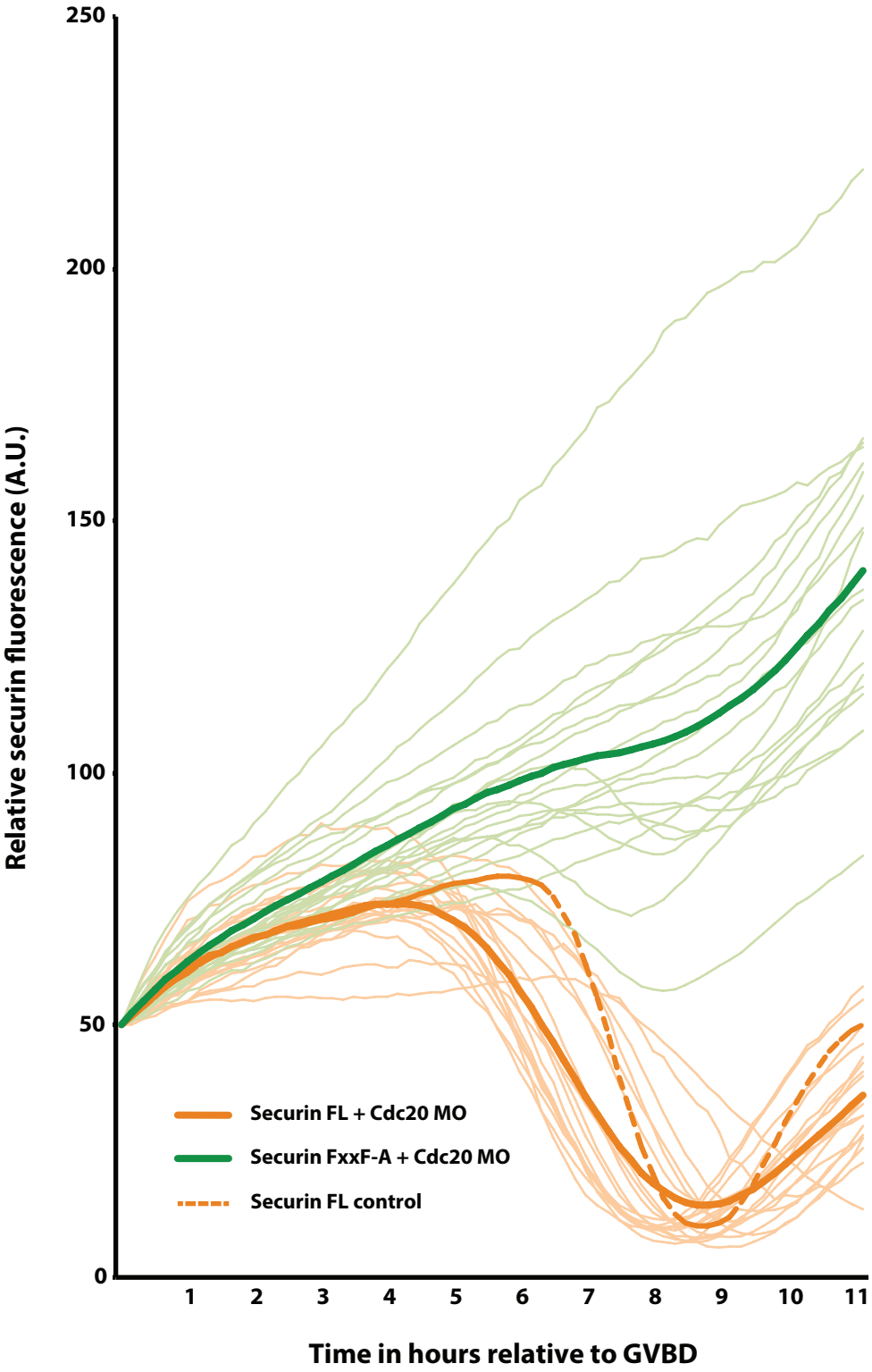
250
200
150
100
50
0
Relative securin fluorescence (A.U.)
1
2
3
4
5
6
7
8
9
10
11
Time in hours relative to GVBD
Securin FL + Cdc20 MO
Securin FxxF-A + Cdc20 MO
Securin FL control

Figure 5.4

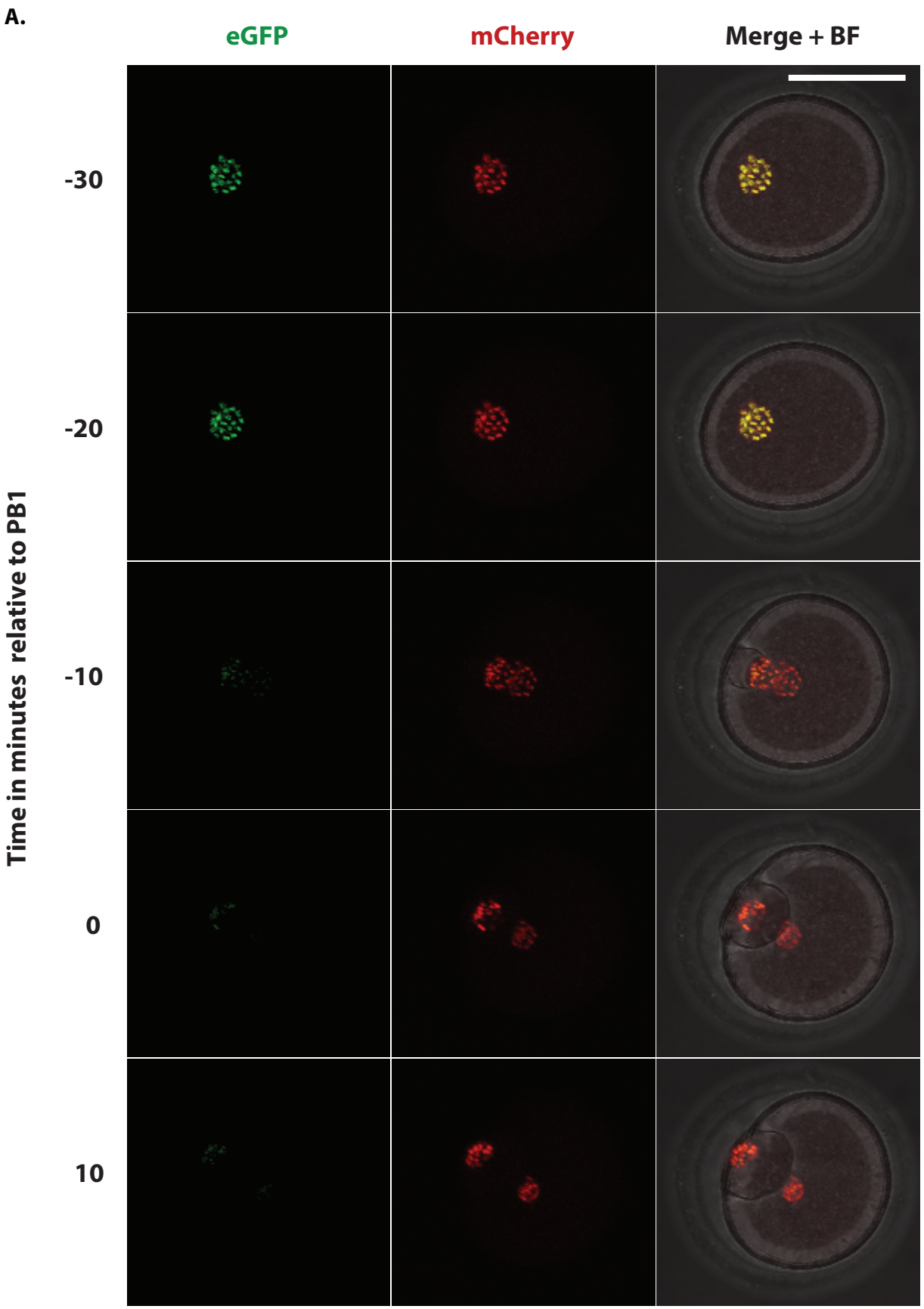
A.
eGFP
mCherry
Merge + BF
Time in minutes relative to PB1
-30
-20
-10
0
10

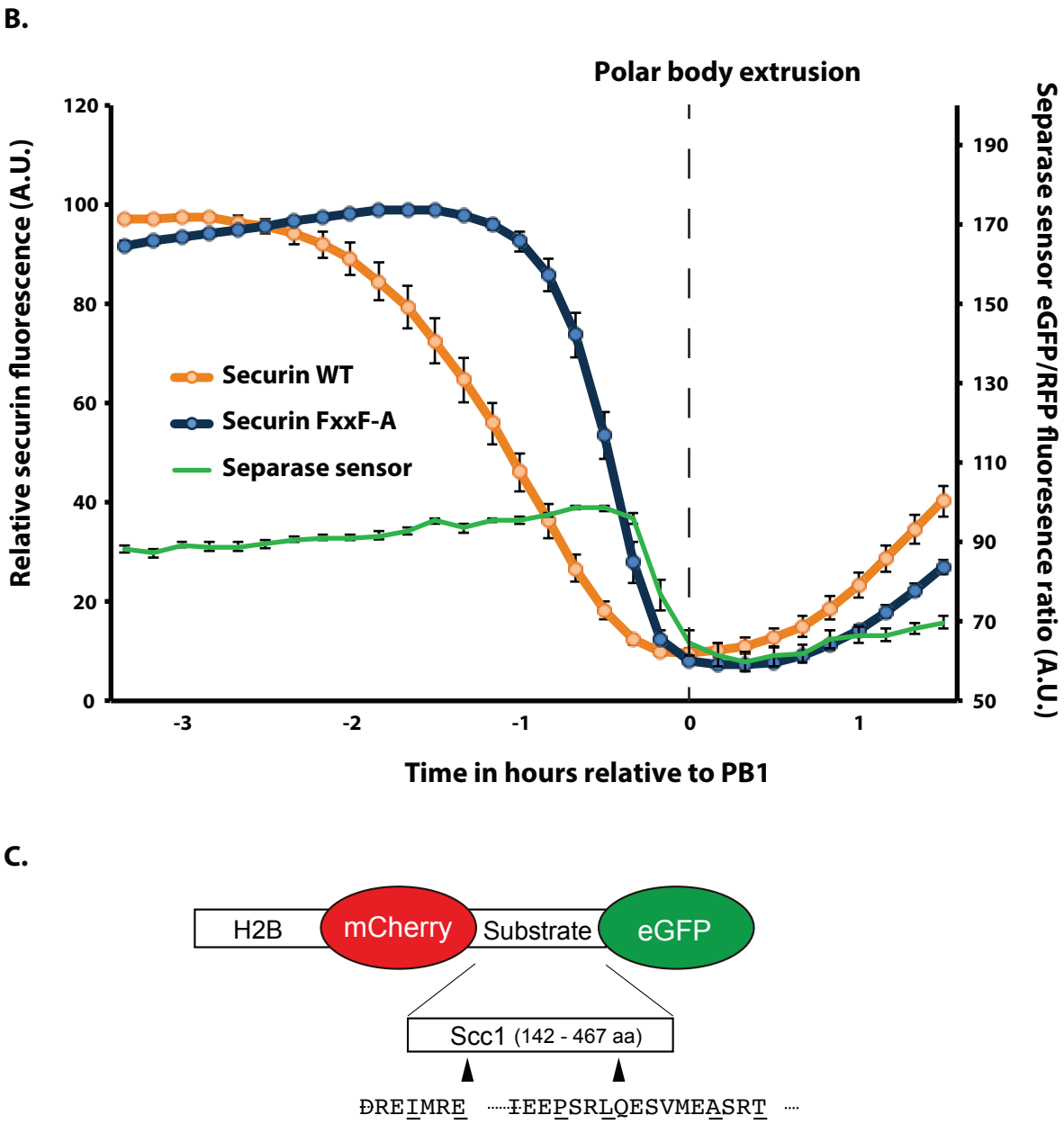

Figure 5.4. Prometaphase securin degradation begins 2.5 hours ahead of separase activation. (A) Time-lapse images of oocyte injected with a H2B-mCherry-Scc1-eGFP separase activity biosensor and imaged at 10 minute time intervals starting 5 hours after GVBD. Representative fluorescence (eGFP in green and mCherry in red) and bright field images are shown during the 50 minutes surrounding PB1 extrusion. Scale bars = 50µm. **(B)** Quantification of separase activity by measuring the average eGFP/mCherry fluorescence ratio from eggs injected with the separase biosensor (green, n= 20), plotted alongside average securin FL::VFP (orange, n=25) and securin FxxF-A::VFP (blue, n=20) destruction profiles produced by taking an average intensity reading from a defined region of interest around the oocyte, plotted over time and aligned at PB1 extrusion. Error bars = +/- SEM. **(C)** Schematic representation of separase activity biosensor adapted from Shindo et al. 2012.

ahead of polar body extrusion as can be seen in a representative oocyte (Fig 5.4A). This timing was confirmed by quantification of the eGFP/mCherry fluorescence ratio which showed that separase became active ~30 minutes ahead of polar body extrusion, 60 minutes after D-box only mediated destruction commences, with the majority of substrate cleavage taking place in the final 20 minutes Fig. 5.4B).

5.2.5 A securin phosphomutant does not significantly affect degradation timing in meiosis I mouse oocytes.

Given that 90 minutes prior to anaphase the D-box alone becomes sufficient to target securin for degradation, yet separase remains inactive for an hour subsequent to this suggests an additional layer of separase regulation once checkpoint signalling ceases. In mitosis, a pool of phosphorylated free securin is targeted for destruction preferentially ahead of a separase-bound securin pool protected by PP2A-mediated dephosphorylation (Hellmuth et al. 2014). I wanted to investigate whether similarly in oocytes the phosphorylation state of securin affects its degradation timing. To address this, 4 residues highlighted to be important for phosphorylation-dependent timing of mitotic securin degradation were replaced with alanines in both a wild-type and FxxF-A securin. Surprisingly neither phosphomutant, securin FL 4A or securin FxxF-A 4A showed a delayed degradation when compared to securin FL and FxxF-A respectively (Fig. 5.5A-B). Interestingly however, securin FxxF-A 4A was in fact targeted ~30 minutes ahead of securin FxxF-A, suggesting that phosphorylation may actually delay degradation in oocytes (as is the case in budding yeast (Lu et al. 2014)), however this would require further investigation to fully characterise (Fig. 5.5B).

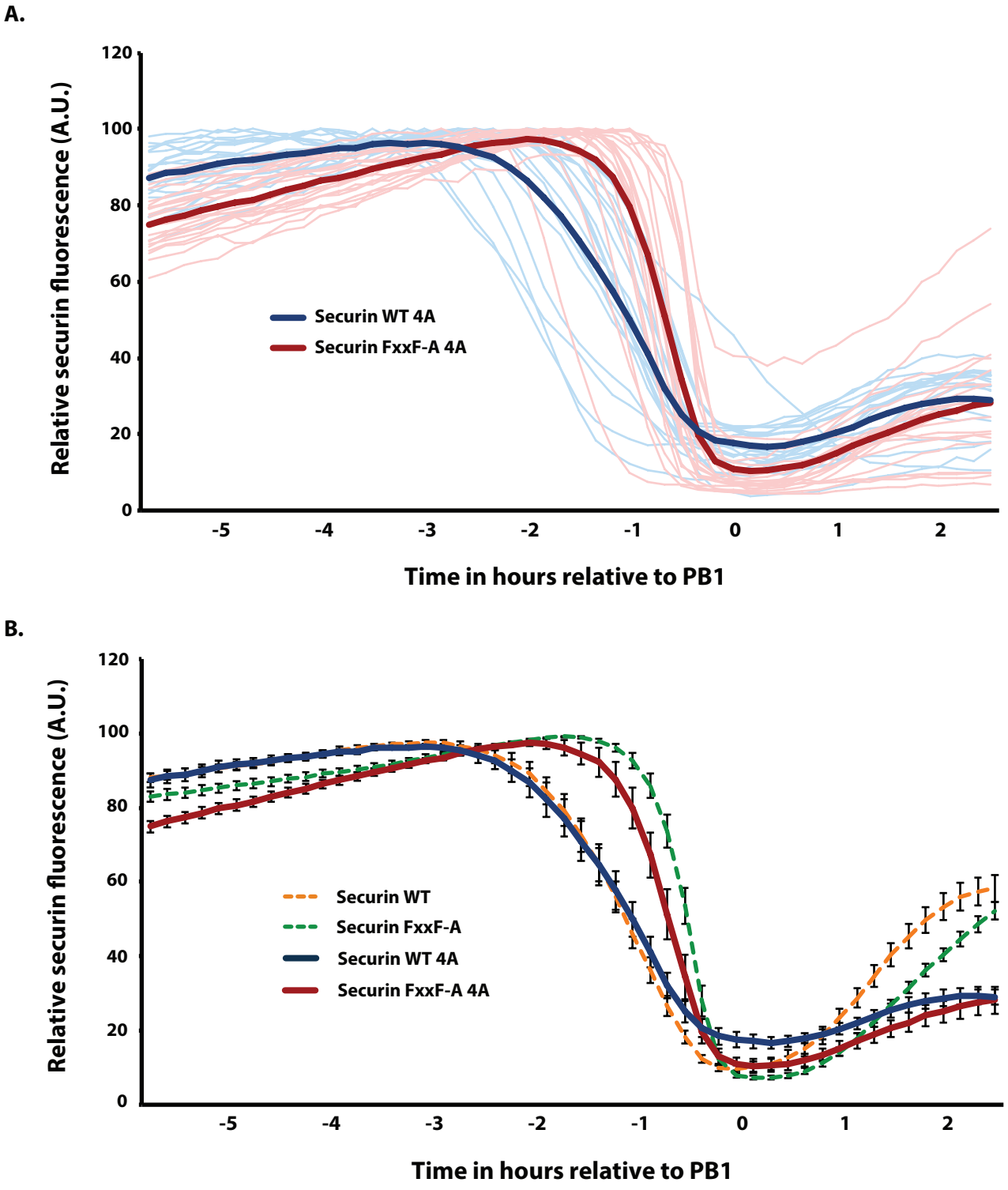

Figure 5.5. A securin phosphomutant does not significantly affect degradation timing in meiosis I mouse oocytes. (A) Average securin WT 4A::VFP (blue, n=17) and securin FxxF-A 4A::VFP (red, n=20) destruction profiles aligned at PB1 extrusion. Fine traces represent destruction profiles from individual oocytes, heavy traces represent the average destruction profile resulting from all injected oocytes for a given construct. **(B)** Average securin WT 4A::VFP (blue, n=17), securin FxxF-A 4A::VFP (red, n=20), securin WT::VFP (orange dashed, n=25) and securin FxxF::VFP (green dashed, n=20) destruction profiles aligned at PB1 extrusion. Error bars = +/- SEM.

5.3 Discussion

Meiotic securin destruction in mouse oocytes is biphasic; consisting of an initial phase during late prometaphase in which free securin is targeted preferentially via a FxxF motif ahead of separase-bound securin in which the FxxF motif is masked in the interface between securin and separase (chapter 4). This is followed by a second phase of destruction initiating 90 minutes ahead of polar body extrusion where the D-box alone is sufficient.

In APC3 knockdown oocytes, securin degradation was drastically reduced in line with the APC/C being the primary E3 ubiquitin ligase mediating meiotic degradation (Fig. 5.3A). To investigate how securin's known APC/C degrons, namely the KEN box and D-box, function alongside the FxxF motif to mediate prometaphase I destruction, securin constructs were tested with either KEN box or D-box mutations or both combined. It was observed that contrary to a previous report (Herbert et al. 2003), when only the D-box is mutated, the KEN box is able to direct minimal degradation. This is not observed in the double KEN/D-box mutant (Fig. 5.1C-D). Unlike in mitotic cells, there was no time delay associated with this switch from D-box to KEN box mediated destruction (Hagting et al. 2002). This could suggest that Cdh1 may not be as strongly inhibited prior to anaphase as it is in mitotic cells where a D-box mutant securin is only targeted for degradation following anaphase once Cdk1-mediated Cdh1 inhibition ceases and the APC/C switches co-activators from Cdc20 to Cdh1 (Hagting et al. 2002). Indeed APC/C-Cdh1 has been shown to moderate the rate of Cdk1 activation prior to GVBD in mouse oocytes, suggesting that especially in early prometaphase, there may be more Cdh1 available to activate the APC/C when compared to that in mitotic cells (Reis et al. 2007; Rattani et al. 2017). Despite this, securin destruction in mouse oocytes was observed to be largely D-box dependent, as a KEN box mutation had no significant effect on destruction profile (Fig. 5.1D). This suggests that securin degradation during late prometaphase in mouse oocytes requires both D-box interaction with the bipartite receptor on APC-Cdc20 and the FxxF motif in order to bypass an active checkpoint and present itself as an APC/C substrate. Other examples of prometaphase APC/C substrates able to bypass an active checkpoint include Nek2A and cyclin A (Zon & Wolthuis 2010). While Nek2A targeting is Cdc20-independent and mediated via direct interaction with the APC/C, cyclin A must liberate Cdc20 from the MCC prior to APC/C activation (Hayes et al. 2006; Di Fiore & Pines 2010). Liberation of Cdc20 is achieved via an ABBA motif within the N-terminus of cyclin A which outcompetes a similar motif in BubR1 for Cdc20 binding, thus freeing Cdc20 from the MCC and activating the APC/C during an active checkpoint.

Interestingly, the FxxF motif shows high sequence similarity to the ABBA motifs identified in cyclin A, BubR1 and Bub1. This will be further explored in chapter 6.

Our hypothesis that the FxxF motif is involved in Cdc20 liberation from the MCC, allowing an APC10/Cdc20 D-box receptor to form during an active checkpoint is further strengthened by observations made in nocodazole-treated oocytes. When oocytes were incubated with nocodazole to depolymerise microtubules and stimulate the checkpoint, a wild-type securin construct was still fully degraded despite the fact that anaphase was blocked. In comparison a mutant construct lacking the FxxF motif was largely stabilised (Fig. 5.2A), evidence that the late prometaphase degradation of securin is not simply due to an inefficient checkpoint, but instead is a controlled mechanism. The FxxF motif functions to bypass an active checkpoint that would otherwise be sufficient to block D-box only mediated degradation since securin FxxF-A is stable in nocodazole treated oocytes.

Morpholino oligo knockdown of Cdc20 reduced securin degradation, however not to the same extent as APC3 knockdown. In Cdc20 knockdown oocytes, wild-type securin was fully degraded yet with much slower degradation dynamics whilst securin FxxF-A mutant was mostly stabilised with only small amounts of degradation observed in certain eggs (Fig. 5.3B). Early securin degradation relying on both the FxxF motif and the D-box is less sensitive to situations where Cdc20 levels are limited, suggesting that perhaps both degrons combined have a higher binding affinity. This leads to the hypothesis that requirement of both an FxxF motif and a D-box for late prometaphase securin destruction would suggest that the destruction machinery mediating this is APC/C-Cdc20, as it is between APC10 and the WD40 domain of Cdc20 that the bipartite D-box receptor is formed (Chao et al. 2012).

The possibility cannot be ruled out that when Cdc20 is knocked down there is the potential for Cdh1 upregulation in order to substitute as primary APC/C co-activator during meiosis I, however further analysis including quantification of relative Cdc20 and Cdh1 levels following MO treatment is required and currently the only conclusion that can be drawn is that Cdc20 is indeed rate limiting for meiotic securin degradation.

While meiotic securin destruction is initiated 3 hours ahead of the first polar body extrusion in mouse oocytes, using a separase biosensor I demonstrate that activation of separase is only observed 20-30 minutes before anaphase (Fig. 5.4A-C). Though it makes sense that separase would only become active over a short time period preceding polar body extrusion, the mechanisms that keep separase inhibited for a further hour after the D-box becomes a sufficient securin degradation signal remain a point of interest. In mitotic cells, securin

phosphorylation serves to protect against premature separase activation. Separase-bound securin is kept in a dephosphorylated state by PP2A and thus protected, while free securin is phosphorylated and thus preferentially targeted for degradation (Hellmuth et al. 2014). However, when these phosphorylation sites were mutated to alanines in a securin FxxF-A mutant, mimicking the dephosphorylated state of mitotic protected separase-bound securin, it was found that rather than being delayed, degradation instead began ~30 minutes ahead of securin FxxF-A (Fig 5.5A-B). This suggests that when securin is phosphorylated, degradation timing may in fact be delayed, a phenomenon previously observed in budding yeast (Lu et al. 2014) but at odds with current mitotic data.

Further clues as to how separase inhibition may be protected after checkpoint signalling reaches a minimum come from oocytes treated with reversine to remove MCC assembly. Even in oocytes lacking an active spindle checkpoint, wild-type securin was consistently targeted for degradation an hour ahead of securin FxxF-A, suggesting that even after checkpoint signalling has ceased, any excess free securin in which both the FxxF motif and D-box are visible will still be targeted preferentially, thus further delaying the point at which separase-bound securin becomes a target for APC/C-mediated degradation. However this potential mechanism for separase protection would only work if there was a sufficient excess of free securin remaining after the initial phase of destruction. Quantification of securin:separase ratio in oocytes is currently under investigation, with initial results suggesting a large excess of securin in oocytes matured for 6 hours post GVBD (data not shown). Following quantification, I intend to use the separase biosensor in securin MO-injected oocytes to investigate how the timing of separase activation varies in a separase knockdown background.

Preliminary imaging data shows securin to be localised throughout the cytoplasm yet absent from chromosomes prior to anaphase onset (data not shown). It is therefore of future interest whether securin-separase complex localisation could play a role in this delayed activation, in which separase relocalisation to chromosomes would be required following the removal of securin-mediated inhibition. To probe this idea, the separase biosensor could be targeted to the cell membrane to investigate whether separase activity is observed with different timing away from chromosomes.

Chapter 6: Cyclin A2 and APC/C processivity in meiosis I.

6.1 Introduction

In chapter 5 it was shown that late prometaphase securin destruction is mediated by both the FxxF motif and the D-box, which work together to permit degradation in the presence of an active checkpoint. Furthermore, it was shown that both APC/C activity and Cdc20 levels were rate limiting to this process. However is was not clear from these experiments how the FxxF motif works alongside the D-box to permit degradation when a D-box alone is insufficient. In this chapter, I will address the possibility that the FxxF motif could be behaving in a similar way to the ABBA motif of cyclin A, a theory based on a high degree of sequence similarity and the relative spatial positioning of the two degrons. I also discuss the potential functionality of a conserved PM motif within cyclin A2, given that a sequence within cyclin A shows homology to the prometaphase APC/C degron identified in cyclin B1 (presented in chapter 3).

Through ubiquitin-mediated hydrolysis, the anaphase promoting complex or cyclosome (APC/C) targets specific substrates for proteolysis at specific times to drive ordered mitotic progression (Pines 2006). In mitosis, the multi-subunit APC/C has a number of prometaphase (Cyclin A, Nek2A and HOXC10), metaphase (Cyclin B and securin) and later substrates (Cdc20, Plk1 and the Aurora kinases) (see Pines 2006 for review). How the same ubiquitin ligase targets each specific substrate at a specific time is still not fully clear even in mitosis and involves a complex balance of a number of factors. These include phosphorylation, co-activator abundance, subcellular localisation, relative substrate abundance, degrons and inhibitor binding (see Sivakumar & Gorbsky 2015 for review).

The APC/C is largely inactive without one of its co-activators; Cdc20 and Cdh1. The presence and position of these co-activators is one of the best known decisive factors in influencing substrate specificity (Vodermaier 2001). Cdh1 is largely responsible for APC/C co-activation in early G1 phase and late M phase of the cell cycle (Pines 2006). However once the cell enters mitosis, cyclin B1-Cdk1 phosphorylation of APC/C subunits, APC3 and APC1, prevents Cdh1 binding and primes the APC/C for Cdc20 co-activation (Fujimitsu et al. 2016). When in complex with Cdc20, the APC/C primarily targets substrates through formation of a putative bipartite destruction box (D-box) receptor between Cdc20 and APC10

(Chao et al. 2012), whereas APC-Cdh1 is able to target substrates with either a D-box or KEN box and does not require a phosphorylated APC/C (Kramer et al. 2000).

In mitosis, the APC/C complexes with Cdc20 until a point when cyclin B1- Cdk1 activity falls and as a result the APC/C loses its priming phosphorylation for Cdc20 binding. At this point there is a switch back towards APC/C co-activation by Cdh1 and Cdc20 itself becomes a target for degradation (Pfleger & Kirschner 2000). Loss of Cdc20 from mitotic cells causes stabilisation of cyclin B1 and securin and results in metaphase arrest (Li et al. 2007; Wolthuis et al. 2008), Cdh1 depletion stabilises the Aurora kinases and causes premature S-phase entry (Floyd et al. 2008). While chromosomes are still aligning during prometaphase both APC/C co-activators are suppressed. The spindle checkpoint acts to inhibit Cdc20, and Cdh1 is inhibited by high cyclin B1-Cdk1 activity. Despite this, the APC/C is still active from very early on in mitosis. Cyclin A, Nek2a and HOXC10 are all degraded rapidly in prometaphase as soon as the nuclear envelope breaks down (NEBD) (Elzen & Pines 2001; Geley et al. 2001; Gabellini et al. 2003; Hayes et al. 2006).

Cyclin A binds to Cdc20 during early mitosis and is targeted to the phosphorylated APC/C in early prometaphase as a Cdc20-Cyclin A2-Cdk2-Cks1 complex (Wolthuis et al. 2008), through the direct binding of Cks1 to phosphorylated APC3 subunits (Di Fiore & Pines 2010; Zon & Wolthuis 2010). Via its ABBA motif, cyclin A2 outcompetes BubR1 for a binding site on Cdc20, rendering cyclin A an APC/C target at a time when the spindle checkpoint is still actively sequestering both APC/C-bound and free Cdc20 (Di Fiore et al. 2016).

While it is clear there is a role for Cks1 in this early degradation, it is not yet fully defined. In one report, when both Cks1 and Cks2 were knocked down using shRNA, cyclin A2 appeared to be stabilised by immunoblot (Wolthuis et al. 2008). However in another study, Di Fiore and Pines instead observe that when cyclin A2 is truncated to its first N-terminal 165 residues (a length lacking the cyclin folds involved in Cdk-binding and thus Cks1 association) it is still targeted for destruction, only this time 20 minutes after NEBD and WT cyclin A2 targeting, yet still 20-25 minutes ahead of anaphase onset (Di Fiore & Pines 2010). Wild-type destruction is then recovered when cyclin A2 N165 is artificially fused to Cks1 (Di Fiore & Pines 2010).

Although depleting Cdc20 largely stabilises cyclin A2 (Di Fiore & Pines 2010), Nek2A degradation is unaffected (Boekhout & Wolthuis 2015). Nevertheless, though direct Cdc20 binding is not required for Nek2A destruction, catalytic activation of the APC/C by Cdc20 at the beginning of the prophase to prometaphase transition is essential (Boekhout & Wolthuis

2015). Nek2A binds directly to TPR motifs in APC/C subunits through its C-terminal MR tail (Hames et al. 2001) and therefore does not require Cdc20 binding to be recruited to the APC/C.

In this chapter the aim was to investigate how cyclin A is regulated in mouse meiosis I and in so doing provide insight to the mechanisms by which cyclin B1 and securin are able to evade the checkpoint in late prometaphase I.

6.2 Results

6.2.1 The FxxF motif in securin resembles an ABBA motif in both positioning and sequence.

The FxxF motif in securin and the PM motif in cyclin B1 both work alongside a D-box to permit APC/C-Cdc20 mediated destruction simultaneously in late prometaphase I (chapters 3 and 4, Levasseur et al. 2017 unpublished). However, other than the seemingly identical temporal degradation profiles, the motifs themselves have very little similarity. While the FxxF motif and the PM motif share no obvious sequence homology, sequence alignment of the region containing the FxxF motif in securin orthologs alongside the ABBA motif-containing regions of cyclin A1, cyclin A2 and BubR1 revealed multiple common features. For the purpose of exploring the similarity between the motifs, investigation was focused on cyclin A2, as this is the primary A-type cyclin expressed in the female germline (Touati et al. 2012).

Both the FxxF motif in securin and the ABBA motif in cyclin A2 typically center around two aromatic residues, either phenylalanine, tyrosine or histidine, in positions 1 and 4, with an upstream proline rich region and a downstream acidic region (Fig. 6.1A). Furthermore, both the FxxF motif of securin and the ABBA motif of cyclin A2 are found in unstructured regions ~50 amino acids downstream of the D-box, while the PM motif of cyclin B1 is located within the N-terminal Helix and is ~120 amino acids downstream of the D-box (Fig. 6.1B).

Due to these common features it became a primary interest to explore how cyclin A2 was regulated in meiosis and if in fact the FxxF motif in securin was working to directly liberate Cdc20 from MCC sequestration via a similar mechanism to the ABBA motif of cyclin A2 in mitosis (Di Fiore et al. 2015).

6.2.2 Cyclin A2 degradation in mouse oocytes begins in early prometaphase I and relies on the Cdk-binding cyclin box/folds.

To investigate the regulation of cyclin A2 in meiosis, initially two constructs were tested, a full-length cyclin A2 (cyclin A2 FL) and a truncated version of cyclin A2 containing only the first N-terminal 165 residues (cyclin A2 N165, Fig. 6.2A). Both constructs contain the D-box and ABBA motif, however cyclin A2 N165 critically lacks the cyclin box/folds essential for Cdk binding (Di Fiore & Pines 2010). Cyclin A2 FL was consistently targeted from early

A.

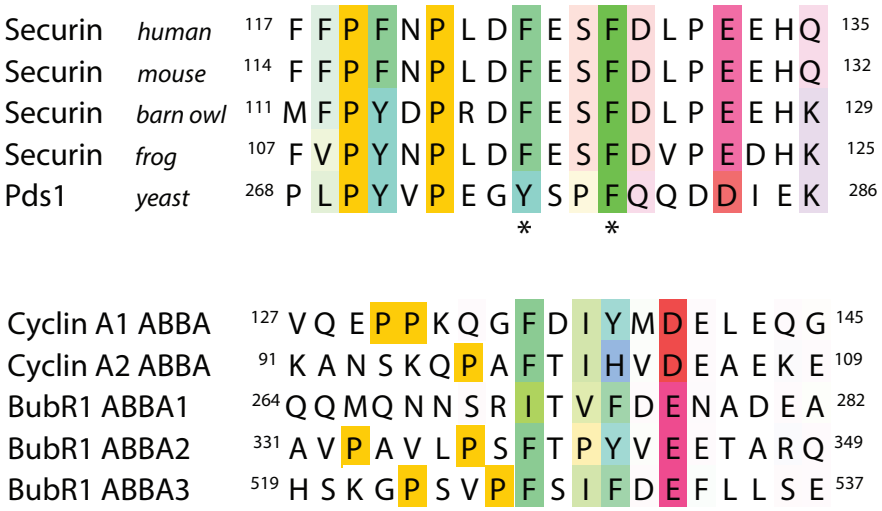

B.

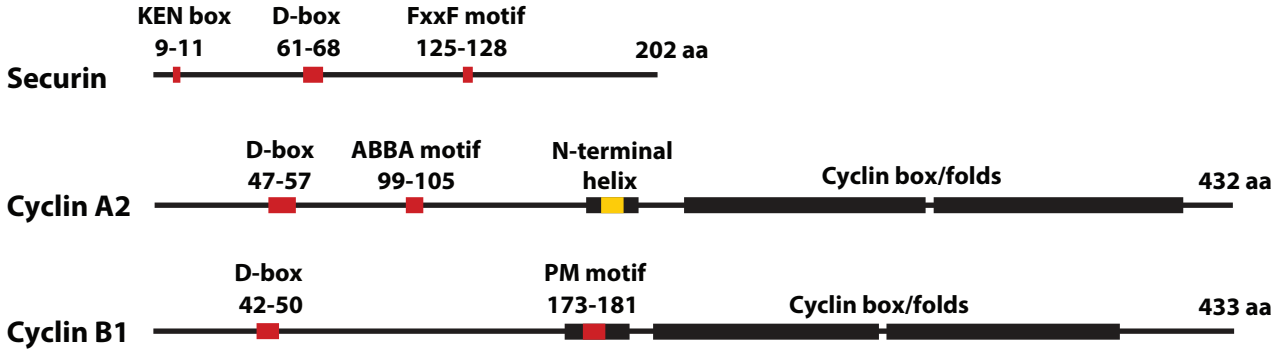

Figure 6.1. The FxxF motif in securin resembles an ABBA motif in both positioning and sequence. (A) Alignment of FxxF motif-containing region in securin orthologs alongside ABBA motif-containing regions from human cyclin A1, cyclin A2 and BubR1. (**B)** Schematic representation showing relative positioning of APC/C degrons within securin, cyclin A2 and cyclin B1. Major structural features are represented by a thick black line, unstructured regions by a thin black line and known degrons highlighted in red. A potential PM motif in cyclin A2 is highlighted in yellow and will be discussed later. All features are to scale.

Figure 6.2

A.

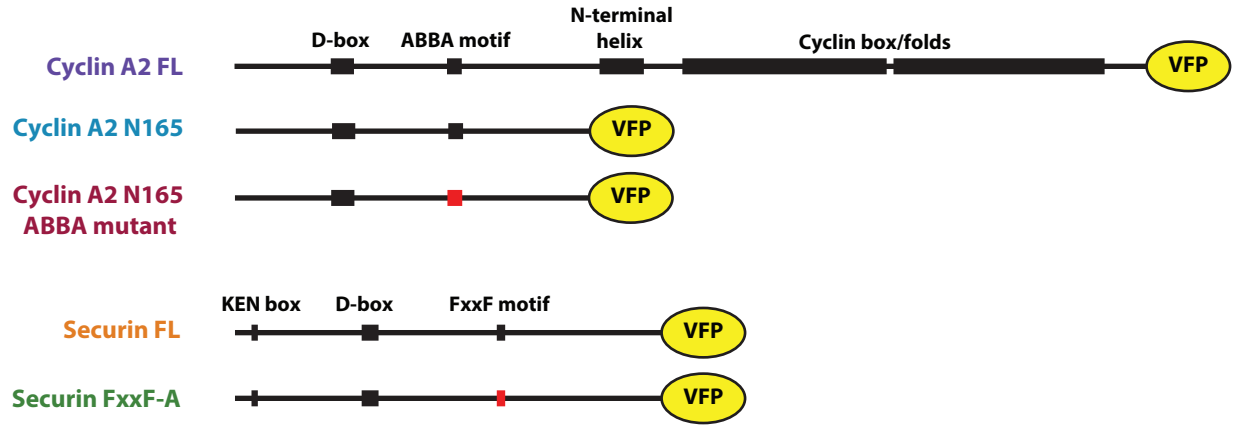

B.

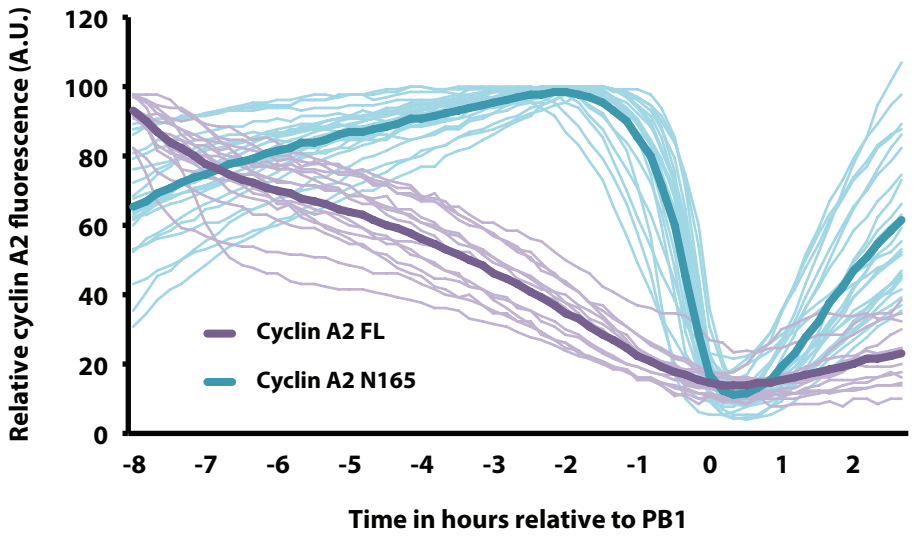

C.

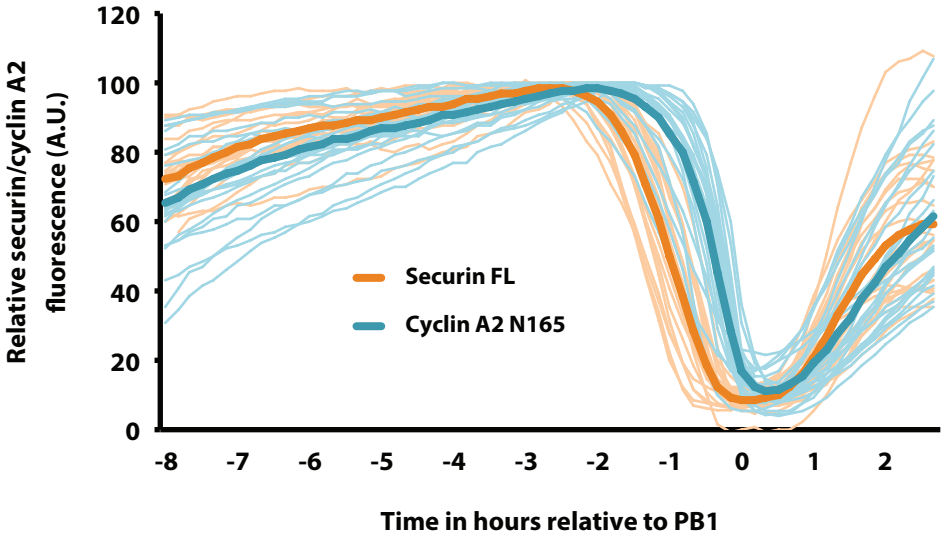

D.

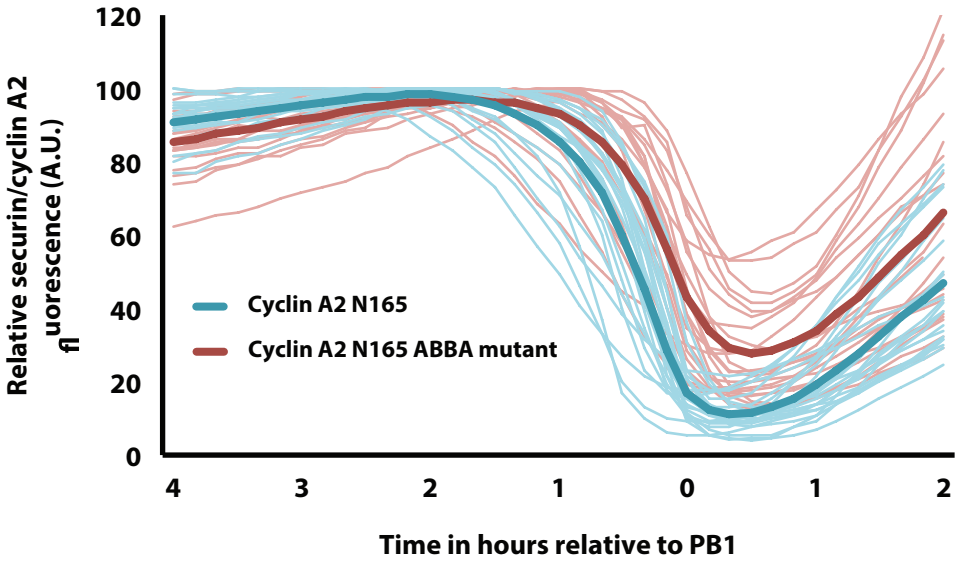

Figure 6.2. The D-box and ABBA motif of cyclin A2 are not sufficient for early prometaphase degradation in meiosis. (A) Schematic showing VFP-tagged cyclin A2 and securin truncations and mutations. **(B)** Average cyclin A2 FL::VFP (purple, n=22) and cyclin A2 N165::VFP (light blue, n=26) destruction profiles aligned at PB1 extrusion. **(C)** Average securin FL::VFP (orange, n=25) and cyclin A2 N165::VFP (light blue, n=26) destruction profiles aligned at PB1 extrusion. **(D)** Average cyclin A2 N165::VFP (light blue, n=26) and cyclin A2 N165 ABBA mutant::VFP (red, n=22) destruction profiles aligned at PB1 extrusion. Fine traces represent destruction profiles from individual oocytes, heavy traces represent the average destruction profile resulting from all injected oocytes of a given contsruct.

prometaphase and had a relatively slow rate of degradation over a period of ~8 hours, eventually reaching a minimum in time with PB1 extrusion (Fig. 6.2B). In contrast, cyclin A2 N165 was completely stable during early prometaphase and only began to be degraded ~2 hours ahead of PB1 extrusion. Therefore the D-box and ABBA motif together are not sufficient to mediate early prometaphase I degradation of cyclin A2. Furthermore, when cyclin A2 N165 was injected alongside securin FL, it was observed that securin was the preferred substrate as N165 degradation began ~1 hour after securin FL (Fig. 6.2C). Interestingly, a cyclin A2 N165 construct lacking its ABBA motif (cyclin A2 N165 ABBA mutant) was targeted for degradation approximately an hour after N165, demonstrating that the ABBA motif does function at this late stage (Fig. 6.2D).

6.2.3 Cks1 binding is required for early prometaphase cyclin A2 destruction in mouse oocytes.

The regions containing the FxxF motif in securin and the ABBA motif in cyclin A2 show strong sequence homology (Fig. 6.2A) and indeed when cyclin A2 is truncated to N165, a construct far more similar to securin (a largely unstructured protein unable to bind Cdk1, yet still containing the D-box and additional degrons), it instead became a target for degradation only 2 hours ahead of PB1 extrusion (Fig. 6.2B). This suggests that rather than a difference in degrons, the dramatic timing difference between cyclin A2 and securin targeting (~5.5 hours) is largely due to the fact cyclin A2 can associate with a Cdk and therefore be targeted to the APC/C via Cks1.

In mitotic cells, early prometaphase cyclin A2 degradation is enabled by Cks1 interaction through Cdk2, which targets cyclin A2 to the phosphorylated APC/C early in mitosis (Wolthuis et al. 2008; Di Fiore & Pines 2010). To test whether the difference in degradation timings between cyclin A2 and securin was in fact largely due to Cks1 targeting of cyclin A2 to the APC/C, a number of Cks1-linked constructs were made (Fig 6.3A). Linking cyclin A2 N165 to Cks1 with a short neutral linker (cyclin A2 N165-Cks1) brought forward destruction which now began as early as 7 hours ahead of PB1 extrusion. Thereby partially rescuing the early prometaphase degradation of cyclin A2 FL (Fig 6.3B). This early degradation was however more gradual than cyclin A2 FL during early prometaphase. Cyclin A2 N165-Cks1 instead showed an increased rate of destruction in the last 4 hours before PB1 extrusion, this is in contrast to cyclin A2 FL where the rate of destruction is largely constant (Fig 6.3B).

Figure 6.3

A.

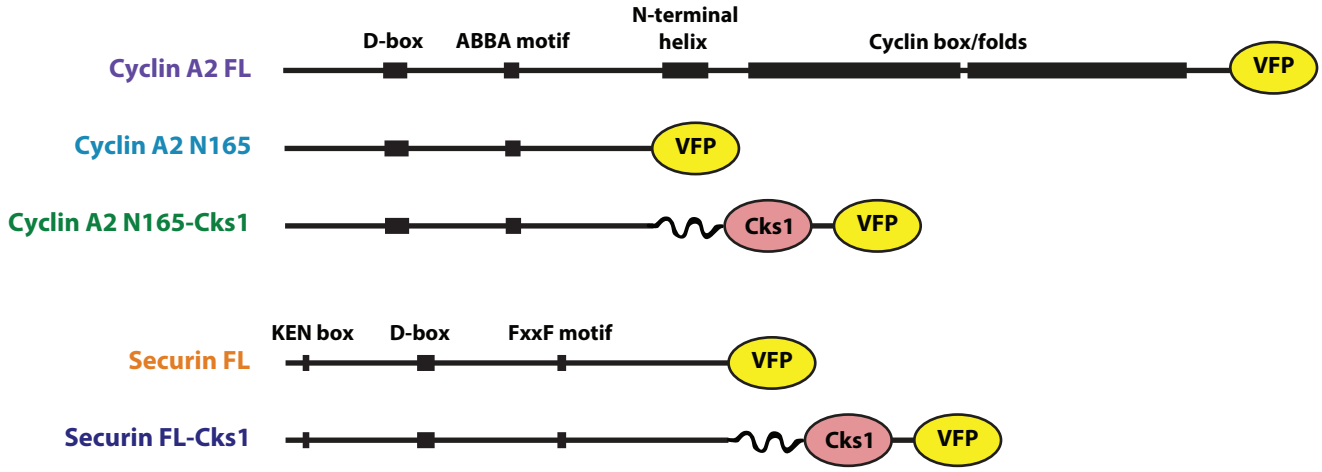

B.

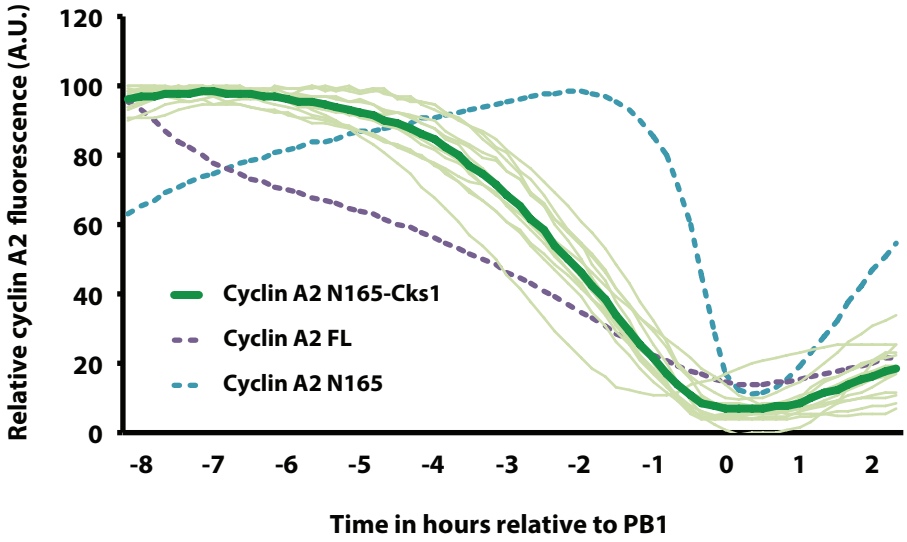

C.

Cks1 WT	118	E	Y	R	H	V	M	L	P	K	D	I	A	K	L	V	P	K	T	H	L	M	S	E	S	E	W	R	N	L	G	147
Cks1 APC/C binding mutant	118	E	Y	A	H	V	M	L	P	K	D	I	A	K	L	V	P	K	T	H	L	M	S	E	S	E	W	R	N	L	G	147
Cks1 APC/C + Skp2 binding mutant	118	E	Y	A	H	V	M	L	P	K	D	I	A	K	L	V	P	K	T	H	L	M	S	E	E	E	W	R	R	L	G	147

Figure 6.3

D.

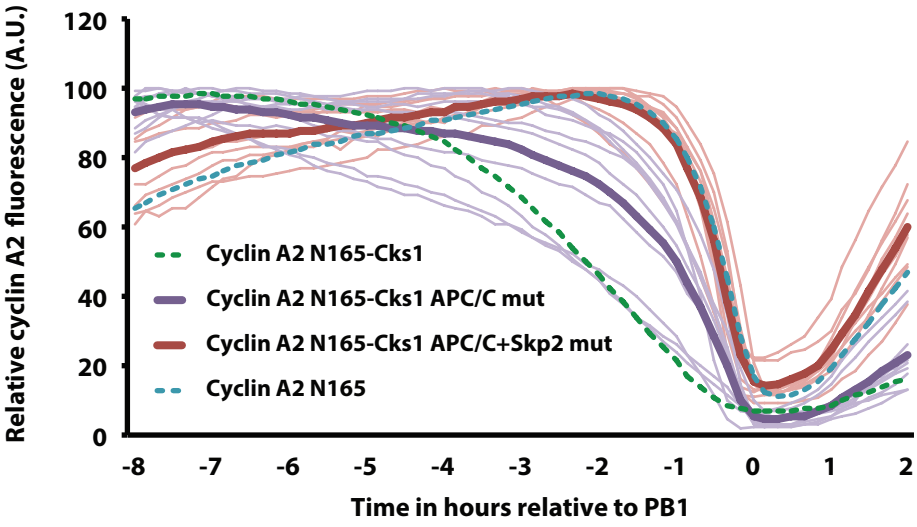

E.

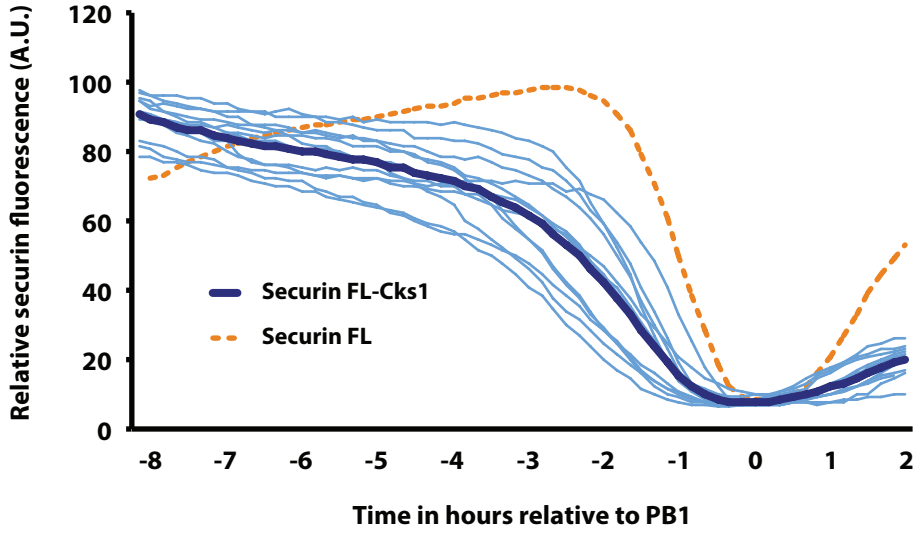

F.

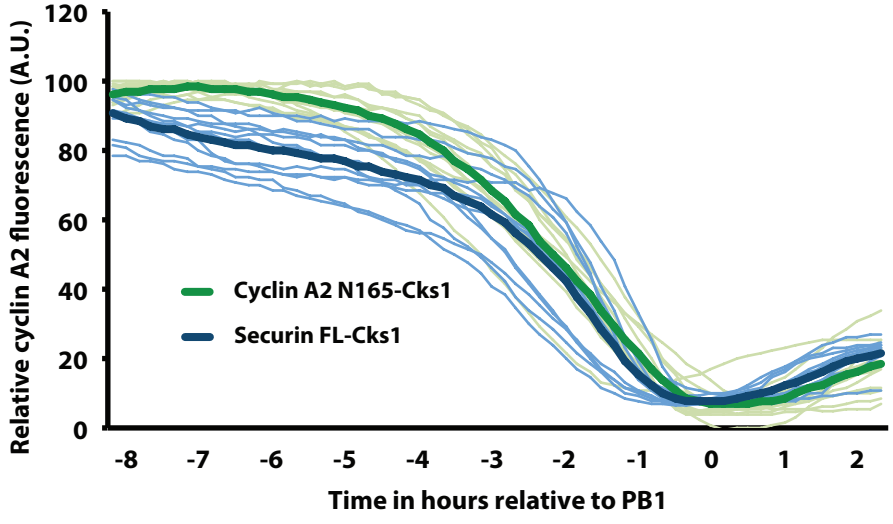

G.

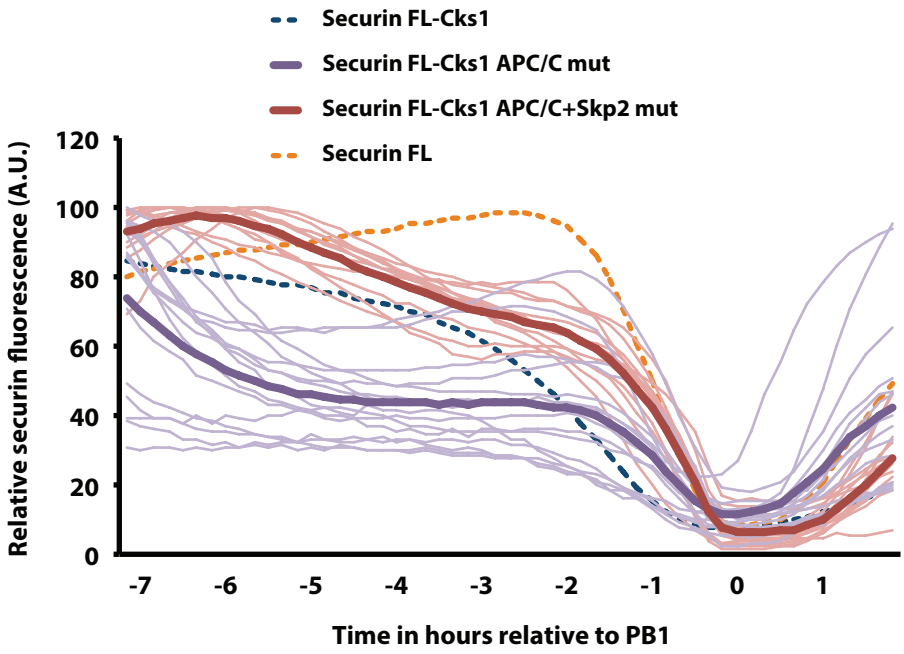

Figure 6.3. Cks1 binding is required for early prometaphase cyclin A2 destruction in oocytes. (A) Schematic showing VFP-tagged cyclin A2 and securin truncations and mutations alongside Cks1-linked constructs. **(B)** Average cyclin A2 N165-Cks1::VFP (green, n=12), cyclin A2 FL::VFP (purple dashed, n=22) and cyclin A2 N165::VFP (light blue dashed, n=26) destruction profiles aligned at PB1 extrusion. **(C)** Cks1 residues 118-147 sequence detail showing the nomenclature of Venus-tagged Cks1 mutations. **(D)** Average cyclin A2 N165-Cks1::VFP (green dashed, n=12), cyclin A2 N165-Cks1 APC/C mutant::VFP (purple, n=15), cyclin A2 N165-Cks1 APC/C+Skp2 mutant::VFP (red, n=9) and cyclin A2 N165::VFP (light blue dashed, n=26) destruction profiles aligned to PB1 extrusion. **(E)** Average securin FL-Cks1::VFP (dark blue, n=12) and securin FL::VFP (orange dashed, n=25) destruction profiles aligned at PB1 extrusion. **(F)** Average cyclin A2 N165-Cks1::VFP (green, n=12) and securin FL-Cks1::VFP (dark blue, n=12) destruction profiles aligned at PB1 extrusion. **(G)** Average securin FL-Cks1::VFP (dark blue dashed, n=12), securin FL-Cks1 APC/C mutant::VFP (purple, n=15), securin FL-Cks1 APC/C+Skp2 mutant::VFP (red, n=13) and securin FL::VFP (orange dashed, n=25) destruction profiles aligned to PB1 extrusion. Fine traces represent destruction profiles from individual oocytes, heavy traces represent the average destruction profile resulting from all injected oocytes of a given contruct.

To test whether linking cyclin A2 N165 to Cks1 caused early degradation by specific targeting to the phosphorylated APC/C during early prometaphase and not through interfering with protein structure for example, the anion-binding site in Cks1 was mutated (Cks1 APC/C binding mutant; Watson et al. 1996; Fig.6.3C). Cyclin A2 N165-Cks1 APC/C mutant was targeted for degradation at a slower rate than cyclin A2 N165-Cks1, yet some degradation still took place from early prometaphase (Fig. 6.3D). I hypothesised that this persisting degradation could be due to the previously reported Cks1 association with Skp2, the F-box protein component of the SCF E3 ubiquitin ligase (Sitry et al. 2002). Indeed, when both the anion-binding site and two residues highlighted to be important in Skp2-binding (Sitry et al. 2002) were mutated together (A2 N165-Cks1 APC/C+Skp2 mutant; Fig. 6.3C), destruction was observed in time with cyclin A2 N165 (Fig. 6.3D).

I reasoned that if Cks1 was able to permit ABBA-mediated cyclin A2 destruction from early prometaphase even without Cdk interaction, then fusing Cks1 to securin may also allow for early prometaphase degradation. Indeed, securin FL-Cks1 degradation consistently began from GV stage and continued at a similar rate until ~4 hours ahead of PB1 extrusion when the rate increased, reaching a minimum in time with polar body extrusion (Fig. 6. 3E). While securin FL-Cks1 was targeted from GV stage, ahead of cyclin A2 N165-Cks1, from mid to late prometaphase the two constructs show similar destruction profiles (Fig. 6.3F).

Surprisingly however, when securin FL-Cks1 was mutated at the Cks1 anion-binding site (securin FL-Cks1 APC/C mutant), rather than simply a reduced early degradation (as in the case of cyclin A2 N165-Cks1 APC/C mutant) the construct was instead rapidly degraded to 50% by 5 hours ahead of PB1 extrusion (Fig. 6.3G). How inhibiting the APC/C interaction could actually make this protein a better substrate is very interesting. I hypothesised that again this may be due to Cks1 interaction with Skp2 and subsequent SCF-mediated degradation. Perhaps by removing the capacity for Cks1 interaction with the APC/C, this increases the portion of the construct targeted to Skp2. Increased initial degradation may be due to the presence of a previously identified SCF recognition motif (DDAYPE) within the C-terminus of securin (Limón-Mortés et al. 2008), not present in cyclin A2, hence why we did not see the effect with cyclin A2 N165-Cks1 APC/C mutant.

However, mutation of both the anion-binding site and the two Skp2-interacting residues does not fully stabilise prometaphase destruction (Fig. 6.3G). Note that while securin FL-Cks1 degradation rate accelerates ~3 hours ahead of PB1 extrusion, APC/C+Skp2 mutant degradation only increases in the last 2 hours before PB1 extrusion.

6.2.4 The ABBA motif is essential for early cyclin A2 degradation in mouse oocytes.

In nocodazole-treated mitotic cells, when the ABBA motif in cyclin A2 is mutated, though the rate of degradation decreases, the mutant is still fully degraded (Di Fiore et al. 2015). This is in contrast to the equivalent securin FxxF-A mutant which is largely stabilised in nocodazole-arrested oocytes (Chapter 5). This prompted the question of whether cyclin A2 contained yet further regions promoting degradation during an active checkpoint. Indeed after sequence alignment and conservation analysis, it was found that the PM motif responsible for late prometaphase I destruction of cyclin B1 is present in all A- and B-type cyclins in humans, yet lost in D- and E-type cyclins (Fig 6.4A). Indeed the motif is highly conserved in cyclins B1 and A2 through Metazoa (Fig. 6.4B-C) and is present in various cyclins of both budding and fission yeast, where the ABBA motif is either divergent or lost completely (Fig. 6.4D-E).

To assess the functionality of this conserved PM motif within cyclin A2, two full-length mutant cyclin A2 constructs were tested, one with the ABBA motif mutated (cyclin A2 FL ABBA mutant) and one with the PM motif mutated (cyclin A2 FL PM mutant) alongside cyclin A2 FL, containing both motifs, and cyclin A2 N165 ABBA containing neither (Fig. 6.5A). It is important to note that all constructs contain a D-box. Though cyclin A2 FL PM mutant was consistently targeted for degradation from early prometaphase, the rate of destruction was slow over the first 6 hours compared to cyclin A2 FL. This was followed by a sharp increase in degradation in the last hour before PB1 extrusion, reminiscent of the cyclin B1 PM mutant as seen in chapter 3 (Fig 6.5B). However, at present we do not have a tested cyclin A2 mutant where Cdk interaction is inhibited (a cyclin B1 Y170A equivalent; see chapter 3). Without a control mutation in both WT and PM mutant constructs, any changes in degradation profile could simply be due to an altered affinity of Cdk and in turn Cks1 binding. As such, while the features of this curve make it tempting to speculate, it is currently not possible to draw any conclusions regarding the function of a cyclin A2 PM motif without such a control.

Cyclin A2 FL ABBA mutant is only a destruction target in the last ~2 hours before PB1 extrusion, however here destruction is rapid (Fig. 6.5C). This is in contrast to mitosis where the reverse is true, mutating the ABBA motif reduces the rate of degradation but does not affect the timing (Di Fiore et al. 2015). Note the particularly late targeting of the cyclin A2 N165 ABBA mutant. This construct contains only a D-box and was expected to be destroyed

in time with the cyclin B1 PM mutant. Instead it appears that the D-box of cyclin B1 is preferred to the D-box of cyclin A2 at this late time point (Fig. 6.5D).

Figure 6.4

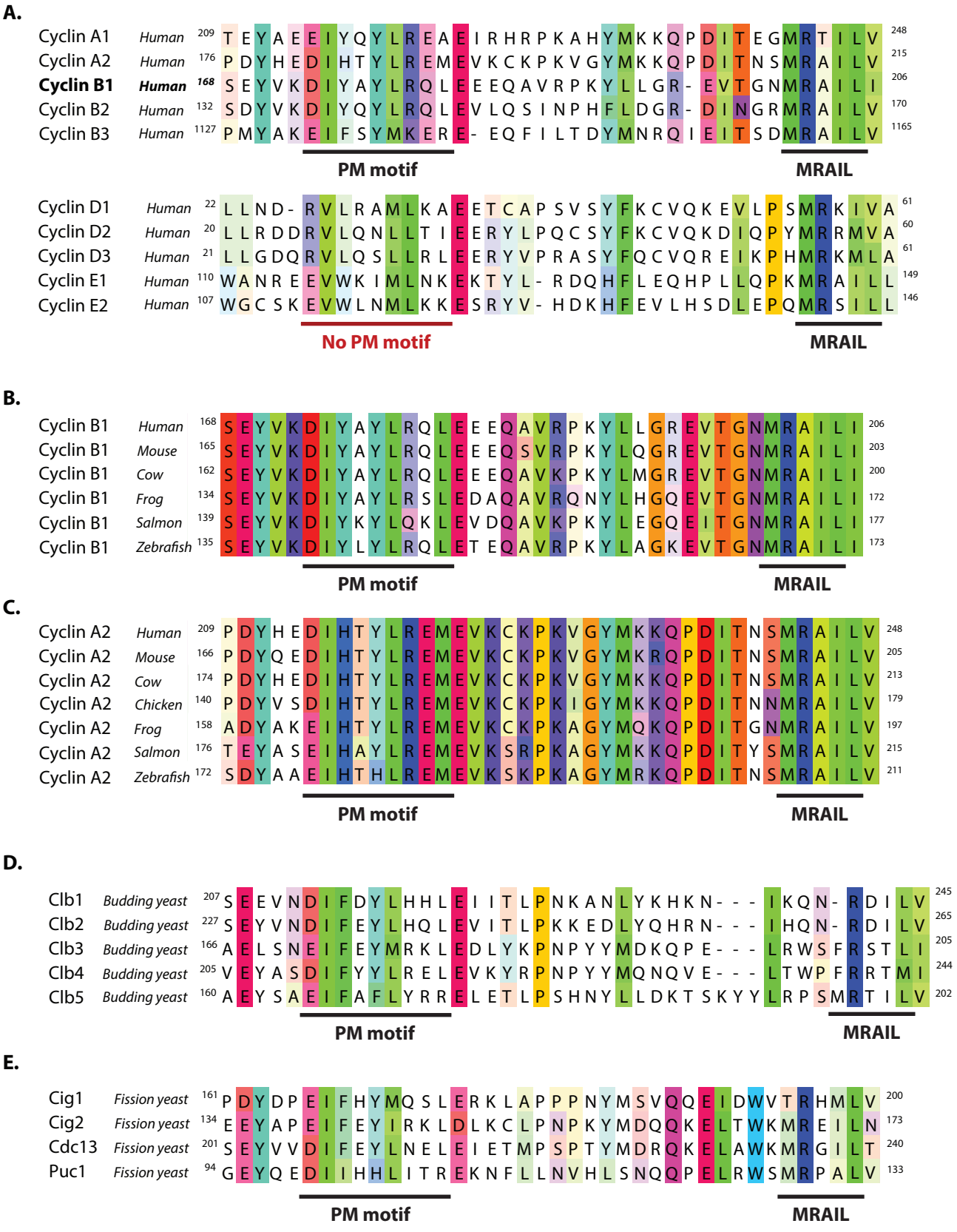
A.
Cyclin A1 Human 209 T E Y A E E I Y Q Y L R E A E I R H R P K A H Y M K K Q P D I T E G M R T I L V 248
Cyclin A2 Human 176 P D Y H E D I H T Y L R E M E V K C K P K V G Y M K K Q P D I T N S M R A I L V 215
Cyclin B1 Human 168 S E Y V K D I Y A Y L R Q L E E E Q A V R P K Y L L G R - E V T G N M R A I L I 206
Cyclin B2 Human 132 S D Y V K D I Y Q Y L R Q L E V L Q S I N P H F L D G R - D I N G R M R A I L V 170
Cyclin B3 Human 1127 P M Y A K E I F S Y M K E R E - E Q F I L T D Y M N R Q I E I T S D M R A I L V 1165
PM motif
MRAIL
Cyclin D1 Human 22 L L N D - R V L R A M L K A E E T C A P S V S Y F K C V Q K E V L P S M R K I V A 61
Cyclin D2 Human 20 L L R D D R V L Q N L L T I E E R Y L P Q C S Y F K C V Q K D I Q P Y M R R M V A 60
Cyclin D3 Human 21 L L G D Q R V L Q S L L R L E E R Y V P R A S Y F Q C V Q R E I K P H M R K M L A 61
Cyclin E1 Human 110 W A N R E E V W K I M L N K E K T Y L - R D Q H F L E Q H P L L Q P K M R A I L L 149
Cyclin E2 Human 107 W G C S K E V W L N M L K K E S R Y V - H D K H F E V L H S D L E P Q M R S I L L 146
No PM motif
MRAIL
B.
Cyclin B1 Human 168 S E Y V K D I Y A Y L R Q L E E E Q A V R P K Y L L G R E V T G N M R A I L I 206
Cyclin B1 Mouse 165 S E Y V K D I Y A Y L R Q L E E E Q S V R P K Y L Q G R E V T G N M R A I L I 203
Cyclin B1 Cow 162 S E Y V K D I Y A Y L R Q L E E E Q A V K P K Y L M G R E V T G N M R A I L I 200
Cyclin B1 Frog 134 S E Y V K D I Y A Y L R S L E D A Q A V R Q N Y L H G Q E V T G N M R A I L I 172
Cyclin B1 Salmon 139 S E Y V K D I Y K Y L Q K L E V D Q A V K P K Y L E G Q E I T G N M R A I L I 177
Cyclin B1 Zebrafish 135 S E Y V K D I Y L Y L R Q L E T E Q A V R P K Y L A G K E V T G N M R A I L I 173
PM motif
MRAIL
C.
Cyclin A2 Human 209 P D Y H E D I H T Y L R E M E V K C K P K V G Y M K K Q P D I T N S M R A I L V 248
Cyclin A2 Mouse 166 P D Y Q E D I H T Y L R E M E V K C K P K V G Y M K R Q P D I T N S M R A I L V 205
Cyclin A2 Cow 174 P D Y H E D I H T Y L R E M E V K C K P K V G Y M K K Q P D I T N S M R A I L V 213
Cyclin A2 Chicken 140 P D Y V S D I H T Y L R E M E V K C K P K I G Y M K K Q P D I T N N M R A I L V 179
Cyclin A2 Frog 158 A D Y A K E I H T Y L R E M E V K C K P K A G Y M Q K Q P D I T G N M R A I L V 197
Cyclin A2 Salmon 176 T E Y A S E I H A Y L R E M E V K S R P K A G Y M K K Q P D I T Y S M R A I L V 215
Cyclin A2 Zebrafish 172 S D Y A A E I H T H L R E M E V K S K P K A G Y M R K Q P D I T N S M R A I L V 211
PM motif
MRAIL
D.
Clb1 Budding yeast 207 S E E V N D I F D Y L H H L E I I T L P N K A N L Y K H K N - - - I K Q N - R D I L V 245
Clb2 Budding yeast 227 S E Y V N D I F E Y L H Q L E V I T L P K K E D L Y Q H R N - - - I H Q N - R D I L V 265
Clb3 Budding yeast 166 A E L S N E I F E Y M R K L E D L Y K P N P Y Y M D K Q P E - - - L R W S F R S T L I 205
Clb4 Budding yeast 205 V E Y A S D I F Y Y L R E L E V K Y R P N P Y Y M Q N Q V E - - - L T W P F R R T M I 244
Clb5 Budding yeast 160 A E Y S A E I F A F L Y R R E L E T L P S H N Y L L D K T S K Y Y L R P S M R T I L V 202
PM motif
MRAIL
E.
Cig1 Fission yeast 161 P D Y D P E I F H Y M Q S L E R K L A P P P N Y M S V Q Q E I D W V T R H M L V 200
Cig2 Fission yeast 134 E E Y A P E I F E Y I R K L D L K C L P N P K Y M D Q Q K E L T W K M R E I L N 173
Cdc13 Fission yeast 201 S E Y V V D I F E Y L N E L E I E T M P S P T Y M D R Q K E L A W K M R G I L T 240
Puc1 Fission yeast 94 G E Y Q E D I I H H L I T R E K N F L L N V H L S N Q Q P E L R W S M R P A L V 133
PM motif
MRAIL

Figure 6.4. The PM motif is conserved in A- and B-type cyclins through Metazoa and various cyclins in both budding and fission yeast. (A) Alignment of PM motif-containing region in human cyclins, showing conservation in A- and B-type cyclins but loss in D- and E-type cyclins. **(B)** Alignment of PM motif-containing region in cyclin B1 orthologs. **(C)** Alignment of PM motif-containing region in cyclin A2 orthologs. **(D)** Alignment of PM motif-containing region in budding yeast cyclins. **(E)** Alignment of PM motif-containing region in fission yeast cyclins. The MRAIL motif, important in Cdk binding, is highlighted as a common feature of most cyclins. Note the conservation of the relative positioning of the PM motif ~18-22 residues upstream of the MRAIL motif.

Figure 6.5

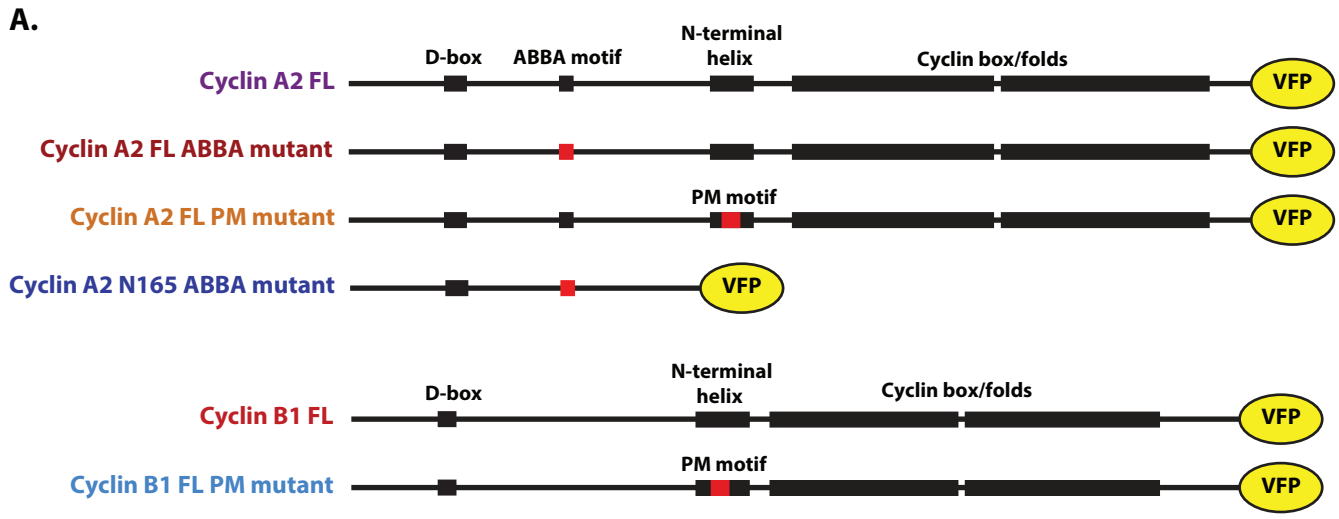
A.
D-box
ABBA motif
N-terminal helix
Cyclin box/folds
Cyclin A2 FL
VFP
Cyclin A2 FL ABBA mutant
VFP
PM motif
Cyclin A2 FL PM mutant
VFP
Cyclin A2 N165 ABBA mutant
VFP
D-box
N-terminal helix
Cyclin box/folds
Cyclin B1 FL
VFP
PM motif
Cyclin B1 FL PM mutant
VFP

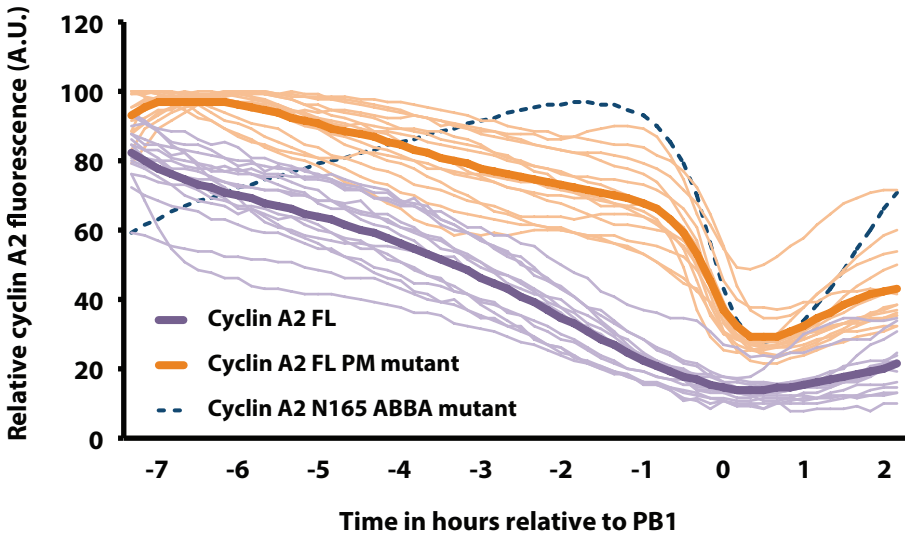
B.
Relative cyclin A2 fluorescence (A.U.)
120
100
80
60
40
20
0
Cyclin A2 FL
Cyclin A2 FL PM mutant
Cyclin A2 N165 ABBA mutant
-7
-6
-5
-4
-3
-2
-1
0
1
2
Time in hours relative to PB1

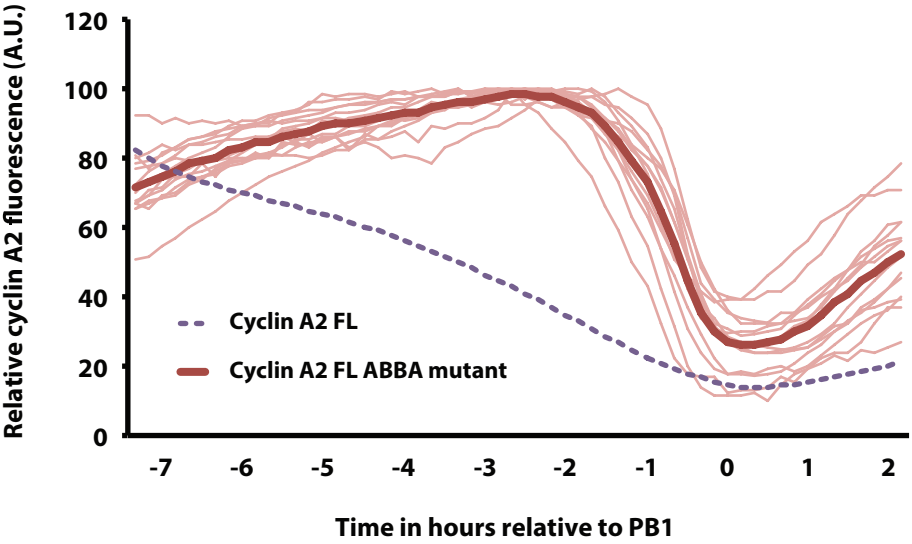
C.
Relative cyclin A2 fluorescence (A.U.)
120
100
80
60
40
20
0
Cyclin A2 FL
Cyclin A2 FL ABBA mutant
-7
-6
-5
-4
-3
-2
-1
0
1
2
Time in hours relative to PB1

D.

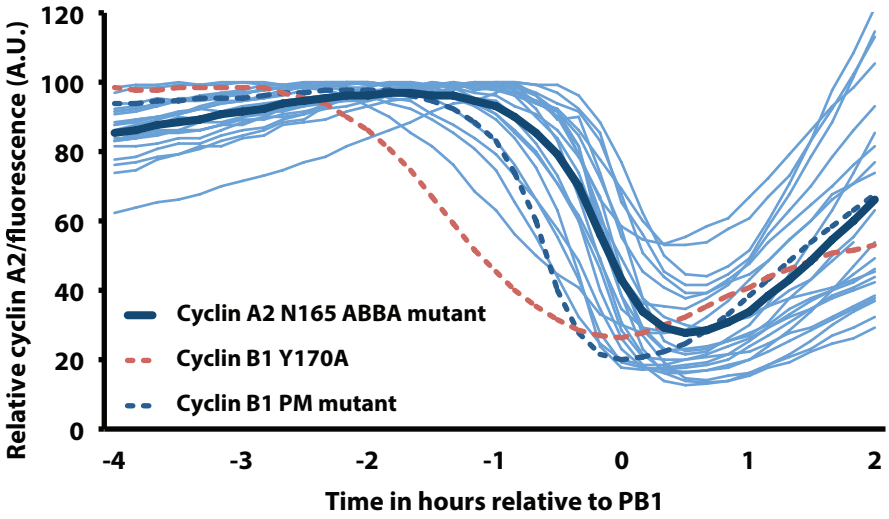

Figure 6.5. The ABBA motif in cyclin A2 is essential for early prometaphase degradation in mouse oocytes. (A) Schematic showing VFP-tagged cyclin A2 and cyclin B1 truncations and mutations. **(B)** Average cyclin A2 FL::VFP (purple, n=22), cyclin A2 FL PM mutant::VFP (orange, n=14) and cyclin A2 N165 ABBA mutant::VFP (dark blue dashed, n=22) destruction profiles aligned at PB1 extrusion. **(C)** Average cyclin A2 FL::VFP (purple dashed, n=22) and cyclin A2 FL ABBA mutant::VFP (red, n=14) destruction profiles aligned at PB1 extrusion. **(D)** Average cyclin A2 N165 ABBA mutant::VFP (blue, n=22), cyclin B1 Y170A::VFP (red dashed, n=32) and cyclin B1 PM mutant::VFP (blue dashed, n=28) destruction profiles aligned at PB1 extrusion. Fine traces represent destruction profiles from individual oocytes, heavy traces represent the average destruction profile resulting from all injected oocytes of a given construct.

6.3 Discussion

In chapters 3 and 4, two novel motifs were identified, the PM motif in cyclin B1 and the FxxF motif in securin that function to permit destruction in late prometaphase I during an active checkpoint. Whilst the degradation timings of cyclin B1 and securin are seemingly identical in both wild-type constructs and in PM/FxxF mutant constructs, the motifs share no discernable similarity either in sequence or position relative to key domains. While the PM motif forms part of the N-terminal helix of cyclin B1, the FxxF motif is found within an unstructured region of securin (Fig. 6.1B). It therefore seems likely that these degrons act to bypass the checkpoint via distinct mechanisms.

Sequence alignment and conservation analysis of other known APC/C degrons revealed that the FxxF motif in securin shares a number of common features with the ABBA motif recently identified in cyclin A1, cyclin A2, Bub1 and BubR1 (Di Fiore et al. 2015). Both motifs typically center around two aromatic residues, either phenylalanine, tyrosine or histidine, in positions 1 and 4, with an upstream proline rich region and a downstream acidic region (Fig. 6.1A). Whilst the FxxF motif does not exactly fit the consensus ABBA motif sequence (Fx[ILV][FHY]x[DE]), it is important to note that the ABBA motif is the most recently characterised APC/C degron and has only been identified a handful of proteins and is therefore likely to evolve as more cases are identified. Also important to note is that ABBA motif in cyclin A was identified using a computational motif search (SLiMSearch; Davey et al. 2011) rather than from experimental data. While the minimal consensus D-box motif is RxxL, there are a number of experimentally identified D-box degrons that do not fit this such as cyclin B3 which has a phenylalanine rather than a leucine in position 4 (Nguyen et al. 2002). Such studies highlight a level of flexibility even in an APC/C degron as well defined as the D-box.

Our data shows that cyclin A2 degradation from early prometaphase I is mediated by Cks1 targeting to the phosphorylated APC/C. A cyclin A2 N165 truncation which includes both the D-box and the ABBA motif, yet lacks Cdk-binding modules is not able to form a complex with Cks1 and only becomes an APC/C target in late prometaphase (Fig. 6.2B). This suggests that while the ABBA motif is essential for a wild-type degradation, the difference between early and late prometaphase APC/C targeting was largely a result of a presence or absence of Cks1. The ABBA motif may offer a higher affinity for the APC/C, but this interaction is only possible when coupled to Cks1-directed recruitment. Indeed, cyclin A2 N165 was targeted an hour after securin FL in late prometaphase suggesting that at this earlier time point the D-box

and FxxF motif of securin have the higher combined binding affinity than the D-box and ABBA motif of cyclin A2 in the absence of Cks1 binding (Fig. 6.2C-D).

Early prometaphase degradation was rescued by linking cyclin A2 N165 to Cks1 (Fig. 6.3B), thus confirming that without Cks1, the D-box and ABBA motif together are insufficient to mediate destruction in early prometaphase. Furthermore, when the linked Cks1 protein contained mutations removing both APC/C and Skp2 interactions, this rescue was abolished (Fig. 6.3F). Interestingly, the APC/C binding mutation alone did not completely abolish the rescue, suggesting that some level of degradation can be mediated via the SCF through direct interaction of Cks1 and the F-box protein Skp2. This finding is supported by a previous study reporting an interaction between cyclin A2-Cdk2 and Skp2 (Yam et al. 1999).

It seemed plausible that the dramatic difference in degradation timing between cyclin A2 and securin may be largely due to Cks1 targeting and that in fact the motifs may function in the same way if similarly localised. To test this, securin was linked to Cks1. Indeed the linked construct was targeted for degradation from early prometaphase. However somewhat unexpectedly, wild-type degradation in late prometaphase was not recovered when both APC/C and Skp2 interacting residues were mutated in Cks1. Whether the FxxF motif can act as an ABBA motif in early prometaphase remains under investigation. Ongoing immunoprecipitation experiments to assess whether the FxxF motif can directly bind to Cdc20's ABBA interacting region will further address this.

In chapter 5, it was demonstrated that late prometaphase degradation of securin is a regulated mechanism, mediated by discrete motifs which permit securin to bypass the spindle checkpoint. An FxxF-A mutant securin was stabilised in nocodazole-treated oocytes. This is in contrast to the ABBA motif in mitotic cyclin A2 destruction, where a cyclin A2 ABBA mutant was still fully degraded in nocodazole-arrested cells, albeit at a reduced rate (Di Fiore et al. 2015). This prompted the question whether cyclin A2 contained additional regions able to mediate degradation during an active checkpoint. Sequence alignment and conservation analysis revealed a conserved PM motif within the N-terminal helix of cyclin A2 (showing high sequence homology to the motif identified in cyclin B1, Fig. 6.4B-C). This conservation carried through to budding and fission yeast cyclins, both of which hold PM motifs consistently ~20 residues upstream of the MRAIL motif critical for Cdk binding (Fig. 6.4D-E; Schulman et al 1998), suggesting this may have important evolutionary significance. Interestingly, while a functional ABBA motif does exist in budding yeast Clb5 (Lu et al. 2014), it bears little resemblance to the mammalian ABBA motif and is completely absent in fission yeast cyclins. It could be argued that the PM motif is so well conserved simply

because it has a role to play in Cdk binding, however human D- and E- type cyclins also have Cdk partners and a well conserved MRAIL motif, yet no PM motif.

We suggest that cyclin A2 contains 3 APC/C degrons; a D-box, an ABBA motif with high sequence homology to the FxxF motif in securin and a PM motif with high sequence homology to that of cyclin B1. To test the functionality of the PM motif would require a non Cdk-binding cyclin A2 with and without a PM motif mutation. An example of this could be a cyclin A2 truncation after the N-terminal helix at around residue 230.

Chapter 7: Conclusion and final remarks.

Accurate cell division is a strictly ordered, highly regulated event that requires complex regulation in order to avoid chromosomal segregation errors during the metaphase to anaphase transition. Errors during segregation often lead to generation of aneuploid daughter cells; cells containing an incorrect number of inherited chromosomes. In mitosis, a robust spindle checkpoint ensures that chromosome division errors occur at a relatively low frequency, by maintaining high levels of cyclin B1 and securin until chromosomes are accurately aligned on the metaphase plate. In contrast, human oocyte meiosis is extremely error prone, with chromosomal abnormalities estimated to be present in as many as 30% of fertilised eggs in younger women, possibly exceeding 50% in those who conceive later in their reproductive lifespan (Hassold & Hunt 2001). This meiotic aneuploidy is the primary genetic cause of miscarriage, congenital disability and mental retardation in foetuses that survive to term (Hassold & Hunt 2001).

It is well observed that in meiosis I mouse oocytes, cyclin B1 and securin degradation initiate in late prometaphase (Homer et al. 2005; Lane et al. 2012) at a time when the spindle is yet to fully migrate to the cortex (Verlhac et al. 2000; Kitajima et al. 2011) and checkpoint proteins are still detected at kinetochores (Lane et al. 2012). This has often been viewed as precocious degradation, missed by a checkpoint that has become insufficient over the large volume of an oocyte. Indeed, the spindle checkpoint does appear to be less robust in oocytes as MPS1 localisation to kinetochores and subsequent kinetochore-dependent MCC assembly is essential for correct prometaphase timing (Hached et al. 2011). In contrast, in mitotic cells MCC complex formation within the cytoplasm is sufficient for correct cell cycle progression (Maciejowski et al. 2010). Thus a diffusible checkpoint able to block premature progression in mitotic cells is not sufficient in oocytes. While a diluted checkpoint may seem like an attractive explanation for the high rates of aneuploidy observed in human oocytes, mouse oocytes are comparable in size and chromosome number but are far less error prone with an estimated 1-2% of fertilised eggs being aneuploid (Bond & Chandley 1983), compared to 25-30% in human eggs (Hassold & Hunt 2001). This implies that cyclin B1 and securin destruction in late prometaphase I is not responsible for segregation errors and consequently seemed worthy of further investigation.

We show that degradation of cyclin B1 and securin in late prometaphase I is not simply due to an insufficient checkpoint but in fact due to controlled novel mechanisms of destruction

within the oocyte. Meiotic destruction of cyclin B1 and securin can be split into two distinct periods; a later period of destruction that resembles mitotic destruction where the D-box is sufficient for APC/C targeting, and a much earlier period of destruction requiring additional previously unidentified motifs able to bypass the spindle checkpoint. The PM motif in cyclin B1 and the FxxF motif in securin constitute novel regions that work alongside a D-box to mediate degradation during an active checkpoint.

Due to the location of these motifs within the proteins, they are likely to be masked when bound to their respective partner proteins; cyclin B1 to Cdk1 and securin to separase. This is supported by the crystal structures of both complexes (Brown et al. 2015; Luo & Tong 2017). We therefore propose a mechanism by which free pools of cyclin B1 and securin are targeted preferentially ahead of bound pools in which the PM motif and FxxF motif respectively would be obscured. This preferential targeting of unbound pools would protect Cdk1 activity and separase inhibition when the spindle checkpoint may become insufficient over the extended prometaphase period in the huge cell volume of an oocyte.

Key experiments to prove this model will involve determination of securin:separase ratio in oocytes, followed by knock down of securin protein level to mimic a mitotic ratio and subsequent measurement of separase activity in a securin knock down background. These would mimic cyclin B1 knock down experiments from our lab in which oocytes are unable to maintain Cdk1 activity and extrude abnormal polar bodies when cyclin B1 protein levels are knocked down such that oocytes contain ~2-fold rather than the usual ~6-fold excess at 5.5 hours post GVBD (Levasseur et al. 2017 unpublished).

It has been suggested that each APC/C substrate is governed in a unique way, ensuring delivery to the proteasome at a particular time and in a specific order (Lu et al. 2014). In the case of cyclin B1 and securin, we expand upon this and suggest processing in a way that is unique to binding state. Our research provides a new insight into fundamental aspects of cell cycle control in meiosis I mouse oocytes, relevant to our understanding of the high rates of aneuploidy in human eggs. We provide substantial evidence for oocyte-specific mechanisms which protect the oocyte from an increased incidence of division error. Destruction mechanisms utilising degrons that would otherwise be masked in complex may be a common principle of proteostasis, this has been suggested (Ravid & Hochstrasser 2008; Harper & Bennett 2016; Davey & Morgan 2016). The position of such degrons allows control over the balance of individual subunits of complexes where their balance becomes misregulated. We would suggest that the oocyte may be exploiting such mechanisms to control the activity of key cell cycle regulators.

We have revised our understanding of both the timing of the oocyte cell cycle and the regulation of cyclin B1, cyclin A2 and securin. Our findings will aid the search for the origins of aneuploidy in oocytes and the design of treatment strategies for women who suffer repetitive miscarriages, a substantial contributor to human infertility. In certain cases, recurrent miscarriage may be due to an imbalance in the ratio of cyclin B1:Cdk1 or securin:separase. Furthermore, given the general conservation of molecular mechanisms in the control of both mitotic and meiotic cell cycles, it is possible that the PM motif and FxxF motif have additional mitotic functions in the 'housekeeping' of cyclin B1 and securin protein levels, or the slippage of cells out of drug-induced mitotic arrest. Beyond cell division, it seems plausible that the masking and unveiling of degrons has a key role to play in proteostasis.

While an error-prone spindle assembly and large cell volume clearly contribute to the high levels of aneuploidy observed in human oocytes, it is also of critical interest whether the protective mechanisms we have identified in mouse oocytes are conserved in humans. Spindle assembly in human oocytes lasts up to 16 hours compared to 3-5 hours in mice (Holubcova et al. 2015). A human oocyte would therefore need much larger excesses of cyclin B1 and securin in order to protect Cdk1 activity and separase inhibition over such an extended time period. The situation in aged oocytes is also very interesting. While all of our studies have been conducted in young mice, we can speculate that the balance of cyclin B1:Cdk1 and securin:separase could be perturbed with age, contributing to the age-dependent exponential increase in error alongside other known problems associated with aged oocytes.

Appendix I: Abbreviations

APC/C	Anaphase promoting complex or cyclosome
CHX	Cycloheximide
CPC	Chromosome passenger complex
FL	Full-length
FRET	Förster resonance energy transfer
GFP	Green fluorescent protein
GV	Germinal vesicle
GVBD	Germinal vesicle breakdown
I2PP2A	PP2A inhibitor 2
IBMX	3-isobutyl-1-methyl xanthine
LH	Luteinising hormone
MI	First meiotic division
MII	Second meiotic division
MCC	Mitotic checkpoint complex
MEFs	Mouse embryonic fibroblasts
MO	Morpholino oligomer
MTOC	Microtubule organising centre
NEBD	Nuclear envelope breakdown
NTH	N-terminal helix
PB1	First polar body extrusion
PP2A	Protein phosphatase 2A
RT	Room temperature
SCF	Skp1-Cullin-F-box complex
Sgo	Shugoshin
SLIC	Sequence- and ligation-independent cloning
VFP	Venus fluorescent protein
WT	Wild-type

Appendix 2. Full sequence alignment of securin orthologs.

References

Arooz, T. et al., 2000. On the concentrations of cyclins and cyclin-dependent kinases in extracts of cultured human cells. *Biochemistry*, 39(31), pp.9494–9501.

Boehm, J.S. et al., 2007. Integrative Genomic Approaches Identify IKBKE as a Breast Cancer Oncogene. *Cell*, 129(6), pp.1065–1079.

Boekhout, M. & Wolthuis, R., 2015. Nek2A destruction marks APC/C activation at the prophase-to-prometaphase transition by spindle-checkpoint-restricted Cdc20. *Journal of Cell Science*, 128(8), pp.1639–1653.

Bond, D. & Chandley, A., 1983. in Aneuploidy 86–91 (Oxford Univ. Press, Oxford, 1983.). , pp.86–91.

Brown, N.R. et al., 2015. CDK1 structures reveal conserved and unique features of the essential cell cycle CDK. *Nature communications*, 6, p.6769.

Brunet, S. et al., 1999. Kinetochore fibers are not involved in the formation of the first meiotic spindle in mouse oocytes, but control the exit from the first meiotic M phase. *Journal of Cell Biology*, 146(1), pp.1–11.

Buonomo, S.B. et al., 2000. Disjunction of homologous chromosomes in meiosis I depends on proteolytic cleavage of the meiotic cohesin Rec8 by separin. *Cell*, 103(3), pp.387–398.

Chambon, J.P. et al., 2013. The PP2A inhibitor I2PP2A is essential for sister chromatid segregation in oocyte meiosis II. *Current Biology*, 23(6), pp.485–490.

Chao, W.C.H. et al., 2012. Structure of the mitotic checkpoint complex. *Nature*, 484(7393), pp.208–213.

Ciosk, R. et al., 1998. An ESP1/PDS1 complex regulates loss of sister chromatid cohesion at the metaphase to anaphase transition in yeast. *Cell*, 93(6), pp.1067–1076.

Clift, D., Bizzari, F. & Marston, A.L., 2009. Shugoshin prevents cohesin cleavage by PP2A Cdc55 -dependent inhibition of separase. *Genes Dev.*, 23(6), pp.766–780.

Clift, D. & Schuh, M., 2013. Restarting life: fertilization and the transition from meiosis to

mitosis. *Nature Reviews Molecular Cell Biology*, 14(9), pp.549–562.

Collin, P. et al., 2013. The spindle assembly checkpoint works like a rheostat rather than a toggle switch. *Nature Cell Biology*, 15(11), pp.1378–1385.

Davey, N.E. et al., 2011. SLiMSearch 2.0: Biological context for short linear motifs in proteins. *Nucleic Acids Research*, 39(SUPPL. 2), pp.56–60.

Davey, N.E. & Morgan, D.O., 2016. Building a Regulatory Network with Short Linear Sequence Motifs: Lessons from the Degrons of the Anaphase-Promoting Complex. *Molecular Cell*, 64(1), pp.12–23.

Davydenko, O., Schultz, R.M. & Lampson, M.A., 2013. Increased CDK1 activity determines the timing of kinetochore-microtubule attachments in meiosis I. *Journal of Cell Biology*, 202(2), pp.221–229.

DiFiore, B. et al., 2015. The ABBA Motif binds APC/C activators and is shared by APC/C substrates and regulators. *Developmental Cell*, 32(3), pp.358–372.

Elzen, N. Den & Pines, J., 2001. Cyclin A is destroyed in prometaphase and can delay chromosome alignment and anaphase. *Journal of Cell Biology*, 153(1), pp.121–135.

Di Fiore, B. et al., 2016. The Mitotic Checkpoint Complex Requires an Evolutionary Conserved Cassette to Bind and Inhibit Active APC/C. *Molecular Cell*, 64(6), pp.1144–1153.

Di Fiore, B. & Pines, J., 2010. How cyclin a destruction escapes the spindle assembly checkpoint. *Journal of Cell Biology*, 190(4), pp.501–509.

Floyd, S., Pines, J. & Lindon, C., 2008. APC/CCdh1 Targets Aurora Kinase to Control Reorganization of the Mitotic Spindle at Anaphase. *Current Biology*, 18(21), pp.1649–1658.

Fujimitsu, K., Grimaldi, M. & Yamano, H., 2016. Cyclin-dependent kinase 1 – dependent activation of APC/C ubiquitin ligase.

Gabellini, D. et al., 2003. Early mitotic degradation of the homeoprotein HOXC10 is potentially linked to cell cycle progression. *EMBO Journal*, 22(14), pp.3715–3724.

Galli, M. & Morgan, D.O., 2016. Cell Size Determines the Strength of the Spindle Assembly Checkpoint during Embryonic Development. *Developmental Cell*, 36(3), pp.344–352.

Gavet, O. & Pines, J., 2010. Progressive Activation of CyclinB1-Cdk1 Coordinates Entry to Mitosis. *Developmental Cell*, 18(4), pp.533–543.

Geley, S. et al., 2001. Anaphase-promoting complex/cyclosome-dependent proteolysis of human cyclin A starts at the beginning of mitosis and is not subject to the spindle assembly checkpoint. *Journal of Cell Biology*, 153(1), pp.137–147.

Gil-Bernabé, A.M. et al., 2006. Protein phosphatase 2A stabilizes human securin, whose phosphorylated forms are degraded via the SCF ubiquitin ligase. *Molecular and cellular biology*, 26(11), pp.4017–27.

Glotzer, M., Murray, A.W. & Kirschner, M.W., 1991. Cyclin is degraded by the ubiquitin pathway. *Nature*, 349(6305), pp.132–138.

Gómez, R. et al., 2007. Mammalian SGO2 appears at the inner centromere domain and redistributes depending on tension across centromeres during meiosis II and mitosis. *EMBO reports*, 8(2), pp.173–180.

Gorbsky, G.J., 2015. The spindle checkpoint and chromosome segregation in meiosis. *The FEBS journal*, 282(13), pp.2471–2487.

Gorr, I.H. et al., 2006. Essential CDK1-inhibitory role for separase during meiosis I in vertebrate oocytes. *Nature cell biology*, 8(9), pp.1035–1037.

Gorr, I.H., Boos, D. & Stemmann, O., 2005. Mutual inhibition of separase and Cdk1 by two-step complex formation. *Molecular Cell*, 19(1), pp.135–141.

Griffin, J. et al., 2006. Comparative analysis of follicle morphology and oocyte diameter in four mammalian species (mouse, hamster, pig, and human). *Journal of Experimental and Clinical Assisted Reproduction*, 3, pp.1–9.

Gui, L. & Homer, H., 2012. Spindle assembly checkpoint signalling is uncoupled from chromosomal position in mouse oocytes. *Development*, 139(11), pp.1941–1946.

Hached, K. et al., 2011. Mps1 at kinetochores is essential for female mouse meiosis I. *Development*, 138(11), pp.2261–2271.

Hagting, A. et al., 2002. Human securin proteolysis is controlled by the spindle checkpoint and reveals when the APC/C switches from activation by Cdc20 to Cdh1. *Journal of Cell Biology*, 157(7), pp.1125–1137.

Hames, R.S. et al., 2001. APC/C-mediated destruction of the centrosomal kinase Nek2A occurs in early mitosis and depends upon a cyclin A-type D-box. *EMBO Journal*, 20(24), pp.7117–7127.

Harper, J.W. & Bennett, E.J., 2016. Proteome complexity and the forces that drive proteome imbalance. *Nature*, 537(7620), pp.328–338.

Hassold, T. & Hunt, P., 2001. To err (meiotically) is human: the genesis of human aneuploidy. *Nat Rev Genet*, 2(4), pp.280–291.

Hayes, M.J. et al., 2006. Early mitotic degradation of Nek2A depends on Cdc20-independent interaction with the APC/C. *Nature cell biology*, 8(6), pp.607–614.

He, J. et al., 2013. Insights into degron recognition by APC/C coactivators from the structure of an Acm1-Cdh1 complex. *Molecular Cell*, 50(5), pp.649–660.

Hellmuth, S. et al., 2015. Human chromosome segregation involves multi-layered regulation of separase by the peptidyl-prolyl-isomerase Pin 1. *Molecular Cell*, 58(3), pp.495–506.

Hellmuth, S. et al., 2014. PP2A delays APC/C-dependent degradation of separase-associated but not free securin. *EMBO Journal*, 33(10), pp.1134–1147.

Herbert, M. et al., 2003. Homologue disjunction in mouse oocytes requires proteolysis of securin and cyclin B1. *Nature cell biology*, 5(11), pp.1023–1025.

Herlands, R.L. & Schultz, R.M., 1984. Regulation of mouse oocyte growth: Probable nutritional role for intercellular communication between follicle cells and oocytes in oocyte growth. *Journal of Experimental Zoology*, 229(2), pp.317–325.

Hodges, C.A. et al., 2005. SMC1β-deficient female mice provide evidence that cohesins are a missing link in age-related nondisjunction. *Nature Genetics*, 37(12), pp.1351–1355.

Holland, A.J. & Taylor, S.S., 2008. Many faces of separase regulation. *SEB experimental biology series*, 59(February 2008), pp.99–112.

Holubcova, Z. et al., 2015. Error-prone chromosome-mediated spindle assembly favors chromosome segregation defects in human oocytes. *Science*, 348(6239), pp.1143–1147.

Homer, H., 2011. New insights into the genetic regulation of homologue disjunction in mammalian oocytes. *Cytogenetic and Genome Research*, 133(2–4), pp.209–222.

Homer, H., 2013. The APC/C in female mammalian meiosis i. *Reproduction*, 146(2).

Homer, H.A. et al., 2005. Mad2 is required for inhibiting securin and cyclin B degradation following spindle depolymerisation in meiosis I mouse oocytes. *Reproduction*, 130(6), pp.829–843.

Hook, E.B., 1985. Aneuploidy. Bond DJ, Chandley AC, (Oxford Monographs on Medical Genetics No. 11). Oxford and New York: Oxford University Press, 1983. *American Journal of Medical Genetics*, 22(2), pp.431–432.

Hornak, M. et al., 2011. Frequency of aneuploidy related to age in porcine oocytes. *PLoS ONE*, 6(4), pp.2–6.

Huang, X. et al., 2009. Preimplantation Mouse Embryos Depend on Inhibitory Phosphorylation of Separase To Prevent Chromosome Missegregation. *Molecular and Cellular Biology*, 29(6), pp.1498–1505.

Hunter, N., 2015. Meiotic recombination: The essence of heredity. *Cold Spring Harbor Perspectives in Biology*, 7(12), pp.1–36.

Izawa, D. & Pines, J., 2011. How APC/C–Cdc20 changes its substrate specificity in mitosis. *Nature Cell Biology*, 13(3), pp.223–233.

Izawa, D. & Pines, J., 2014. The mitotic checkpoint complex binds a second CDC20 to inhibit active APC/C. *Nature*, 517(7536), pp.631–634.

Jeong, J.Y. et al., 2012. One-step sequence-and ligation-independent cloning as a rapid and versatile cloning method for functional genomics Studies. *Applied and Environmental Microbiology*, 78(15), pp.5440–5443.

Jin, L. et al., 2008. Mechanism of Ubiquitin-Chain Formation by the Human Anaphase-Promoting Complex. *Cell*, 133(4), pp.653–665.

Jonak, K. et al., 2017. APC/C-Cdc20 mediates deprotection of centromeric cohesin at meiosis II in yeast. *Cell Cycle*, 16(12), pp.1145–1152.

Kamenz, J. et al., 2015. Robust Ordering of Anaphase Events by Adaptive Thresholds and Competing Degradation Pathways. *Molecular Cell*, 60(3), pp.446–459.

Kamenz, J. & Hauf, S., 2014. Slow checkpoint activation kinetics as a safety device in anaphase. *Current Biology*, 24(6), pp.646–651.

Kamenz, J. & Hauf, S., 2017. Time To Split Up: Dynamics of Chromosome Separation.

Trends in Cell Biology, 27(1), pp.42–54.

Kanatsu-Shinohara, M., Schultz, R.M. & Kopf, G.S., 2000. Acquisition of meiotic competence in mouse oocytes: absolute amounts of p34(cdc2), cyclin B1, cdc25C, and wee1 in meiotically incompetent and competent oocytes. *Biol Reprod*, 63(6), pp.1610–1616.

Kitajima, T.S., Ohsugi, M. & Ellenberg, J., 2011. Complete kinetochore tracking reveals error-prone homologous chromosome biorientation in mammalian oocytes. *Cell*, 146(4), pp.568–581.

Kolano, A. et al., 2012. Error-prone mammalian female meiosis from silencing the spindle assembly checkpoint without normal interkinetochore tension. *Proceedings of the National Academy of Sciences*, 109(27), pp.E1858–E1867.

Kraft, C. et al., 2005. The WD40 propeller domain of Cdh1 functions as a destruction box receptor for APC/C substrates. *Molecular Cell*, 18(5), pp.543–553.

Kramer, E.R. et al., 2000. Mitotic regulation of the APC activator proteins CDC20 and CDH1. *Molecular biology of the cell*, 11(5), pp.1555–69.

Lane, S.I.R. & Jones, K.T., 2014. Non-canonical function of spindle assembly checkpoint proteins after APC activation reduces aneuploidy in mouse oocytes. *Nature Communications*, 5, pp.1–9.

Lane, S.I.R., Yun, Y. & Jones, K.T., 2012. Timing of anaphase-promoting complex activation in mouse oocytes is predicted by microtubule-kinetochore attachment but not by bivalent alignment or tension. *Development (Cambridge, England)*, 139(11), pp.1947–55.

Lara-Gonzalez, P., Westhorpe, F.G. & Taylor, S.S., 2012. The spindle assembly checkpoint. *Current Biology*, 22(22), pp.R966–R980.

Ledan, E. et al., 2001. Meiotic Maturation of the Mouse Oocyte Requires an Equilibrium between Cyclin B Synthesis and Degradation. *Developmental Biology*, 232(2), pp.400–413.

Lee, J. et al., 2008. Unified mode of centromeric protection by shugoshin in mammalian oocytes and somatic cells. *Nature Cell Biology*, 10(1), pp.42–52.

Lee, S.B. et al., 2015. Parkin Regulates Mitosis and Genomic Stability through Cdc20/Cdh1. *Molecular Cell*, 60(1), pp.21–34.

LeMaire-Adkins, R., Radke, K. & Hunt, P.A., 1997. Lack of checkpoint control at the metaphase/anaphase transition: A mechanism of meiotic nondisjunction in mammalian females. *Journal of Cell Biology*, 139(7), pp.1611–1619.

Li, C. et al., 2010. Anterior visceral endoderm SMAD4 signaling specifies anterior embryonic patterning and head induction in mice. *International Journal of Biological Sciences*, 6(6), pp.569–583.

Li, M., York, J.P. & Zhang, P., 2007. Loss of Cdc20 causes a securin-dependent metaphase arrest in two-cell mouse embryos. *Molecular and cellular biology*, 27(9), pp.3481–3488.

Limón-Mortés, M.C. et al., 2008. UV-induced degradation of securin is mediated by SKP1-CUL1-beta TrCP E3 ubiquitin ligase. *Journal of cell science*, 121(Pt 11), pp.1825–31.

Lin, Z., Luo, X. & Yu, H., 2016. Structural basis of cohesin cleavage by separase. *Nature*, 532(7597), pp.131–134.

Lister, L.M. et al., 2010. Age-related meiotic segregation errors in mammalian oocytes are preceded by depletion of cohesin and Sgo2. *Current Biology*, 20(17), pp.1511–1521.

Lu, D. et al., 2014. Multiple mechanisms determine the order of APC/C substrate degradation in mitosis. *Journal of Cell Biology*, 207(1), pp.23–39.

Lukinavičius, G. et al., 2015. SiR–Hoechst is a far-red DNA stain for live-cell nanoscopy. *Nature Communications*, 6, p.8497.

Luo, S. & Tong, L., 2017. Molecular mechanism for the regulation of yeast separase by securin. *Nature*, 542(7640), pp.255–259.

Maciejowski, J. et al., 2010. Mps1 directs the assembly of Cdc20 inhibitory complexes during interphase and mitosis to control M phase timing and spindle checkpoint signaling. *Journal of Cell Biology*, 190(1), pp.89–100.

Martin, R.H., 2008. Meiotic errors in human oogenesis and spermatogenesis. *Reproductive biomedicine online*, 16(4), pp.523–31.

Mei, J., Huang, X. & Zhang, P., 2001. Securin is not required for cellular viability, but is required for normal growth of mouse embryonic fibroblasts. *Current Biology*, 11(15), pp.1197–1201.

Minshull, J. et al., 1994. A MAP kinase-dependent spindle assembly checkpoint in Xenopus

egg extracts. *Cell*, 79(3), pp.475–486.

Miyano, T. et al., 2007. Formation of Pig Oocytes. , 24, pp.92–98.

Musacchio, A., 2015. The Molecular Biology of Spindle Assembly Checkpoint Signaling Dynamics. *Current Biology*, 25(20), pp.R1002–R1018.

Musacchio, A. & Salmon, E.D., 2007. The spindle-assembly checkpoint in space and time. *Nature Reviews Molecular Cell Biology*, 8(5), pp.379–393.

Nabti, I. et al., 2008. Securin and not CDK1/cyclin B1 regulates sister chromatid disjunction during meiosis II in mouse eggs. *Developmental Biology*, 321(2), pp.379–386.

Nagao, K. & Yanagida, M., 2006. Securin can have a separase cleavage site by substitution mutations in the domain required for stabilization and inhibition of separase. *Genes to Cells*, 11(3), pp.247–260.

Nagaoka, S.I. et al., 2011. Oocyte-specific differences in cell-cycle control create an innate susceptibility to meiotic errors. *Current Biology*, 21(8), pp.651–657.

Nagaoka, S.I., Hassold, T.J. & Hunt, P.A., 2012. Human aneuploidy: mechanisms and new insights into an age-old problem. *Nat Rev Genet*, 13(7), pp.493–504.

Nam, H.-J. & van Deursen, J.M., 2014. Cyclin B2 and p53 control proper timing of centrosome separation. *Nature Cell Biology*, 16(6), pp.538–549.

Nerusheva, O.O. et al., 2014. Tension-dependent removal of pericentromeric shugoshin is an indicator of sister chromosome biorientation. *Genes and Development*, 28(12), pp.1291–1309.

Nguyen, T.B. et al., 2002. Characterization and expression of mammalian cyclin B3, a prepachytene meiotic cyclin. *Journal of Biological Chemistry*, 277(44), pp.41960–41969.

Nilsson, J. et al., 2009. Europe PMC Funders Group The APC / C maintains the spindle assembly checkpoint by targeting Cdc20 for destruction. *Nature Cell Biology*, 10(12), pp.1411–1420.

Pfleger, C.M. & Kirschner, M.W., 2000. The KEN box: An APC recognition signal distinct from the D box targeted by Cdh1. *Genes and Development*, 14(6), pp.655–665.

Pines, J., 2011. Cubism and the cell cycle: the many faces of the APC/C. *Nature Reviews*

Molecular Cell Biology, 12(7), pp.427–438.

Pines, J., 2006. Mitosis: A matter of getting rid of the right protein at the right time. *Trends in Cell Biology*, 16(1), pp.55–63.

Rattani, A. et al., 2017. APC/CCdh1 Enables Removal of Shugoshin-2 from the Arms of Bivalent Chromosomes by Moderating Cyclin-Dependent Kinase Activity. *Current Biology*, 27(10), p.1462–1476.e5.

Rattani, A. et al., 2014. Dependency of the spindle assembly checkpoint on Cdk1 renders the anaphase transition irreversible. *Current Biology*, 24(6), pp.630–637.

Ravid, T. & Hochstrasser, M., 2008. Diversity of degradation signals in the ubiquitin–proteasome system. *Nature Reviews Molecular Cell Biology*, 9(9), pp.679–689.

Reis, A. et al., 2007. Prometaphase APCcdh1 activity prevents non-disjunction in mammalian oocytes. *Nature Cell Biology*, 9(10), pp.1192–8.

Rieder, C.L. et al., 1994. Anaphase Onset in Vertebrate Somatic Cells Is Controlled by a Checkpoint That Monitors Sister Kinetochore Attachment to the Spindle. , 127(5), pp.1301–1310.

Sánchez-Puig, N., Veprintsev, D.B. & Fersht, A.R., 2005. Human full-length Securin is a natively unfolded protein. *Protein science : a publication of the Protein Society*, 14(6), pp.1410–8.

Santaguida, S. et al., 2010. Dissecting the role of MPS1 in chromosome biorientation and the spindle checkpoint through the small molecule inhibitor reversine. *Journal of Cell Biology*, 190(1), pp.73–87.

Santamaría, D. et al., 2007. Cdk1 is sufficient to drive the mammalian cell cycle. *Nature*, 448(7155), pp.811–815.

Schindelin, J. et al., 2012. Fiji: an open-source platform for biological-image analysis. *Nat Meth*, 9(7), pp.676–682.

Schuh, M. & Ellenberg, J., 2007. Self-Organization of MTOCs Replaces Centrosome Function during Acentrosomal Spindle Assembly in Live Mouse Oocytes. *Cell*, 130(3), pp.484–498.

Schulman, B. a, Lindstrom, D.L. & Harlow, E., 1998. Substrate recruitment to cyclin-

dependent kinase 2 by a multipurpose docking site on cyclin A. *Proceedings of the National Academy of Sciences of the United States of America*, 95(18), pp.10453–10458.

Sczaniecka, M. et al., 2008. The spindle checkpoint functions of Mad3 and Mad2 depend on a Mad3 KEN box-mediated interaction with Cdc20-anaphase-promoting complex (APC/C). *Journal of Biological Chemistry*, 283(34), pp.23039–23047.

Sebestova, J. et al., 2012. Lack of response to unaligned chromosomes in mammalian female gametes. *Cell Cycle*, 11(16), pp.3011–3018.

Shindo, N., Kumada, K. & Hirota, T., 2012. Separase Sensor Reveals Dual Roles for Separase Coordinating Cohesin Cleavage and Cdk1 Inhibition. *Developmental Cell*, 23(1), pp.112–123.

Silkworth, W.T. et al., 2009. Multipolar spindle pole coalescence is a major source of kinetochore mis-attachment and chromosome mis-segregation in cancer cells. *PLoS ONE*, 4(8).

Sitry, D. et al., 2002. Three different binding sites of Cks1 are required for p27-ubiquitin ligation. *Journal of Biological Chemistry*, 277(44), pp.42233–42240.

Sivakumar, S. & Gorbsky, G.J., 2015. Spatiotemporal regulation of the anaphase-promoting complex in mitosis. *Nature Reviews Molecular Cell Biology*, 16(2), pp.82–94.

Stemmann, O. et al., 2001. Dual inhibition of sister chromatid separation at metaphase. *Cell*, 107(6), pp.715–726.

Sullivan, M. & Morgan, D.O., 2007. Finishing mitosis, one step at a time. *Nature Reviews Molecular Cell Biology*, 8(11), pp.894–903.

Sun, S.C. & Kim, N.H., 2012. Spindle assembly checkpoint and its regulators in meiosis. *Human Reproduction Update*, 18(1), pp.60–72.

Tanenbaum, M.E. & Medema, R.H., 2010. Mechanisms of Centrosome Separation and Bipolar Spindle Assembly. *Developmental Cell*, 19(6), pp.797–806.

Touati, S.A. et al., 2012. Cyclin A2 Is Required for Sister Chromatid Segregation, But Not Separase Control, in Mouse Oocyte Meiosis. *Cell Reports*, 2(5), pp.1077–1087.

Touati, S.A. & Wassmann, K., 2016. How oocytes try to get it right: spindle checkpoint control in meiosis. *Chromosoma*, 125(2), pp.321–335.

Uhlmann, F., Lottspeich, F. & Nasmyth, K., 1999. Sister-chromatid separation at anaphase onset is promoted by cleavage of the cohesin subunit Scc1. *Nature*, 400(6739), pp.37–42.

Verlhac, M.H. et al., 2000. Asymmetric division in mouse oocytes: With or without Mos. *Current Biology*, 10(20), pp.1303–1306.

Vodermaier, H.C., 2001. Cell cycle: Waiters serving the destruction machinery. *Current Biology*, 11(20), pp.834–837.

Wang, H. et al., 2001. Pds1 phosphorylation in response to DNA damage is essential for its DNA damage checkpoint function. *Genes and Development*, 15(11), pp.1361–1372.

Wassmann, K., 2013. Sister chromatid segregation in meiosis II : Deprotection through phosphorylation. *Cell Cycle*, 12(9), pp.1352–1359.

Watanabe, Y. & Nurse, P., 1999. Cohesin Rec8 is required for reductional chromosome segregation at meiosis. *Nature*, 400(6743), pp.461–464.

Waterhouse, A.M. et al., 2009. Jalview Version 2-A multiple sequence alignment editor and analysis workbench. *Bioinformatics*, 25(9), pp.1189–1191.

Watson, M.H. et al., 1996. A mutation in the human cyclin-dependent kinase interacting protein, CksHs2, interferes with cyclin-dependent kinase binding and biological function, but preserves protein structure and assembly. *Journal of molecular biology*, 261(5), pp.646–657.

Webster, A. & Schuh, M., 2017. Mechanisms of Aneuploidy in Human Eggs. *Trends in Cell Biology*, 27(1), pp.55–68.

Wei, R. et al., 2017. Smurf1 targets Securin for ubiquitin-dependent degradation and regulates the metaphase-to-anaphase transition. *Cellular Signalling*, 38(June), pp.60–66.

Wolthuis, R. et al., 2008. Cdc20 and Cks Direct the Spindle Checkpoint-Independent Destruction of Cyclin A. *Molecular Cell*, 30(3), pp.290–302.

Yam, C.H. et al., 1999. Regulation of cyclin A-Cdk2 by SCF component Skp1 and F-box protein Skp2. *Molecular and cellular biology*, 19(1), pp.635–645.

Yamano, H. et al., 1998. The role of the destruction box and its neighbouring lysine residues in cyclin B for anaphase ubiquitin- dependent proteolysis in ssion yeast: de ning the D-

box receptor. , 17(19), pp.5670–5678.

Yuan, L., 2002. Female Germ Cell Aneuploidy and Embryo Death in Mice Lacking the Meiosis-Specific Protein SCP3. *Science*, 296(5570), pp.1115–1118.

Zachariae, W., 1998. Control of Cyclin Ubiquitination by CDK-Regulated Binding of Hct1 to the Anaphase Promoting Complex. *Science*, 282(5394), pp.1721–1724.

Zon, W. van & Wolthuis, R.M.F., 2010. Cyclin A and Nek2A: APC/C–Cdc20 substrates invisible to the mitotic spindle checkpoint. *Biochemical Society Transactions*, 38(1), pp.72–77.

Zur, A. & Brandeis, M., 2001. Securin degradation is mediated by fzy and fzr, and is required for complete chromatid separation but not for cytokinesis. *EMBO Journal*, 20(4), pp.792–801.

Zur, A. & Brandeis, M., 2002. Timing of APC/C substrate degradation is determined by fzy/fzr specificity of destruction boxes. *EMBO Journal*, 21(17), pp.4500–4510.